A deep cyclonic gyre in the Australian–Antarctic Basin

Michael S. McCartney
Physical Oceanography Department, Woods Hole Oceanographic Institution, Woods Hole, MA, 02543 USA

Kathleen A. Donohue
Graduate School of Oceanography, University of Rhode Island, Narragansett, RI 02882, USA

Abstract

The traditional image of ocean circulation between Australia and Antarctica is of a dominant belt of eastward flow, the Antarctic Circumpolar Current, with comparatively weak adjacent westward flows that provide anticyclonic circulation north and cyclonic circulation south of the Antarctic Circumpolar Current. This image mostly follows from geostrophic estimates from hydrography using a bottom level of no motion for the eastward flow regime and typically yield transports near 170 Sv. Net eastward transport for this region of about 145 Sv results from subtracting those westward flows. This estimate is compatible with the canonical 134 Sv through Drake Passage with augmentation from Indonesian Throughflow (around 10 Sv).

A new image is developed from World Ocean Circulation Hydrographic Program sections I8S and I9S. These provide two quasi-meridional crossings of the South Australian Basin and the Australian–Antarctic Basin, with full hydrography and two independent direct-velocity measurements (shipboard and lowered acoustic Doppler current profilers). These velocity measurements indicate that the belt of eastward flow is much stronger, 271 ± 49 Sv, than previously estimated because of the presence of eastward barotropic flow. Substantial recirculations exist adjacent to the Antarctic Circumpolar Current: to the north a 38 ± 30 Sv anticyclonic gyre and to the south a 76 ± 26 Sv cyclonic gyre. The net flow between Australia and Antarctica is estimated as 157 ± 58 Sv, which falls within the expected net transport of 145 Sv.

The 38 Sv anticyclonic gyre in the South Australian Basin involves the westward Flinders Current along southern Australia and a substantial 33 Sv Subantarctic Zone recirculation to its south. The cyclonic gyre in the Australian–Antarctic Basin has a substantial 76 Sv westward flow over the continental slope of Antarctica, and 48 ±6 Sv northward-flowing western boundary current along the Kerguelen Plateau near 57ºS. The cyclonic gyre only partially closes within the Australian–Antarctic Basin. It is estimated that 45 Sv bridges westward to the Weddell Gyre through the southern Princess Elizabeth Trough and returns through the northern Princess Elizabeth Trough and the Fawn Trough – where a substantial eastward 38 Sv current is hypothesized. There is evidence that the cyclonic gyre also projects eastward past the Balleny Islands to the Ross Gyre in the South Pacific.

The western boundary current along Kerguelen Plateau collides with the Antarctic Circumpolar Current that enters the Australian–Antarctic Basin through the Kerguelen–St. Paul Island Passage, forming an energetic Crozet–Kerguelen Confluence. Strongest filaments in the meandering Crozet-Kerguelen Confluence reach 100 Sv. Dense water in the western boundary current intrudes beneath the densest water of the Antarctic Circumpolar Current; they intensely mix diapycnally to produce a high potential vorticity signal that extends eastward along the southern flank of the Southeast Indian Ridge. Dense water penetrates through the Ridge into the South Australian Basin. Two escape pathways are indicated, the Australian–Antarctic Discordance Zone near 125°E and the Geelvinck Fracture Zone near 85°E. Ultimately, the bottom water delivered to the South Australian Basin passes north to the Perth Basin west of Australia and east to the Tasman Basin.

Abstract 1
1. Introduction 4
2. Data 7
3. Qualitative description of regional circulation elements and water masses 10
3.1. The Western Boundary Current 12
3.2. Sources for the Western Boundary Current 13
3.3. Antarctic Circumpolar Current west of the Australian–Antarctic Basin 15
3.4. Conditions west of and in the Fawn Trough 17
3.5. Conditions west of and in the Kerguelen–St. Paul Island Passage 18
3.6. Antarctic Circumpolar Current at I8S 20
3.7. The Crozet–Kerguelen Confluence 21
3.7.1. Waters colder than 0.7ºC 22
3.7.2. Waters warmer than 0.7ºC 23
3.7.3. The front associated with the Crozet–Kerguelen Confluence 24
3.7.4. Potential vorticity structure of the Crozet–Kerguelen Confluence 25
3.8. Antarctic Circumpolar Current at I9S 26
3.9. Leakage of cold water through the Australian–Antarctic Discordance 27
4. Combining the geostrophic shear with a velocity reference. 29
4.1. ADCP referencing of geostrophic shear 29
4.2. SADCP-referenced transport adjustment 31
4.3. Final transport adjustments 32
4.3.1. Transport between I9S and Australia 33
4.3.2. Transport south of I8S in the southern Princess Elizabeth Trough 35
4.3.3. Transport south of I9S over the continental slope off the Adélie Coast. 35
4.3.4. The final SADCP bias adjustment. 36
4.4. Discussion of the quality of the transport estimates 37
4.4.1. The remaining errors of SADCP referencing and its effect on transport estimates 37
4.4.2. How strong is the Antarctic Slope Current? 38
4.4.3. Summary of estimated section transports, implied convergence, and error. 40
5. Quantification the strength and structure of the regional circulation 40
5.1 The large-scale circulation in the southeastern Indian Ocean 41
5.2 The dominant current elements 45
5.2.1. Flow through Kerguelen–St. Paul Island Passage 45
5.2.2. Flow along and across the Southeast Indian Ridge 48
5.2.3. Westward recirculation south of Australia 50
5.2.4. The collision of the western boundary and Fawn Trough currents east of Kerguelen Plateau 51
5.2.5. The Crozet–Kerguelen Confluence meander field 53
5.2.6. The connection between the cyclonic gyres of the Weddell–Enderby and Australian–Antarctic Basins 55
5.2.7. The zonal overturning and the eastward closure of the cyclonic gyre 57
5.2.8. The connection between the cyclonic gyre of the Australian–Antarctic Basin and the Ross Gyre 60
5.3. The flow of bottom water from the Australian–Antarctic Basin to the South Australian Basin 61
5.3.1. Hypothesized northward dense water flow through the Geelvinck Fracture Zone 61
5.3.2. Escape of dense water out of the cyclonic gyre in the Australian–Antarctic Basin 63
6. Conclusions 65
Acknowledgments 67
References 67

1. Introduction

The Indian Ocean has no northern source of deep and bottom water. Deep water enters from the south and subsequently warms, upwells, and ultimately returns southward within intermediate and thermocline depths (Schmitz, 1995; 1996). Estimates of northward deep-water transports below ~2000 m range from 5 to 25 Sv (1 Sv ≡ $10^6 m^2 s^{-1}$) (Toole & Warren, 1993; Robbins & Toole, 1997; Macdonald, 1998; Sloyan & Rintoul, 2001b; Ganachaud, 2003). Three deep mid-latitude basins, Madagascar, Mid-Indian Ocean, and Wharton Basins[1] (Fig. 1) receive deep and bottom water. This deep northward flow is constrained by a complicated set of ridges and fracture zones. Here we focus on the circulation in the southeast Indian Ocean within the Antarctic–Australian Basin where cold deep and bottom water transits from high latitudes near Antarctic to subtropical latitudes by crossing under the deep-reaching Antarctic Circumpolar Current.

In the southeast Indian Ocean, cold deep water negotiates two major basin sequences from the Australian–Antarctic to the Mid-Indian Ocean Basin: 1) Australian–Antarctic to South Australian to Perth to Wharton to Mid-Indian Ocean and 2) Australian–Antarctic to South Australian to Mid-Indian Ocean. We briefly review these pathways

The Australian–Antarctic Basin supplies deep water to the South Australian Basin. The Australian–Antarctic Discordance Zone, depths near 4000 m, was early identified as a pathway for northward bottom-water flow across the Southeast Indian Ridge (Wyrtki, 1971; Rodman & Gordon, 1982). Bottom waters south of the saddle are typically < 0.0°C[2], while immediately north of the saddle they are distinctly warmer, ~ 0.4°C (Fig. 2). The Southeast Indian Ridge crest rises east-to-west from the Discordance and outcrops at the St Paul and Amsterdam Islands; northward flow of deep and bottom waters from the Australian–Antarctic Basin to the South Australian Basin are therefore progressively blocked east-to-west. The progressive rise is interrupted by the Geelvinck Fracture Zone near 85°E, sill near 3400 m (Smith & Sandwell, 1997). Here we suggest that the Geelvinck Fracture Zone enables deep-water communication between the Crozet, Australian–Antarctic and South Australian Basins at temperatures warmer than 0.6–0.7°C, a hitherto not-recognized pathway.

The South Australian Basin exchanges deep cold water with both the Perth Basin to its the north and the Tasman Basin to its east. Geostrophic estimates indicate that the South Australian Basin provides about 5–6 Sv of deep water to the Perth Basin through the gap between Broken Ridge and

[1] We use names from GEBCO (2005). Gazetteer of Undersea Feature Names - December 2005. *http://www.ngdc.noaa.gov/mgg/gebco/*). IHO-IOC..

[2] All temperatures in this paper are potential temperatures referenced to zero pressure and will be referred to simple as temperatures.

the Naturaliste Plateau (Warren, 1981; Toole & Warren, 1993; Talley & Baringer, 1997), while current-meter based estimates yield 3.7 Sv through the gap for temperatures colder than 1.4°C (B.M. Sloyan, personal communication, material discussed in Sloyan, 2006). From the Perth Basin, where coldest waters are typically 0.6°C, deep water flows northward into the Wharton Basin where coldest waters are slightly warmer near 0.6–0.7°C. The South Australian Basin exchange of cold deep water with the Tasman Basin is limited to warmer than ~0.7°C by the ~ 4150 m sill between the Tasman Rise and the Southeast Indian Ridge (Smith & Sandwell, 1997).

The Mid-Indian Basin, with coldest waters typically 0.8–0.9°C, receives cold deep and bottom water from the Wharton Basin via westward flow through zonal fractures in the Ninety East Ridge with estimated amplitude of 2 Sv (Warren & Johnson, 2002). The South Australian Basin also supplies deep water directly to the Mid-Indian Ocean Basin over the saddle between the Broken and Southeast Indian Ridges (Reid, 2003). The controlling depth of that saddle is near 3600 m (Smith & Sandwell, 1997). Temperatures just southeast of the saddle at sill depths are near 0.94°C, comparable with temperatures in westward flow through the 28°S fracture in the Ninety East Ridge (Talley & Baringer, 1997).

The Australian–Antarctic Basin, the southernmost Indian Ocean Basin and the focus of this paper, has two major sources of deep water. The eastward-flowing Antarctic Circumpolar Current delivers relatively warm deep water from the Crozet Basin. The Kerguelen Plateau, the Southeast Indian Ridge and the sill between them block a portion of deep Antarctic Circumpolar Current water and limit eastward transport north of Kerguelen Plateau to temperatures warmer than 0.7°C (Park, Gamberoni & Charriaud, 1991; 1993). Additional deep-water input arrives in a western boundary current along the Kerguelen Plateau which brings dense water as cold as -0.4°C north from the margins of Antarctica (Speer & Forbes, 1994). Contributions to this dense water derive from as far east as the Adélie Coast, and also from the west as the southern Weddell–Enderby Basin (Donohue, Hufford & McCartney, 1999; Heywood, Sparrow, Brown & Dickson, 1999)

A first estimate of the deep boundary current transport off the southern Kerguelen Plateau by Speer and Forbes indicated a modest amplitude of 6 Sv net transport for a 460 km wide hydrographic section (below 2500 m, the net resulting from a 10 Sv western boundary current minus a 4 Sv offshore recirculation). Direct-velocity estimates (Donohue et al., 1999) indicated a much stronger current with large transports of deep and bottom water (<1°C): 28 ± 17 Sv using hydrography referenced with shipboard acoustic Doppler current profile data, and 49 ± 9 Sv using lowered acoustic Doppler current profile data. These estimates exceed the estimated 5 Sv of deep and bottom water flowing northward into the mid-latitude Indian Ocean indicating that the western boundary current transport is part of a cyclonic gyre within the Australian–Antarctic Basin; the net transport between the northward-flowing western boundary current and the southward recirculation to its

east leaves a small residue that passes across the Southeast Indian Ridge to the South Australian Basin (Donohue et al., 1999).

Additional evidence for a strong cyclonic gyre is found in deep property maps (Orsi, Johnson & Bullister, 1999). Furthermore, analysis of deep-sea sediments and hydrography indicated strong bottom currents along the northern flank of the Kerguelen Plateau, the deep western boundary current, and along the southern flank of the Southeast Indian Ridge, the eastward flowing limb of cyclonic circulation (Kennett & Watkins, 1976; Kolla, Sullivan, Streeter & Langseth, 1976; Houtz, Hayes & Markl, 1977; Kolla, Henderson, Sullivan & Biscaye, 1978; Dezileau, Bareille, Reyss & Lemoine, 2000). The recent full Indian Ocean circulation estimate of Reid (2003), however, does not include a deep Australian–Antarctic gyre component; instead broad weak northward deep-water flow (~ 6 Sv) converges and traverses the Australian–Antarctic Discordance Zone.

The existence of a cyclonic gyre also follows from consideration of the zonal flow. The eastward turning of the separated western boundary current substantially augments the total eastward flow of the Antarctic Circumpolar Current. This augmented eastward transport requires compensatory westward flow in the south, in order for the net eastward flow between Australia and Antarctica to be within the constraints of measured circumpolar flow. Limited direct-velocity measurements have revealed that westward flow along the Antarctic continental slope (Heywood et al., 1999; Bindoff, Rosenberg & Warner, 2000). Together the various measurements indicate a strong cyclonic gyre, a major element of the world ocean general circulation not previously recognized.

In this paper we extend our preliminary work on the western boundary current off the southern Kerguelen Plateau (Donohue et al., 1999). World Ocean Circulation Hydrographic Program sections I8S and I9S provide two quasi-meridional crossings of the South Australian and the Australian–Antarctic Basins. Full water-column conductivity and temperature profiles, silicate measurements, and two independent direct-velocity measurements (shipboard and lowered acoustic Doppler current profilers) are used to describe the deep-water circulation, quantify the strength of the deep cyclonic gyre within the Australian–Antarctic Basin, and examine its relation to the Antarctic Circumpolar Current. Additional World Ocean Circulation Hydrographic Program sections and historical hydrography are utilized to determine the pathways of deep and bottom waters from the Australian–Antarctic Basin into the South Australian Basin and to further define the structure of the cyclonic gyre.

Circulation patterns developed in this study are shown in Fig. 3. These patterns reflect an attempt to provide a comprehensive basin-wide circulation scheme, made quantitative through the transport constraints developed here from I8S and I9S. We note that this region of the Indian Ocean remains data sparse, particularly near Kerguelen Plateau, and that there have been few attempts to describe the regional circulation.

In the southwest Australian–Antarctic Basin, a western boundary current flows northward flow along the eastern side of the Kerguelen Plateau. This western boundary current originates from the northward extension of westward flow along the Antarctic continental slope (blue contours) augmented by eastward flow through the Princess Elizabeth Trough (purple contours). Near 56°S the western boundary current is further augmented by eastward flow through the Fawn Trough (green contours). The Crozet–Kerguelen Confluence forms where the boundary current encounters the portion of the Antarctic Circumpolar Current that enters the Basin north of Kerguelen Plateau. Eastward flow from the Crozet Basin, a combination of Antarctic Circumpolar Current waters from Drake Passage and warmer waters from the South Atlantic and the Agulhus Return Current, passes north of Kerguelen Plateau into the South Australian and Australian–Antarctic Basins (red contours). The Confluence is a meandering front extending eastward from the western boundary current's separation point. Along the Confluence dense waters from the western boundary current intrude beneath the lighter waters to the north: a folding-under process not represented in the depth-integral field. The Confluence extends eastward along the southern flank of the Southeast Indian Ridge and thus delivers dense waters to the area immediately south of the Australian–Antarctic Discordance. The pathways inferred for the dense water flow are show in black, beneath the colored contours of depth-integral flow.

The eastward Antarctic Circumpolar Current flows north of Kerguelen, enters the Australian–Antarctic Basin, merges with eastward flow from the western boundary current and progressively crosses the Southeast Indian Ridge into the South Australian Basin. The western boundary current off Kerguelen Plateau and the Crozet–Kerguelen Confluence form the western and northern limbs of a strong cyclonic gyre in the Australian–Antarctic Basin. The cyclonic gyre does not, however, appear to completely close within the Australian–Antarctic Basin. It clearly extends westward linking to the cyclonic Weddell Gyre and may extend eastward into the South Pacific.

2. Data

From 1 December 1994 to 19 January 1995 aboard the R/V Knorr, as part of the World Ocean Circulation Experiment Hydrographic Program (WHP), a series of full-depth closely spaced hydrographic casts were occupied across the South Australian and Australian–Antarctic Basins (Fig. 1); these sections are known as I8S and I9S in the WHP dataset. Both sections were terminated in the south in fringe sea-ice half way up the Antarctic continental slope. Station spacing for the full-depth hydrographic casts was nominally 55 km, with closer spacing near topographic features and Antarctic Circumpolar Current fronts, and extended to 65 km within the Australian–Antarctic Basin along I9S. Hydrographic casts performed with a 36-bottle rosette/CTD to within about 10 m of the bottom yielded full water-column conductivity and temperature profiles as well as water samples for salinity, oxygen, and a suite of nutrients at all stations. On four stations, 31, 32, 48, and 49, a 24-bottle ro-

sette/CTD was used. For sections I8S and I9S we show (panels a and b, respectively) temperature (Fig. 4), salinity (Fig. 5), silicate (Fig. 6), CFC-11 (Fig. 7), potential vorticity (Fig. 8), and neutral density (Fig. 9). Potential vorticity is calculated as fN^2/g where f is the Coriolis parameter, N^2 is the squared Brunt-Väisälä frequency and g is the acceleration due to gravity. Neutral density γ^n is calculated using the methodology described by Jackett and McDougall (1997).

Two independent acoustic Doppler current profiling systems measured ocean velocity. A lowered ADCP (LADCP) mounted on the hydrographic frame provided full depth profiles of horizontal currents at all hydrographic stations using the 36-bottle rosette while a shipboard ADCP (SADCP) continuously (on station and underway between stations) monitored upper-ocean currents (Fig. 10).

Details regarding the LADCP instrument and data processing have been given by Hacker et al. (1996) and Fischer et al. (1993). Two stations, 6 and 32, have incomplete LADCP records because the instrument stopped recording on the upcast, and the LADCP processing requires full down- and up-cast profiles. Four stations, 31, 33, 48 and 49, made with a heavy weather small rosette package did not include LADCP sampling. Depth-averaged LADCP instrument error has been estimated as 1.0 cm s^{-1} by Hacker et al. (1996). The uncertainty in velocity at any given depth is larger and harder to quantify. Waters at high latitudes tend to have good deep scattering amplitudes, minimizing the depth-dependent part of the velocity error.

The SADCP measurements were made with a hull-mounted 153 kHz sonar (RD Instruments model VM-150, "narrowband"), with position fixes provided by military P/Y-code GPS receivers, and with the gyrocompass errors corrected in postprocessing using heading measurements by an Ashtech 3DF GPS attitude sensor (King & Cooper, 1993). Current was sampled at 8 m intervals in the vertical, typically to as deep as 300 m in the subtropics and 400 m in high latitudes. SADCP data is not available for the last 180 km of I9S near the coast of Australia. Standard water track calibration methods (Joyce, 1989; Pollard & Read, 1989) provided a velocity scale factor and constant angular offset between the transducer and the Ashtech antenna array. Heading accuracy is 0.1º or better, leading to uncertainty of 1 cm s^{-1} in the cross-track velocity component. This bias, while of small speed, can accumulate a large cross-track transport for long sections like the I8S and I9S sections. Because the I8S and I9S sections were steamed in opposite directions, respectively north to south and south to north, the bias error is oppositely signed for the two sections. This enables us to place limits on the bias by placing tolerance limits on the estimated transport convergence between the sections. Ultimately, this bias contributes the greatest uncertainty to quantitative circulation calculation, Fig. 3.

The barotropic tide is removed from the SADCP and LADCP measurements using the tidal prediction from the TPXO.3 TOPEX/Poseidon global tide model (Egbert, Bennett & Foreman, 1994; Egbert, 1997). The amplitude of the barotropic tide is generally less than 1 cm s^{-1} except over the Kerguelen Plateau where the amplitude reaches 5 cm s^{-1} (Fig. 11). The resulting LADCP velocity sections are

dominated by columnar unidirectional flows with frequent lateral flow reversals. These reversals align with small-scale isopycnal slope reversals and therefore velocity shear reversals. There is a strong consistency between the measured and geostrophic velocity fields.

High-quality on-station SADCP measurements provide additional information about LADCP instrument performance. The difference between on-station SADCP and LADCP cross-track velocities averaged over the same depth range, typically 75 to 300 m depth, for stations deeper than 500 m has a small mean of 0.79 (-0.16) cm s^{-1} and 2.2 (2.1) cm s^{-1} standard deviation for I8S (I9S). Difference between along-track velocities also has a small mean of -0.01 (-0.18) cm s^{-1} with 3.5 (3.6) cm s^{-1} standard deviation

Three additional WHP sections (locations on Fig. 1) are used in more limited fashion in this study: one of the multiple repeats of the SR3 section (December 1994 to January 1995, contemporaneous with I8S and I9S), S5 (November to December 1994, nearly contemporaneous with I8S and I9S), and P11A (April to May 1993, ~ 20 months before I8S and I9S). SR3 stations form a section from Tasmania to Antarctica crossing the central South Australian Basin and eastern Australian–Antarctic Basin. The reader is referred to Rintoul and Bullister (1999), Rintoul and Sokolov (2001) and Yaremchuk et al. (2001) for analyses of SR3 sections. S5 meridionally spans the South Australian Basin at nominal longitudes of 120ºE and 132ºE with additional sampling along 48ºS between the two meridional sections. This zonal segment lies just north of the deepest sills of the Australian–Antarctic Discordance. Schodlok and Tomczak (1997b) and Schodlok et al. (1997) provide analyses of the S5 section. P11A is mostly in the Tasman Basin, but crosses the southeastern Australian–Antarctic Basin; there is yet no published treatment of that section.

In order to put the WHP observations in a regional context, we utilize the hydrographic atlas created by Gouretski and Jancke (1998), an update from Olbers et al. (1992). This global climatology provides temperature and salinity on a 1º by 1º grid. This climatology has several advantageous features. First, the vertical resolution is superior to the World Ocean climatology produced by the National Ocean Data Center (NODC) Ocean Climate Laboratory (Levitus & Boyer, 1994; NODC, 1998) and therefore allows the examination of deep water masses. Second, the climatology is created from the NODC data set and augmented with WOCE and WOCE-era data. Third, the optimal interpolation is performed on neutral surfaces (Jackett & McDougall, 1997) rather than depth or pressure surfaces and therefore avoids the production of false water masses (Lozier, McCartney & Owens, 1994; Lozier, Owens & Curry, 1995). Here will use the atlas distributions of dynamic height and deep planetary potential vorticity. Unfortunately, the atlas is not without its drawbacks. Mapped bottom temperatures were unsatisfactory because we were limited to the value at the deepest standard level reported within the grid, which is not strictly the bottom temperature due to the vertical grid resolution. Instead we chose to show mapped bottom temperatures from the preliminary ver-

sion Indian Ocean HydroBase provided by R. Curry, an extension to this ocean of the database and tools described by Lozier et al. (1994; 1995); after completion of our project, this was subsequently published (Kobayashi & Suga, 2006).

Beyond that of the WHP section work of the 1990s, the bulk of the hydrographic regional coverage is from the USNS Eltanin in the 1960's and early 1970's; that data fades in concentration west of 85°E because of the termination of the Eltanin program in 1972. To address specific local issues we extract various Eltanin and other ship stations from the NODC World Ocean Database (NODC, 2000), including important sections across the Kerguelen–St. Paul Island Passage (location MD91 on Fig. 1) discussed by Park et al. (1991; 1993).

Sea level anomaly data are provided by the CLS Space Oceanography Division. Here we will use a high-resolution, 1/3º Mercator grid, map of merged (ERS-1, ERS-2, and Topex/Poseiden) sea level anomaly (Le Traon & Dibarboure, 1999; Ducet, Le Traon & Reverdin, 2000) to explore the nature of an eddy/ meander structure encountered on I9S, and to highlight the intensity of variability immediately east of Kerguelen Plateau.

3. Qualitative description of regional circulation elements and water masses

In the following discussion of circulation patterns in Antarctic–Australian Basin refer to our regional circulation schematic (Fig. 3) and the dynamic-height field from climatology (Fig. 2).

We begin our discussion by highlighting two important points. First, the belt of eastward shear and flow that we refer to as the "Antarctic Circumpolar Current" contains significant contributions from the regional gyres in addition to circumpolar flow. Second, the upper ocean dynamic height contours can be misleading because they don't include a barotropic component.

The Gouretski and Jancke (1998) atlas provides a regional context for the WHP sections and represents a smoothed time-mean climatology. We proxy the portion of Antarctic Circumpolar Current that passes north of Kerguelen Plateau using dynamic height values at 100 m referenced to 1000 m (Fig. 2). Using I8S and I9S (dynamic height distribution included on Figs. 4a&b) as a guide along with the above referenced frontal studies, we use the nominal range 0.6–1.0 dyn m to represents the eastward flow of the Antarctic Circumpolar Current through the Kerguelen–St. Paul Island Passage. The 0.6 dyn m contour (interrupted at the northern edge of the Plateau in the gridded climatology) is a reasonable proxy for the Polar Front, using its traditional marker of the northern limit of the Antarctic Surface Water temperature minimum being less than 2°C. The higher valued contours, 1.1 and 1.2 dyn m, are associated with the Subtropical Front, with their northward turn indicating the eastern subtropical gyre recirculation. The 0.4 and 0.5 dyn m contours are discontinuous across Kerguelen Plateau, but with the lack of deep stations around Fawn Trough their continuity there is possible: We later describe a Fawn Trough Current bringing Weddell–Enderby and Crozet Basins' waters across the Plateau to the Antarctic–Australian Basin. The 0.3 dyn m contour passes

eastward through the Princess Elizabeth Trough, and loops north, which we will associate with a source flow to the western boundary current.

As will be shown later, the barotropic flow components are substantial in the Australian–Antarctic Basin. For the Passage flow and its projection across the Antarctic–Australian Basin, the barotropic flows significantly increase transports because bottom velocities are in the same direction as the shear, although the dynamic height contours still capture the sign and pathways of the flow. For the western boundary current regime and the southern parts of the Basin, the barotropic components overwhelm the patterns of upper-ocean dynamic height for values less than about 0.6 dyn m, such that dynamic height does not reveal pathways or even flow direction. Thus in Fig. 2 there is no particular indication of western boundary current flow, and no suggestion of the westward flow in the southern Australian–Antarctic Basin that we show in Fig. 3. These elements represent surface referenced currents, often with surface velocities oppositely directed from the sign of the shear. [3]

Overall the Antarctic Circumpolar Current (0.6–1.0 dyn m) follows the large-scale orientation of the Southeast Indian Ridge, trending somewhat south of east as the Current traverses from the Kerguelen–St. Paul Island Passage to south of Tasmania, with a net southward shift of about 800 km. One by one the contours cross the crest of the Ridge. The northern parts of the Antarctic Circumpolar Current, contours 1.0 and 0.9 dyn m, gradually cross the Ridge crest west of the Discordance Zone. The 0.8 dyn m contour reaches the crest near 100°E, but doesn't clearly get north of the crest until about 140°E. The rest of the Antarctic Circumpolar Current passes by the broad saddle of the Discordance Zone and crosses the Ridge east of 140°E; a recent study documents that crossover (Sokolov & Rintoul, 2002). The climatology of the 0.6–1.0 dyn m contours reveals surprisingly small influence of the broad deep saddle in the Ridge centered at the Australian–Antarctic Discordance Zone; there is no evidence in upper-ocean dynamic height for the Antarctic Circumpolar Current preferentially crossing from the poleward to equatorward side of the Southeast Indian Ridge at the Discordance Zone.

The near-bottom temperature fields and the upper-ocean dynamic height in Fig. 2 reveals the interplay of the Passage Current and the cold dense waters brought northward in the boundary current regime to the east of Kerguelen Plateau. The sill in Passage limits temperatures there to no colder than around 0.7°C. The distribution shows that waters colder than this are found all along the southern flank of the Southeast Indian Ridge, beneath dynamic height contours as high as 0.8 dyn

[3] Most of the shear profiles in our domain are monotonic. Bottom and surface levels of no motion are normal usages for geostrophic calculations, leading to currents in the same/opposite direction as the sign of the geostrophic shear. More generally we will refer to bottom- and surface- referenced flows for situations where, rather than applying a zero speed at the bottom/surface, a velocity with the same/opposite sign as the geostrophic shear is applied at the bottom/surface. For the typical monotonic shear these lead to full water-column unidirectional flow in the same/opposite direction as the sign of the shear, with speed amplitudes larger than those resulting from bottom/ surface levels of no motion.

m, these originate in the northward flow of the deep western boundary current water, and intrude beneath the Passage Current. The distribution shows that the northward passage of cold water through the Australian–Antarctic Discordance is essentially orthogonal to the overlying eastward flow.

A first look at our sections' temperature distributions (Fig. 4) shows the relationship between the Antarctic Circumpolar Current and the regional gyres. The Passage Current flows obliquely along the southeast Indian Ridge, which truncates deep isotherms. Along I8S, the Southeast Indian Ridge crest interrupts isotherms colder than 1.3ºC, while to the east at I9S, 0.8ºC is the coldest isotherm continuous across the crest suggesting that waters between 1.3º and 0.8ºC may pass over the Ridge crest between the two sections (Figs. 4a and 4b); this is consistent with the dynamic height inference that some of the Antarctic Circumpolar Current crosses the Ridge before reaching the Discordance. Most of the Current has crossed the Ridge by section I9S: the Subantarctic Front is north of the crest, while the Polar Front and the 0.6 dynamic height contour is essentially at the crest. This position is a more northward position compared to climatology (Fig. 2) which reflects the particular synoptic structure of I9S. In the South Australian Basin, along both sections, colder bottom water reappears where depths exceed 4000 m, about 0.64°C on I8S and 0.44°C on I9S. These waters, ultimately from the western boundary current, have found their way to that Basin predominately through the Discordance east of I9S.

We now elaborate on these circulation elements using the full hydrographic dataset.

3.1. The Western Boundary Current

The sharp rise of isotherms and isoneutral density surfaces towards the southern Kerguelen Plateau along I8S (Figs. 4a and 9a, stations 64 through 68) mark the western boundary current. ADCP velocities for I8S indicate that surface flow is northwestward along the eastern flank of the southern Kerguelen Plateau (Figs. 10 left and 11a). This confirms the early inference of such surface flow from iceberg drifts (Tchernia, 1974; Tchernia & Jeannin, 1980). The rise in isopycnals (Fig. 9a) extends throughout the water column indicating monotonic geostrophic shear to the southeast. The boundary current flows in the opposite direction of that shear: the LADCP data show that velocities are nearly in the same direction at all depths (Fig. 11a), yielding a substantial northwestward depth-averaged flow (Fig. 10 right). Therefore, there is not a level of no motion within the deep western boundary current and even a surface level of no motion will underestimate the western boundary current transport. Direct-velocity measurements are necessary to reference geostrophic velocities in the current.

Speer and Forbes' (1994) small estimate of a deep western boundary current transport of 6 Sv resulted from their use of a favored 2500 m level of no motion – which generated a southward flowing 12 Sv transport above that level, and a net water-column transport of southward 6 Sv. They in-

dicated doubt that the level could be much shallower than that, nor that the deep water transport could be larger than 10 Sv. They did tabulate transports for shallower levels of no motion to illustrate their dependency on reference level, while advocating the deep reference level. A surface level of no motion resulted in a water-column transport of 54 Sv – which is comparable to the absolute transports later reported in Donohue et al. (1999) and revisited below.

3.2. Sources for the Western Boundary Current

The western boundary current off southern Kerguelen Plateau derives from two main sources (Fig. 3). These sources have been identified through a combination of water mass characteristics and flow estimation (Speer & Forbes, 1994; Frew, Heywood & Dennis, 1995; Donohue et al., 1999; Heywood et al., 1999). Here is what has emerged from the analysis. Westward flow along the Antarctic continental slope, which we will call the Antarctic Slope Current rather than the Antarctic Slope Front, has origins in deep water formed in the Ross Sea and along the Adélie coast (Gordon & Tchernia, 1972; Rintoul, 1998; Whitworth III, Orsi, Kim & Nowlin Jr, 1998; Bindoff et al., 2000), but has transports much larger than estimated deep-water formation. This Current bifurcates in the southwestern Australian–Antarctic Basin to supply both a continued westward flow through the southern Princess Elizabeth Trough into the Weddell–Enderby Basin and a northward turning branch into the western boundary current off the Kerguelen Plateau (Speer & Forbes, 1994; Donohue et al., 1999; Heywood et al., 1999). Additional input to the western boundary current comes from eastward flow of Weddell–Enderby Basin water, which passes through the northern Princess Elizabeth Trough and then turns northwest into the western boundary current (Donohue et al., 1999; Heywood et al., 1999). Here is some of the evidence for these sources; the absolute transports will be estimated in section 4.

Within the deep western boundary current, silicate reveals both a vertical layering and an onshore–offshore transition indicating and differentiating the two cold water-mass sources mentioned above; this is discussed in detail by Donohue et al. (1999). Due to the significant silicate flux from opaline sediments (Edmond, Jacobs, Gordon, Mantyla & Weiss, 1979), silicate is not a conservative tracer and we use it only qualitatively. In deep western boundary current core stations, 66–67, the deep waters are consistently lower in silicate on γ^n surfaces than further offshore (Figs. 6a and 12). This lower silicate in the western boundary current is attributed to the waters over the Antarctic continental slope. This is a general characteristic of deep waters near Antarctic, stemming from the plumes of dense, nutrient-depleted deep water formed near the shelves (e.g., Carmack, 1973; Bindoff et al., 2000). The interior waters of the Antarctic–Australian and Weddell–Enderby Basins have silicate values that are too high (Mantyla & Reid, 1995; Reid, 2003) to be a plausible source for the lower silicate deep waters of the western boundary current. Because the measured flows over

the Antarctic continental slope are generally westward, the continental slope east of I8S is implicated as the immediate origin for the low silicate water in the western boundary current.

We sampled the westward flow of the Antarctic Slope Current along the southern part of I9S. A water-mass transition from low silicate water onshore (south) to higher concentrations offshore (north) occurs near station 91 (Figs. 6b and 12). Lowered ADCP velocities (Fig. 11b) indicate westward flow for stations 85–91 for waters colder than 1°C ($\gamma^n \geq 28.15$). Note that isotherms and isopycnals rise southward across this water-mass transition and are generally parallel with depth. So while the shear is unidirectional, the transition from eastward to westward flow indicates a shift of level of no motion from the bottom to the surface. While the silicate changes across this transition could be taken simply as indicating the effects of mixing and the accumulation of silicate from underlying sediments along a long and slow circuitous pathway around the western Antarctic–Australian Basin, there also is a contribution from the changing source characteristics (Whitworth, 2002).

Part of the Antarctic Slope Current turns north to feed the deep western boundary current. Evidence indicates this flow is the sole source for deep-water temperatures less than about 0.1ºC ($\gamma^n \geq 28.31$) in that current. The rest of the westward flow passes from the Antarctic–Australian Basin to the Weddell–Enderby Basin along the continental slope in the southern Princess Elizabeth Trough, where low silicate concentration is seen in the temperature range -0.3ºC to -0.4ºC along I9S (γ^n range 28.32–28.34, Fig. 12), and the flow has been measured as westward. Waters from the Weddell–Enderby Basins are not a plausible source for the cold deep western boundary current because water in this temperature range is not found in the eastward flow regime in the northern Princess Elizabeth Trough; the coldest waters flowing east are about 0.1ºC (Donohue et al., 1999).

At temperatures warmer than 0.1ºC, besides the contribution from the northward turning branch from the Antarctic Slope Current, input to the deep western boundary current also comes from the Weddell–Enderby Basin. Waters warmer than 0.1ºC ($\gamma^n \leq 28.31$) inshore of the deep western boundary current core, stations 68–72, are similar to those found in the northern Princess Elizabeth Trough and dissimilar to those found along the Adélie coast in the southern part of I9S. South of the Kerguelen Plateau in I8S, isotherms descend well into the Princess Elizabeth Trough (Fig. 4a). The lowered ADCP velocities show eastward flow in the northern Princess Elizabeth Trough that is consistent with a bottom-referenced situation (Fig. 11a). For temperatures greater than 0.1ºC ($\gamma^n \leq 28.31$) eastward flow through the northern Princess Elizabeth Trough converges with the westward flow of deep water along the continental slope as a combined source for the deep western boundary current. The eastward flow branch through the northern Trough contributes higher silicate Weddell–Enderby Basin deep water to the inshore part of deep western boundary current.

The I8S section did not extend all the way south across the Princess Elizabeth Trough because of ice cover. Speer and Forbes (1994) report data from the southern Trough area sampled in 1992

from an icebreaker; conversely to us, they did not have a synoptic section in the northern Trough. Deep water in the southern Trough was as cold as -0.45°C, and shared water-mass characteristics with those we observed in the westward flow regime at the southern end of I9S. Because they used a mid-depth level of no motion, westward deep flow along the Antarctic continental slope appears beneath the level of no motion but eastward flow occurs above the level of no motion, counter to the traditional image of the westward flowing Antarctic Slope Current. Speer and Forbes (1994) assumed that this derived eastward flow in the southern Trough branches northward to contribute to the shallower part of the western boundary current. Heywood et al. (1999) used shipboard ADCP to reference geostrophic velocities in the Princess Elizabeth Trough and found that there is no level of no motion within the Trough. They report a full water-column eastward (westward) flow in the northern (southern) Princess Elizabeth Trough, with the southern Trough situation contradicting the Speer and Forbes (1994) construction from a level of no motion, and re-establishing the westward flowing Antarctic Slope Current. We note that Heywood et al. (1999) also identified the eastward pathway in the northern Trough as a source for the deep western boundary current concurrently noted by Donohue et al. (1999) but additionally found some involvement of waters slightly colder than 0.1°C in that eastward flow, which they attributed to the action of a frontal meander in mid-Trough during their 1993 cruise.

3.3. Antarctic Circumpolar Current west of the Australian–Antarctic Basin

The Antarctic Circumpolar Current brings deep water from west of Kerguelen to the Australian–Antarctic Basin, but must negotiate the topographic complex consisting of the Southeast Indian Ridge, Kerguelen Plateau, the intervening sill between them, and, as just described, the Princess Elizabeth Trough between the Plateau and Antarctica. This subsection describes the Antarctic Circumpolar Current structure in the Crozet and Weddell Enderby Basins west of the topographic complex.

The Antarctic Circumpolar Current alone is associated with at least 3 fronts, Subantarctic, Polar and Southern ACC Front. These fronts mark regions of concentrated flow and transport within the Antarctic Circumpolar Current. To a limited degree it is possible to use established circumpolar frontal definitions that apply to these fronts over the entire Southern Ocean (Orsi, Whitworth III & Nowlin, 1995; Belkin & Gordon, 1996; Pollard, Lucas & Read, 2002). Buoyancy forcing leads to significant transformation following the flow, and a frontal definition at one longitude may become inappropriate at another. Inevitably there are significant departures from the above-defined open-ocean frontal system in several regions, reflecting the interaction of the Antarctic Circumpolar Current with the subtropical gyres to its north and the subpolar domain to its south. The Kerguelen Plateau sector is one such region of complexity; there the difficulties are compounded by the extreme sparseness of hydrographic data, particularly subsurface data.

We will adopt a regional *ad hoc* set of front terminology derived from the study of the area immediately west of Kerguelen Plateau as developed by Sparrow et al. (1996) and Holliday and Read (1998); the former authors' rendition is show here as Fig. 13. South of about 35°S, flow is generally eastward and 5–7 fronts have been identified within this belt; these fronts shift and cluster in a variety of configurations (Park et al., 1993; Read & Pollard, 1993; Holliday & Read, 1998; Park, Charriaud, Craneguy & Kartavtseff, 2001; Pollard & Read, 2001; Park, Leboucher, Pollard & Read, 2002). The overall pattern west of 50ºE has two primary concentrations of eastward transport, one near 40–45°S, associated with Agulhus Return Current, Subtropical Front, and Subantarctic Front, and another near 50–55°S, associated with the Polar Front. The transports and pathways for the southernmost frontal grouping are ill-defined because that region has the poorest station concentration of the whole Southern Ocean.

The northern group includes subtropical waters from the Agulhus Current flowing east within the Agulhus Return Front, and waters from the South Atlantic and Drake Passage flowing east within the Subtropical and Subantarctic Fronts. The distinctness of these origins is progressively lost eastward through buoyancy forcing, which produces the array of Subantarctic Mode Waters that dominates the Subantarctic zone from the central Indian Ocean eastward across the South Pacific to Drake Passage (McCartney, 1977; 1982; Fine, 1993; Park et al., 1993; Fine, Maillet, Sullivan & Willey, 2001). This pattern reminds us that this concentration of eastward flow is tied to exchange between the southern Indian and South Pacific subtropical gyres and the great belt of eastward flow in the Southern Ocean. Eastward flow in the Southern Ocean receives a net contribution of warm waters from the Agulhus Current and from the South Atlantic and in compensation returns Subantarctic Mode Water and Antarctic Intermediate Water to the subtropical gyres. Subantarctic Mode Water is produced by buoyancy forcing along the eastward flow, and Antarctic Intermediate Water is produced remotely in and west of Drake Passage (McCartney, 1977; 1982; Sloyan & Rintoul, 2001a), with perhaps locally a secondary source south of the Subantarctic Front (Park & Gamberoni, 1997).

Classically the Subantarctic Front is described as having the Polar Frontal Zone to its south separated by a significant distance from its southern boundary the Polar Front, yet data from the region west of the Kerguelen complex often show a merger of the Subantarctic and Polar Fronts (e.g. Read & Pollard, 1993). In 1991 Park et al. (1993) crisscrossed the northern transport concentration four times between 51°E and 79°E. The Agulhus Return, Subtropical and Subantarctic Fronts were found compressed together into a < 200 km wide belt of baroclinic transport. It appears that the northern concentration of transport in the Crozet Basin essentially wholly passes through the Kerguelen–St. Paul Island Passage, forming the Passage Current.

How the southern concentration of transports from the western Crozet Basin approaches the Kerguelen Plateau is less clear. In the southwestern Indian Ocean that concentration is linked to the

Polar Front (Read & Pollard, 1993; Sparrow et al., 1996; Park et al., 2001), and it can be identified by the traditional marker of the northern limit of the Antarctic Surface Water temperature minimum being less than 2°C. After the flow system passes ~45°E, that traditional Polar Front indicator trends nearly due east and passes immediately to the north or south of Kerguelen Island. But Park et al (1993) noted that traditionally defined Polar Front was a weak baroclinic feature – only about 5-7 Sv with a bottom level of no motion. It appears that after passing mostly between del Caño Rise and Conrad Rise, ~50°E, the southern concentration of eastward transport trends south of east towards the middle of Kerguelen Plateau, dissociated with the classical definition of the Polar Front. Using the smoothed fields of the Olbers et al. (1992) atlas dataset, and a bottom level of no motion, Sparrow et al. (1996) quantified this southern transport pathway at two longitudes, one near 52°S at 50°E and the other at 60°E near 56°S. They developed a surface temperature definition to map this front, but also noted a corresponding shift in characteristics of the subsurface Antarctic Surface Water temperature minimum and associated the front with the northern limit of the 0°C isotherm of this minimum (rather than the traditional marker of 2ºC. Holliday and Read (1998) revisited the dual Polar Front using underway ship data including XBTs and surface thermosalinograph data. They confirmed both the surface and temperature minimum definitions of the southern of the two fronts. They further noted from 1500 m XBT data a deeper signature of the front as the southern limit of the upper circumpolar deep-water temperature maximum of 2°C.

Orsi et al. (1995) indicate a circumpolar "Southern ACC Front" passing through the northern Princess Elizabeth Trough. We therefore associate that front with our western-originating source flow path for Weddell–Enderby Basin waters contributing to the western boundary current east of Kerguelen Plateau. They indicated that the Southern ACC Front turns sharply northward along the eastern flank of the southern Kerguelen Plateau, which we take as indicating a boundary in the western boundary current regime between the Princess Elizabeth Trough source waters and those of from the northward turning branch from the westward flowing Antarctic Slope Current.

Besides the eastward flow of dense water through the northern Princess Elizabeth Trough, we identify two other dense water pathways from the Crozet and Weddell–Enderby Basins through the topographic complex to the Antarctic–Australian Basin, discussed in the next two subsections.

3.4. Conditions west of and in the Fawn Trough

Holliday and Read (1998) three times encountered the southern Polar Front at or immediately west of the narrows of Fawn Trough on cruises transiting to and from Princess Elizabeth Trough. Without intending anything more than a regional name, we will refer to this as the Fawn Trough Front or Fawn Trough Current, and will later associate with it with significant eastward transport across the Kerguelen Plateau.

Focusing on the Fawn Trough, the bathymetry of the central Kerguelen Plateau is shown in Fig. 14. We extracted the indicated two groups of hydrographic stations from the NODC World Ocean Database (NODC, 2000), and Fig. 15 shows the average temperature profiles for the two groups. The frontal markers indicated by Holiday and Read (1998), Antarctic Surface Water 0°C temperature minimum and 2°C upper deep-water temperature maximum must pass between the two groups. Below the temperature maximum isotherms at the southern group are considerable uplifted compared to the northern group, indicative of deep reaching geostrophic shear at this front. The bathymetric data indicates the Fawn Trough sill depth between 2575 and 2600 m (Smith & Sandwell, 1997). Using 2600 m, the two mean profiles give temperatures of 0.40 and 0.91. We adopt 0.4ºC as the estimate of the coldest waters that potentially could cross the Fawn Trough sill. Another estimate we will later use is the depth of the 1ºC isotherm (close to the γ^n = 28.15 kg m^{-3}) surface we use to divide in two the thick dense water layer of the Australian–Antarctic Basin. The mean profiles place that isotherm at 2500 and 1800 m, indicating that Fawn Trough represents a potentially significant pathway for contributing denser waters from the Weddell–Enderby Basin to the Australian–Antarctic Basin. The NODC database has only a single station (Discovery from 1937) close to the Fawn Trough sill (100 km southwest), in 2730 m water depth, with deepest observation of 0.50ºC at 2460 m, with 1ºC near 1950 m. We take this as confirming the delivery of dense water to the sill by the Fawn Trough Current.

3.5. Conditions west of and in the Kerguelen–St. Paul Island Passage

A sill in the blocks deep eastward flow of the Antarctic Circumpolar Current through the Kerguelen–St. Paul Island Passage (Fig. 16). The sill depth is about 3400–3450 m (Smith & Sandwell, 1997); on Fig. 16 we use a shade break at 3350 m, with the peaks of the rough topography of the sill starting to appear near 80ºE showing this to be a wide and broad sill regime

In the southern Passage the Gallieni Spur extends northeast from Kerguelen Island delimiting the southern part of the sill, while in the northern Passage the Geelvinck Fracture Zone projects northeast penetrating the Southeast Indian Ridge with depths similar to the sill depth (Fig. 16). The sill limits the coldest deep-water temperatures that can flow from the Crozet Basin through the Passage to the Australian–Antarctic Basin, and presumably similarly limits temperatures of flow through the Fracture Zone. We now characterize that coldest water.

A 1991 section (Fig. 17a) 450 km west of the sill from the Suzil Expedition (Park et al., 1993) has a coldest bottom temperature of 0.73ºC at a station with 3620 m depth. Along the section temperatures are in the range 0.86–1.02ºC for most the estimated 3400–3450 m depth range of the Passage sill, with a slightly colder range, 0.77–0.79ºC at that station with the coldest bottom water temperature. As described by Park et al., the section shows all the fronts discerned in the northern Crozet Basin (Fig. 13) compressed into a narrow band over the deepest part of the section, except for the

classical Polar Front marker (2°C temperature minimum), which is in shallow water over the northern flank of the Kerguelen Plateau. The coldest bottom water observation lies beneath the band of strongest eastward baroclinic shear. This is illustrated with the same 100/1000 dynamic height index used in other section plots, showing the band spanning 1.3–0.77 dyn m (with the southern low value poorly resolved by the stations over the topography). The shear reaches the seafloor.

Fig. 18 shows temperature profiles for several stations in the southern part of the Passage (and other stations discussed later). The USNS Eltanin station 1315 (blue symbol) just west of the Gallieni Spur (location on Fig. 16) further defines characteristics at the southern side of the Passage sill: 0.77°C at 35 m above the stations bottom sounding of 3242 m. This is colder by 0.08°C than the coldest waters at the same depth 1991 section station (e.g., station 50 in Fig. 17), suggesting that sometimes the geostrophic flow over the southern part of the sill uplifts isotherms more than observed in the 1991 west of this location. A 200 m uplift of the station 50 profile from the Suzil section would match the 3242 m temperature, and give a 0.73°C temperature at sill depth. A 1987 occupation of nearly the same section had (Park et al., 1991) similar compression of the fronts, with more isotherm uplift in the south giving coldest water reaching 0.711°C (section not shown, but the profiles are on Fig. 18). We conclude that the coldest water brought to the area immediately west of the sill of the Kerguelen–St Paul Island Passage within the Antarctic Circumpolar Current is likely to fall in the temperature range between 0.7–0.8ºC, with no evidence that it is colder than 0.7°C.

Looking west of the Passage to see if those inferences make sense with the deep flow approaching from the west, the concentration of fronts noted by Park et al. (1993) is evident in these deeper areas well west of the Passage (Fig. 17b and 17c). The shear reaches the seafloor in these areas also. Focusing on the stations which match best with the band of concentrated shear in the Passage (dynamic heights from 0.7–1.3 dyn m), and looking in the 3400–3450 m depth range of the Passage sill, we find the temperatures ranges at these two sections are, respectively, 0.87–1.19ºC and 0.58–1.20ºC. The section across the mouth of the Passage is again poorly resolved over the topography, but the two southern stations shows bottom temperatures of 0.62 and 0.65ºC (depths 3310 m and 3125 m. Those are consistent with the westernmost section's waters in that depth range near the southern side of the dynamic height band.

It thus appears that the deep flow of the Antarctic Circumpolar Current in the Crozet Basin (manifested by the deep shear in the western sections and the presumption that is associated with eastward flow) delivers waters just colder that 0.7ºC to the entrance of the Kerguelen–St. Paul Island Passage. West of the sill, all observations available indicate the coldest deep water is slightly above 0.7ºC. We adopt that temperature as the indicator for the cold limit for Crozet Basin waters at the Passage sill. The Passage Current therefore is likely to carry deep water no colder than 0.7ºC. That deep-water temperature is considerably warmer than much of the deep western boundary cur-

rent along the eastern flank of the Kerguelen Plateau, where the 0.7°C isotherm shoals to about 1500 m. and the 3450 m temperature is about -0.2°C (Fig. 4a).

3.6. Antarctic Circumpolar Current at I8S

Along I8S the dynamic height, isotherms and isoneutral surfaces (Figs. 4a and 5a) and the direct-velocity measurements (Figs. 10 and 11a) reveal an eddy-rich flow field. This concentrated variability may be the circulation structure that causes enhanced diapycnal mixing estimated from the CTD finestructure and LADCP profiles (Polzin & Firing, 1997; Sloyan, 2005). Because of the strong eddy action, there is some ambiguity in defining the locations of one of the canonical Southern Ocean fronts. The Subantarctic Front, the poleward boundary of Subantarctic Mode Water, is unambiguously between 42ºS and 45ºS with the poleward edge directly over the Southeast Indian Ridge crest. This is a typical configuration in the Australasian sector east of here (Callahan, 1971; McCartney, 1976). I8S crossed the Polar Front three times at 51.5ºS, 52.0°S and 53ºS, using the classical definition of the 2°C temperature of the Antarctic Surface Water temperature minimum layer. The northern and southern crossings are marked on the I8S property sections. This reflects either a frontal re-crossing of the section due to a meander of the frontal marker, or the presence of a cutoff cyclonic or anticyclonic eddy north or south of the front. Cutoff eddies have been observed in the Australasian sector of the Southern Ocean (e.g. Savchenko, Emery & Vladimirov, 1978), with typical scale 50–100 km.

Cross-track LADCP velocities indicate a general tendency for the near-bottom cross-track velocity to have the same sign as the deep-referenced shear and the near-surface velocity (Fig. 11a). This character of the Antarctic Circumpolar Current system has been reported in the Pacific sector (Donohue, Firing & Chen, 2001), in current-meter measurements just north of the Southeast Indian Ridge at 143°E (Phillips & Rintoul, 2000), and inferred as circumpolar using float data (Gille, 2003).

Along I8S a broad southward rise of isotherms and isopycnals (Figs. 4a and 5a) is seen throughout the water column. While this could be simply identified as the Antarctic Circumpolar Current; it is actually something more than that as indicated by two aspects of the distributions.

First, vertically within the broad band of eastward shear, the deeper waters do not originate by flow through the Kerguelen–St. Paul Island Passage, they instead come from the western boundary current. In the Passage section (Fig. 17a) the shear signature of eastward flow through the Passage is the dynamic height span from about 1.3–0.77 dyn m. Along I8S the highest dynamic height values, in the north, are only about 1.21 dyn m, consistent some northward flow into the subtropical gyre between the sections. The first significant gradient of dynamic height along I8S, at the Subantarctic Front, is due east of the Passage, but the 0.77 dyn m value corresponding to the southern Passage is encountered more than 1000 km farther south near the first Polar Front marker. The compression of fronts in the Passage is clearly gone, and in the Passage Current the Subantarctic

and Polar Fronts have markedly diverged by I8S. Beneath the 1.2–0.77 dyn m span along I8S, waters too cold (< 0.7ºC) to have emerged from the Passage are encountered, first at station 43, the tip of a wedge thickening southward to 1600 m at the Polar Front, where the bottom temperature is -0.27ºC. This layering is not simply the flow from the Passage moving eastward over quiescent bottom water in the Australian–Antarctic Basin, but rather the result of the confluence of two strong currents, the Antarctic Circumpolar Current flow through the Kerguelen–St. Paul Island Passage and the western boundary flow. The former is topographically limited to shallower than 3450 m and warmer than 0.7ºC, while the latter has a vast layer of waters colder than 0.7ºC spanning depths from as shallow as 1250 m to as deep as 4750 m.

Second, laterally within broad band of eastward shear, a depth dependent transition occurs from waters emerging from the Passage in the north to waters originating in the western boundary current in the south. The transition is well north at 0.7ºC (as just described), while in the upper kilometer it is near the Polar Front, where the dynamic height drops from the ~ 0.7–0.8 dyn m values that are consistent with origins in the southern Passage to much lower values, ~ 0.3–0.4 dyn m, far lower than the southern Passage values. This lateral transition also reflects the confluence between the western boundary current and the eastward flow through the Kerguelen–St. Paul Island Passage.

3.7. The Crozet–Kerguelen Confluence

Working northward along the eastern flank of the Kerguelen Plateau from our I8S observations near 58ºS, the western boundary current encounters a succession of four obstacles to continued northwest flow along the flank, two dynamical (current confluences) and two topographical. The western boundary current encounters the eastward Fawn Trough Current above 2600 m near 56ºS, the first of two current confluences There is a substantial ridge, the Chun Spur, projecting southeast from the plateau near 53ºS that appears to topographically steer the merged western boundary and Fawn Trough currents, which then undergo a second confluence, with the strong eastward flow through the silled Kerguelen–St. Paul Island Passage. Below the Passage sill depth near 3450 m the deeper flow of the western boundary current is topographically blocked by the sill and by the Southeast Indian Ridge to the north. A meandering and energetic front is the result of the interplay of topographic steering and the current confluences; we term it the Crozet–Kerguelen Confluence, and note that it is marked by a strong front with coincident substantial concentration of eastward flow across I8S.

In Fig. 3 we represent the Confluence using the synoptic pattern from I8S. Fig. 19a shows altimeter derived sea surface height variance, suggestive of the mesoscale variability of the confluence relative to the synoptic picture from I8S. Based on the eddy variability revealed in I8S and in the altimetry, it is apparent that the broad smooth gradient of dynamic height in the dynamic height climatology (Fig. 2) does not reflect the synoptic reality of a sharper gradient with mesoscale mean-

ders, eddies and position variability. In the climatology this smooth picture is caused as much by data scarcity as by the two dimensional smoothing algorithm.

Work on the distribution of sediments has revealed a minimum in sediment thickness beneath the location of this Confluence, attributed by investigators as due to resuspension caused by strong bottom-water currents (Kennett & Watkins, 1976; Kolla et al., 1976; Houtz et al., 1977; Kolla et al., 1978; Dezileau et al., 2000). We next examine the hydrographic evidence for the deep currents.

3.7.1. Waters colder than 0.7°C

Below 0.7ºC the topographic blocking of the deep western boundary current flow seems complete. There is no evidence for a westward turning boundary current branch bringing cold dense waters into the Kerguelen–St. Paul Island Passage past the Gallieni Spur to potentially counterflow westward to the Crozet Basin (Park et al., 1993). As discussed above bottom temperatures west of the sill are warmer than 0.7°C, and are most plausibly flowing eastward as part of the Passage Current, not westward undercutting it. Waters colder than 0.7ºC coming north in the boundary current penetrate northward to the flank of the Southeast Indian Ridge: along I8S, the northward limit of penetration of 0.7ºC is at station 43, defined by a 100 m thick layer over the 3450 m isobath.

I8S, the Passage sill, and the Ridge form an abyssal cul-de-sac below about 3400 m in the northwest corner of the Australian–Antarctic Basin. The Geelvinck Fracture Zone intersects the Passage sill, and is a potential pathway for deep water escape, and defines the effective depth limit for the cul-de-sac. The Fracture Zone itsself is indicated as having a sill depth near 3350 m (Smith & Sandwell, 1997), probably not significantly different from the Passage sill. There are no stations in or close to the Fracture or atop the sill to the south of its entrance to enable assessment of conditions. Later we discuss the possibility of deep flow through the Geelvinck Fracture Zone.

The colder waters of the western boundary current turn east and intrude beneath the Antarctic Circumpolar Current. This accounts for the presence of cold waters beneath the band of strong eastward shear of the Passage Current, and reflects the first stage of the migration of southern source deep water across the Antarctic Circumpolar Current in this quadrant. Continued northward penetration of this colder deep water is limited until the eastward descent of the crest of the Southeast Indian Ridge towards the Australian–Antarctic Discordance Zone enables cold deep flow into the South Australian Basin.

The waters colder that 0.7ºC that intrude under the eastward flow from the Passage have three origins. As discussed in section 3.2, the western boundary current is initiated at the southern Kerguelen Plateau by northward turning flows from the westward Antarctic Slope Current and the eastward flow through the northern Princess Elizabeth Trough (blue and purple contours in Fig. 3, respectively). The former source includes a wide range of dense water temperatures down to the coldest observed deep water. The latter source is limited to warmer than about 0.1ºC. The subse-

quent confluence of the western boundary current flow with the Fawn Trough Current (green contours in Fig. 4) might involve waters as cold as about 0.4ºC (section 3.4), and later when we estimate transports we will conclude that this is a strong and vigorous confluence.

3.7.2. Waters warmer than 0.7ºC

At these warmer temperatures the confluence of the western boundary current flow with the Antarctic Circumpolar Current creates a pronounced lateral density difference across the confluence front. Isotherms in the Antarctic Circumpolar Current within the Kerguelen–St. Paul Island Passage are considerable deeper than in the western boundary current at I8S and in the waters we associate with the Fawn Trough Current (Fig. 18). If the successive confluences of the western boundary current with the Fawn Trough involved horizontal flow and were columnar in nature, then one would diagnose the origins of the various regimes of the belt of eastward shear in I8S. For example, in Fig. 18 the Passage profiles all have 1ºC between 2750 m and 3500 m, with the isolated USNS Eltanin station west of Gallieni Spur reaching 2500 m, waters from the Fawn Trough Current have that isotherm between 2500 and 1900 m, while data in the southern part of the western boundary current has it between 1000 and 1900 m. Along I8S the 2500 and 1900 m depths of 1ºC then are estimates of the regime boundaries: stations 58 and 50, respectively, for the transitions between the Passage flow, the Fawn Trough Current contribution, and the separated flow from the western boundary current.

It is likely, of course, that the confluences involve non-columnar elements, and the transitions between the waters originating in the individual currents are depth dependent. This clearly happens with the waters colder than 0.7ºC, where the northern tip of its intrusion beneath the Passage Current falls about 350 and 700 km north of the regime boundaries defined in the last paragraph. The confluence does not create purely parallel eastward flows separated by a vertical boundary. Instead the western boundary current waters, denser at a given level than the Fawn Trough Current waters, intrude or fold under the Fawn Trough Current waters to some degree. In turn, the waters of that system, denser at a given level than the waters emerging from the Kerguelen–St. Paul Island Passage, intrude and fold under the Passage Current waters.

The folding under appears to involve vertical descent. This is most obvious for the wedge of water colder than 0.7ºC beneath the Passage waters along the Southeast Indian Ridge. In the above defined regime of eastward flow of Passage waters north of station 50, 0.7ºC is everywhere deeper than 2500 m. In the western boundary current in I8S adjacent to the southern platform of the Kerguelen Plateau, 0.7ºC, are no where deeper than about 1500 m. Offshore of there, where the meanders of the combined flow of the western current and the Fawn Trough Current cross and recross I8S, 0.7ºC is deeper, but no deeper than 2250 m. Thus in the process of confluence and turn-

ing offshore and intruding beneath the Passage Current, waters from the western boundary current descend by about 1000 m.

Clearly there are some interesting dynamics going on in this confluence system. There has been some theorizing about the collision of baroclinic western boundary currents and the eastward turning of the merged currents (Agra & Nof, 1993; Lebedev & Nof, 1996; 1997), mostly applied to the Brazil Malvinas Confluence. With the quantification of our current system developed later in this paper some of these ideas may find application, for example in understanding the pathways the separated currents follow, and perhaps relating its apparently variability of position to changes in the strengths of the colliding currents.

3.7.3. The front associated with the Crozet–Kerguelen Confluence

A particularly strong front is associated with the Crozet–Kerguelen Confluence. As noted by Park et al. (1993), the classically defined Polar Front is a weak feature (5-7 Sv bottom referenced) in the Kerguelen–St. Paul Island Passage (Fig. 17), where it is close to but distinctly south of the main baroclinic front at mid-Passage. We noted above that this concentrated front diverges into two distinct fronts along I8S. There the southern front contains the classically defined Polar Front indicator, but unlike within the Passage, on I8S there is a large baroclinic strength associated with the front, bottom referenced about 50 Sv.

The I8S section shows an enhanced Polar Front as measured by the extent of southward rise of isotherms and isopycnals near stations 49–52 (Figs. 4a & 9a). The deep isotherms 1.0 and 1.5°C, for example, rise to 2300 and 1800 m, respectively. These depths are about 800 m shallower that their shallowest occurrence in the Park et al. (1993) synoptic survey of the Kerguelen–St. Paul Island Passage, Fig. 17. This supports our inference that in our sections the Polar Front represents the Crozet–Kerguelen Confluence, a Polar Front enhanced through the juxtaposition of the western boundary current waters south of the Antarctic Circumpolar Current waters that enter the basin through the Kerguelen–St. Paul Island Passage. In Fig. 18 we show the only deep sampled stations (green symbols) along the western boundary north of Fawn Trough. These suggest that the very cold waters of the western boundary current observed south of the Trough (red symbols) have been displaced offshore by the Fawn Trough Current waters (the green profiles fit inside the envelope of profiles from west of the Trough.) These profiles have isotherm depths consistent with being the southern part of the enhance Polar Front even if there were no descent involved with their confluence with the Passage Current. With descent, even some of the western boundary current waters from farther sough may contribute to the enhance Polar Front.

This frontal enhancement and its eastward persistence seem analogous to that of the Weddell–Scotia Confluence (Patterson & Sievers, 1980), where the western boundary current of dense water within the Weddell Gyre encounters the Antarctic Circumpolar Current emerging from the Drake Pas-

sage–Scotia Sea choke point. That also leads to an enhanced Polar Front from the South Scotia Arc near 40°W extending well to the east at the Greenwich Meridian (Whitworth & Nowlin, 1987) and south of Africa (e.g. 40ºE Read & Pollard, 1993; and 30ºE Park et al., 2001).

3.7.4. Potential vorticity structure of the Crozet–Kerguelen Confluence

A potential vorticity signature is associated with the confluence system: high potential vorticity is found at the interface between the deep waters brought eastward by the Passage Current and the cold deep waters brought into the Australian–Antarctic Basin by the deep western boundary current. The three meridional WOCE sections in the Australian–Antarctic basin all show a deep potential vorticity maxima centered near γ^n = 28.2 kg m^{-3}, and nominal temperature 0.5ºC along the southern flank of the Southeast Indian Ridge (Figs. 8, 20 and 21).

The collision of the Passage Current and the western boundary current has vertically layered the two water sources near 3000 m. The layering of two water masses produces a sharp local density gradient and hence high potential vorticity. We find no high potential vorticity water mass upstream in either the deep western boundary current east of Kerguelen or the Antarctic Circumpolar Current north of Kerguelen (Park et al., 1993) instead this appears to be an extrema induced by the Confluence. This layer is too deep and dense to have advected from the Crozet Basin across Kerguelen–St. Paul Island Passage sill and into the Australian–Antarctic Basin, instead it lies just below the coldest waters brought over the sill.

The high potential vorticity induced by the collision is robust enough to survive the smoothing inherent in averaging data to produce the climatology. Figs. 21 and 22 show that this high potential vorticity signal extends across the zonal breadth of the Australian–Antarctic Basin. Consistent with our above discussion of the Antarctic Circumpolar Current only gradually crossing the Southeast Indian Ridge, the patch of elevated potential vorticity appears to parallel the upper-ocean Current and stays contained within the Australian–Antarctic Basin without indication of crossing over into the South Australian Basin. This is interesting because the while the γ^n = 28.2 surface intersects the southern flank of the Southeast Indian Ridge west of and along I9S, it reappears north of the Ridge along I9S, indicating that water this dense does pass through the Australian–Antarctic Discordance. So the passage through the Discordance alters the potential vorticity signature from relatively high values south of the Discordance to relatively low values to the north.

Close examination of station profiles with the deep potential vorticity maxima exhibit steppiness indicative of mixing processes (Fig. 23). Two methods have been applied to the I8S and I9S data sets. Polzin and Firing (1997) calculated density strain and velocity shear variance from the LADCP data while Sloyan 2005 calculated density strain variance and applied fine-structure parameterizations. Near 55ºS, in the Australian–Antarctic Basin and below depths of 1000 m, they estimated mixing as enhanced by a factor of 40 relative to an estimate for the Garrett and Munk (1972) wave

field. Polzin and Firing (1997) speculate that elevated dissipation within the Australian–Antarctic Basin is due to internal lee waves created as the Antarctic Circumpolar Current flows over small-scale bottom topography.

3.8. Antarctic Circumpolar Current at I9S

Similar to the I8S section, along I9S (115ºE), isotherms and isopycnals generally rise southwards (Figs. 4a and 5a), and are parallel with depth. LADCP velocities indicate a bottom-referenced system (Fig. 4b and 11b) except for a surface-referenced westward flow regime in the south over the Antarctic continental slope. The Subantarctic Front lies between 46ºS and 49ºS, just north of the Southeast Indian Ridge crest. The Polar Front is now close to the Subantarctic Front and coincides with the Southeast Indian Ridge crest near 51ºS; their divergent positions along I8S has been replaced by a closeness reminiscent of the Kerguelen–St. Paul Island Passage (Fig. 17). However, the enhanced strength and full water column character of the Polar Front observed at I8S persists at I9S, as does the presence in the deepest levels of deep water colder than observed in the Passage. The net rise of isotherms and isopycnals is more substantial that along I8S, typically reaching 300 to 500 m shallower depths over the Antarctic continental slope. As with I8S, I9S's southern terminus was in the fringe ice, and the Antarctic Slope Current regime was only partially sampled.

Along I9S general the southward rise of isotherms is interrupted by a slope reversal between 52ºS to 55ºS; this is larger in scale that the several slope reversals along I8S. LADCP cross-track velocity shows westward flow here consistent with a bottom-referenced system. SADCP velocity vectors show strong flow curvature in this area (Fig. 19b). In an axisymmetric eddy, vectors normal to the velocity vectors intersect at the center of the eddy. Fig. 19 shows that vectors perpendicular to the velocity vectors intersect near 55º S 115.5º E, and that this "center" coincides with a positive sea surface height anomaly as discerned from altimeter data. Without a mean field to reference the sea surface height anomaly maps, it is difficult to ascertain whether this feature is a large-scale (~ 200–300 km) eddy or a meander. Additionally it cannot be determined how often this feature occurs at this location except to note that reversed shear has been observed south of the crest before in this sector (Callahan, 1971; McCartney, 1976; Rintoul & Bullister, 1999), raising the possibility that it is a permanent structure. We note that on the larger scale (Fig. 19b) this region has relatively low variability in sea surface height anomaly compared to the area northwest of Kerguelen Plateau and over the Australian–Antarctic Discordance.

In contrast to the discussion of the mean climatology at the beginning of this section, I9S shows the belt of dynamic height associated with the Passage Current having almost completely crossed the Southeast Indian Ridge before even reaching the Discordance (the coincidence of the Polar Front with the Ridge crest). Within the deep levels of that Front, the 0.7ºC isotherm lies at 2790 meters, some 300 m above the Ridge crest at the section, so its flow across the Ridge has initiated by this

longitude. But this may not be the normal configuration: because of the large scale eddy or meander, the Front may be abnormally far north, uplifting deep isotherms and enabling deep flow across the Ridge west of the Discordance

3.9. Leakage of cold water through the Australian–Antarctic Discordance

Cold dense water makes its way northward through the Australian–Antarctic Discordance. Rodman and Gordon (1982) Mantyla and Reid (1995) used relatively sparse pre-WHP data to map bottom temperature, suggesting water as cold as 0.3°C just penetrates the sills. The Discordance is a heavily fractured area. The large-scale bathymetry corresponds to a broad sill as deep near 3800 m with several narrow (~ 10–20 km) fractures reaching deeper than 3900 m (Fig. 24). The deepest fracture, blocked below 4100 m, traces northwards to where the coldest water (< 0.3°C) is observed in S5 (Fig. 25). The temperature distribution (Fig. 2) does indicate a favored pathway at those deepest fractures. The bottom-water temperatures warm en route through diapycnal mixing within the fractures, from the -0.1–0°C waters presented to the southern ends of the fractures to the typical 0.2–0.4°C observed immediately north of the fractures. A large area within the South Australian Basin has temperatures just warmer than 0.4°C (Fig. 2).

There are no direct-velocity measurements of deep flow near the Discordance, but existing hydrographic data sets suggest flow is weak. Schodlok and Tomczak (1997a) report 3.3 Sv of northward flow beneath neutral density γ^n = 28.19 kg m^{-3} across the 48ºS segment of the S5 section (location on Fig. 1). Their estimate derives from an inverse model calculation initialized with a level of no motion at neutral density γ^n = 28.08 kg m^{-3} (~3000 m depth). As often is the case, the inversion does not depart much from the prescribed initial condition. This estimate is likely an upper limit to the deep geostrophic transport over the Discordance Zone. Isotherms along the 48ºS S5 section are parallel with depth and generally rise to the west (Fig. 25), indicating southward shear. In order to achieve deep northward flow a mid-depth level of no motion is required. In Fig. 25 we show transports below neutral density γ^n = 28.21 kg m^{-3} (~ 0.5°C) for a range of level of no motions between 2500 m and the deepest common level. The magnitude of northward geostrophic transport decreases with increasing depth of level of no motion. The shallowest reference level results in about 3 Sv of northward into the South Australian Basin, and the transport goes to essentially zero for a bottom level of no motion. This section was within a month of I9S, so westward rise in isopycnals may reflect the large-scale meander in the I9S section to the west of the Discordance and S5. If the eastward baroclinic flow across I9S was concentrated more to the north than usual, the southward geostrophic flow component across the 48ºS S5 section would reflect the eastward flow returning to normal latitudes east of I9S. The SADCP reference along the I9S section does not support a level of no motion within the water column near the Southeast Indian Ridge and the Subantarctic Front, nor does current-meter data at SR3 (Phillips & Rintoul, 2002). (SADCP data exists for the S5 cruise, but

to our knowledge it has not been combined with the hydrography to produce an absolute circulation estimate.) It is quite possible that the northward flow of cold bottom water is small scale within the deeper fissures across the Discordance, and not quantifiable from the geostrophic shear of this section given its station spacing relative to the rough bathymetry

The climatology also suggests that northward geostrophic flow through the Discordance Zone would require a mid depth level of no motion, but with even less potential northward transport than the synoptic S5 section. The Antarctic Circumpolar Current and the Ridge are essentially parallel according to the climatology (Fig. 2): upper-ocean dynamic height contours trend southeast across the Discordance Zone. Note this climatology includes about a dozen meridional sections between 155° and 135°S. Deep dynamic height parallels upper-ocean (Gordon, Molinelli & Baker, 1978; Olbers et al., 1992). Northward geostrophic flow of bottom water requires a level of no motion above that water. There is little along-Ridge density gradient to support a cross-Ridge geostrophic shear that would in turn support geostrophic flow of bottom water across the Ridge. Bottom-water flow through the Discordance does not reflect the large-scale mean geostrophic shear, which is predominately zonal and in a bottom-referenced regime. Instead, we suggest that it occurs as small-scale seeps through the deeper fracture zones of the Discordance.

At levels where the larger-scale topography interrupts the meridional pressure gradient, the deeper fractures through the Ridge have heavier water at the southern ends than at the northern ends. That could drive northward flow through the fractures, limited by some combination of hydraulic control and dissipative effects, but only if there is a northward pressure gradient. If the mean zonal flow is eastward top to bottom, that will impress a southward pressure difference at the ends of the fractures, and instead tend to drive southward flow through the fractures. The fact that bottom water does evidently seep northward suggests that either it is intermittent, perhaps occurring during occasions when an eddy or meander passes over the Discordance and momentarily alters the pressure field, or that there is a permanent zonal flow reversal near the bottom, with the westward flow providing the necessary northward geostrophic pressure gradient at the general depth of the Ridge crest at the Discordance to drive the northward flow of the dense water through the fractures.

Indirect evidence for the absence of direct geostrophic flow of bottom water across the Australian–Antarctic Discordance is found in I9S (Figs. 8B and 9B), in SR3 (Fig. 20), in S5 (not shown) and in the climatology (Figs. 21 and 22). South of the Discordance the waters have elevated potential vorticity, as described in section 3.8. The bottom water layer north of the Discordance is several hundreds of meters thick beneath γ^n = 28.2 kg m^{-3} and is very low potential vorticity, < 5 x 10^{-12} $cm^{-1}sec^{-1}$. A rather thin transition caps that low potential vorticity layer, with potential vorticity rising to > 10 x 10^{-12} $cm^{-1}sec^{-1}$ over a hundred meter span. That transition could represent a boundary between potential vorticity conserving water that flows adiabatically, geostrophically and essentially

zonally along the Discordance and initially high potential vorticity water that seeps northward through the Discordance fractures which is vertically homogenized by mixing in the fractures below the Discordance's nominal sill depth, with the homogenization yielding the low potential vorticity of the bottom water of the South Australian Basin.

4. Combining the geostrophic shear with a velocity reference.

Hydrography alone is not adequate to determine the strength and vertical structure of the western boundary current, flows within the Princess Elizabeth Trough, the westward flow regime along the Antarctic coast, and the Antarctic Circumpolar Current (Speer & Forbes, 1994; Donohue et al., 1999; Heywood et al., 1999; Bindoff et al., 2000; Donohue et al., 2001). Here we reference the geostrophic velocities with the ADCP data and make specific adjustments that reflect sampling issues, transport constraints, and data errors. These velocities are then integrated to estimate transport; Fig. 3 is the smoothed representation of our best estimate. Ultimately, the quality of our quantitative regional circulation is limited by the lack of data between the I8S and I9S sections, by the synoptic nature of the sections, by the errors inherent in referencing geostrophic shears with direct velocities, and errors of the implementation of large-scale transport constraints caused by the I8S and I9S sections ending at the fringe sea ice off the Antarctic continent.

4.1. ADCP referencing of geostrophic shear

Geostrophic velocities could be referenced with either the SADCP or the LADCP velocity. For either measurement, the cross-track ADCP velocity profile is matched to the geostrophic shear profile. For the SADCP reference velocity (shown in upper panels of Fig. 26), in the horizontal we average between stations, in the vertical we average from 150 m to 250 m. For the LADCP reference velocity, in the horizontal we average profiles from the two stations used to construct a geostrophic shear, in the vertical we average from the surface to the deepest common level between stations. The geostrophic shear profile then is "shifted" to yield an adjusted geostrophic profile whose depth average matches the ADCP average over the same depth range. Here we define a bottom velocity as the velocity at the deepest common level and is thus the offset between the geostrophic velocity profile referenced to the bottom and the geostrophic velocity referenced to the ADCP. Resulting bottom velocity estimates for the two methods are compared in Fig. 26.

Errors in the SADCP reference derive mainly from two sources: instrument error and ageostrophic motion. The major contributors to the SADCP-measured ageostrophic motion are assumed to be barotropic tides, internal tides and near-inertial oscillations. As mentioned previously, the barotropic tide as estimated using the OSU TOPEX/Poseidon Cross-Over Global Inverse Solution, version 3.1 (Egbert et al., 1994) has been removed from our SADCP and LADCP profiles. Separately, we estimate that baroclinic tides and near-inertial motions would together yield a reference velocity standard deviation of about 3 cm s^{-1} using a methodology detailed in Donohue et al. (2001). Briefly, we

use the on-station SADCP time series of velocity to estimate internal tidal amplitude and near-inertial oscillations by assuming that variability in the on-station velocity is due to the semidiurnal internal tide and near-inertial oscillations and that the two phenomenon can be separated by their different length scales. The internal tide is assumed to have a larger vertical scale than the near-inertial oscillations. Additionally, since this method is crude, we average the individual station estimates over the I8S and I9S sections to yield a single rms error, rather than using localized estimates. These error estimate are conservative. A portion of the low vertical wavenumber near-inertial signal contributes to the internal tide estimate. Additionally, the vertical average of the residual (on-station minus semidiurnal signal) likely overestimates the contribution of the near-inertial signal to the vertically averaged reference velocity.

Comparison between the geostrophic shears and the between-station cross-track SADCP velocity shear profiles gives an independent estimate of the ageostrophic velocity at small vertical scales. The root-mean-square of the differences between the SADCP and geostrophic velocity shear profiles over the reference depth interval ranges from 0.2 to 4.2 cm s^{-1} with typical root-mean-square values near 1 cm s^{-1} suggesting that ageostrophic noise is minimal.

Errors in the LADCP reference derive mainly from same sources as in the SADCP (instrument error and ageostrophic motion) but also occur when the station sampling fails to resolve the horizontal scales of the velocity field i.e., when the true horizontal average between stations is not the same as the horizontal average of two stations. Numerous examples of LADCP resolution failures are evident in Fig. 26, e.g. station groups 26–29 and 46–47 along I8S and 90–91, 94–95, 97–99, 116–119, along I9S.

It is striking how well the ADCP references agree with one another (Fig. 26). The overall pattern is similar: bottom velocities tend to be the same sign as the upper-layer cross-track velocities, particularly south of the Southeast Indian Ridge. The magnitudes are comparable: the rms differences in bottom velocity are 4.0 cm s^{-1} and 2.7 cm s^{-1} for I8S and I9S, respectively. The mean offset is not statistically different than zero for either section: 0.30 cm s^{-1} with standard error 0.36 cm s^{-1} and 0.6 cm s^{-1} with standard error of 0.46 cm s^{-1} for I8S and I9S, respectively.

For a first look at how ADCP referencing translates into transports, Fig. 27a shows transports accumulated northward along both sections from their southernmost stations, estimated with different approaches to reference velocities: using the deepest common level of stations pairs as a level of no motion, and using LADCP and SADCP referencing. Both forms of ADCP referencing yield accumulated transports that significantly exceed the conventional bottom referencing. The disparity would be even larger if in the south a surface level of no motion were used rather than the deepest common level – this being a minimal requirement to give westward flow along the continental slope (e.g., Rintoul & Bullister, 1999).

We note that the LADCP referencing yields a curious accumulation of westward flow across I8S in the South Australian Basin, yielding a westward 76 Sv north of the Subantarctic Front compared to only 13 and 11 Sv with SADCP and deepest common level referencing. We do not know of any claim for substantial strength broad westward flows in this domain. This large transport instead may reflect an undiagnosed bias issue for the LADCP. There are anecdotal reports of LADCP biases (Hacker et al., 1996; Dengler, Fischer, Quadfasel & Schott, 2002), but as of yet there is no definitive causality determined. We do note that the first 1/3 of I8S exhibited particularly low deep water scattering levels, and therefore a relatively poor signal to noise ratio.

4.2. SADCP-referenced transport adjustment

We will use integrated transports based on the SADCP referencing to construct the regional absolute circulation. This choice reflects the compatibility between geostrophy which determines the average geostrophic shear between two stations and SADCP velocity averaged between station. Spatial aliasing can result when the average velocity between two stations is poorly represented by the average velocity of the two stations. Additionally, LADCP referencing could not be used along portions of I8S when the small rosette was employed. We will, however, compare several current features estimated by both methods since the degree of agreement, given the independence of SADCP and LADCP data, helps build confidence in the SADCP estimates we use for the overall circulation estimate. Error of the reported transports will be estimated using an ageostrophic component of 3 cm s^{-1} (uncorrelated station pair to station pair). We next discuss the error due to a systematic bias in the SADCP estimate.

Transport calculations demand extremely accurate velocities, with systematic bias errors being most problematic. As mentioned previously, the SADCP heading accuracy could be as large as 0.1º leading to an uncertainty of 1 cm s^{-1} in the cross-track velocity component. For an individual station pair spaced 60 km in 4000 m water depth, 1 cm s^{-1} amounts to only 2.4 Sv. But because the bias error due to heading accuracy is constant, it steadily accumulates along a section. A 1 cm s^{-1} error applied to a 4000 m depth section of 3000 km length (the approximate average depth and length of each of our two sections) represents 120 Sv. In some studies mass balance for a land to land section provides a constraint that enables refinement of the ADCP referencing to correct for residual bias errors (e.g., Joyce, Hernandez-Guerra & Smethie, 2001; Hall, Joyce, Pickart, Smethie & Torres, 2004). We cannot easily do this for I8S and I9S because we have incomplete sampling at the southern ends of both I8S and I9S, and there is likely considerable westward transport there. Isotherms rise so dramatically at the southern ends of both sections that we also cannot use constraints on convergence into dense layers between the sections because the isotherms intersection with the seafloor occur beyond the sections' southern sampling limits. We will address these sampling issues in the next section.

As a starting point we adopt, a basin-scale constraint to estimate an initial bias correction. We assume that for the bottom water, the net mass transport along I8S within the Antarctic-Australian Basin between Kerguelen Plateau and the Southeast Indian Ridge should be small, as the topography forms a near cul-de-sac northwest of I8S. This provides an imperfect constraint on our SADCP reference. The Kerguelen–St. Paul Island Passage sill blocks deep flow colder below 0.7–0.9°C (discussion in section 3.4 and Figs 17 and 18). The SADCP-referenced I8S flow before any bias adjustment yields a net transport below neutral density 28.185 (~0.7ºC) of -12.8 Sv (negative is to northwest), a convergence into the cul-de-sac. Requiring instead that the net transport be zero translates into a bias of -0.51 cm s^{-1}. This adjustment is within the uncertainty for the calibration of the SADCP transducer alignment.

Treating the SADCP bias as constant for the I8S and I9S sections, we initially adjust the SADCP reference by subtracting 0.5 cm s^{-1} from each SADCP cross-track reference velocity. At the Fawn Trough the sill depth is shallower than in the Kerguelen–St. Paul Island Passage (Fig. 14), but because deep waters are colder (uplifted) to its west (Fig. 15), somewhat colder deep water, perhaps 0.3–0.5°C, may flow though that Trough. Thus the constraint is imperfect, and we treat the resulting bias only as a starting point, to be refined after consideration of other aspects of the transport distribution.

The large-scale impact of the initial bias adjustment is to increase the total estimated transport through I8S and diminish the total transport through I9S, since the ship traversed these sections in opposite directions, Fig. 27b. An encouraging aspect of the bias adjustment is that it reduces the implied convergence between the sections. Any difference in mass flow through I8S and I9S must be compensated by some combination of northward flow into the eastern subtropical gyre, and, in the south, the zonal flows across the two sections between their southern ends and Antarctica. Before the bias adjustment the I9S total transport exceeded the I8S total by about 170 Sv (310 Sv versus 140 Sv). After the initial bias adjustment, the differential reduces to 43 Sv (243 Sv versus 200 Sv), an improvement which, however, before considering other adjustments, still requires a southward flow past Australia, an unlikely circumstance.

4.3. Final transport adjustments

We will ultimately (after some other adjustments) constrain the flow though I9S to be the sum, 145 Sv of two estimated flows: the Antarctic Circumpolar Current at Drake Passage, estimated at 134 Sv by Whitworth (1983) and an additional eastward transport compensating for the net westward flow through the Indonesian Archipelago estimated as ~ 10–12 Sv (Gordon, 2001; Talley & Sprintall, 2005). The uncertainty of the combined transport is dominated by the Drake Passage component. Whitworth noted a annual average transport standard deviation of ± 11 Sv, and Cunningham and colleagues later interpreted the 134 Sv estimate as having an associated transport error of ± 15-27

Sv (Cunningham, Alderson, King & Brandon, 2003). The original dataset that is the basis for the 134 Sv had significant mooring failures at the Subantarctic Front, deteriorating the estimation of 500 m velocity and is the largest contributor to the error estimate. Here we will ad hoc adapt ± 25 Sv as the error of our constraint of 145 Sv for the combined flow. Thus, before our initial bias constraint, the I9S estimate of 310 Sv is unacceptable, while the 243 Sv after applying that bias is an improvement – and with other adjustments developed below actually can be brought into tolerance.

A second constraint we adopt is on the implied zonal convergence between the sections. Once issues with the incomplete sampling at the southern ends of the two sections are addressed, we will constrain that convergence (I9S – I8S) to be -30 ± 30 Sv, requiring northward transport between the two sections. We estimate that net flow to be northward because there a consensus that deep water flows northward into the Perth Basin and an expectation is that the thermocline will have a net northward flow (or perhaps seasonally a slight southward net when the Leeuwin Current is at its maximum transport in winter). The most direct estimate for the deep flow is the recent one by Sloyan (2006) using a WOCE current meter array, an annual average 4.4–5.8 Sv northward flow below γ^n = 28.1 kg m^{-3}, somewhat smaller than an earlier hydrographic section inversion estimate of 7.5 Sv (Sloyan & Rintoul, 2001b). We adopt 0– 10 Sv as a broad constraint for the deep zonal convergence, consistent with those estimates and other inversion estimates (Toole & Warren, 1993; Talley & Baringer, 1997; Macdonald, 1998; Ganachaud, Wunsch, Marotzke & Toole, 2000). For the upper ocean there are only inversion estimates, in those same papers, and broadly ranging between as 0 to 35 Sv between 95ºW and the coast of Australia. Our adopted constraint represents the combination of these estimates into a net of 30 Sv with a tolerance defined by limiting the convergence to a northward transport and a consideration that twice the convergence (2*30 Sv) would be unacceptably large as it would imply a subtropical gyre that would carry most of the upper ocean Agulhus Return Current flow across I8S and then north.

Fig. 27c shows the transports integrated northward from Antarctica, after several final adjustments have been made, including a iterative final adjustment of the SADCP bias as described below. Because our aim is to produce a comprehensive quantitative transport diagram, we need to estimate transports for the "missing pieces" along I8S and I9S. There are three such regions: the un-sampled regions between the southern end of each section and Antarctica and the region from the northern tip of I9S to Australia where the SADCP was not operational. Two of these three estimates are based directly on other measurements while the third is a deduction. In our discussion of the three estimates, we will refer to the section transport elements with the final SADCP bias applied and provide the value using the initial bias estimate to indicate the impact of the second bias readjustment.

4.3.1. Transport between I9S and Australia

At the northern end of I9S, the SADCP system became dysfunctional about 160 km before the end of the section. The LADCP velocity data, directly integrated, indicated a westward 24 Sv flow in that part of the section, part of a northern boundary current structure described by Hufford et al. (1997). Here we applied the more refined approach of LADCP referencing of the geostrophic shear, which reduces that estimated westward flow to a net 16 Sv. In lieu of an SADCP-based estimate, we append that LADCP-estimated westward flow to the northern end of the SADCP referenced I9S, reducing the I9S transport estimate with the initial bias from 243 Sv to 227 Sv. The appended 16 Sv, is formed from 17 Sv in our lighter layer, opposed by 1 Sv eastward flow in the denser layer (below nominally 3800 m in this area). This 16 Sv represents a northern boundary current (about 80 km width) contribution to the westward flow of the Flinders Current (Bye, 1972) at the southwestern extremity of Australia (see Middleton & Cirano, 2002, for recent interpretations of the Flinders Current). Beneath the 16 Sv eastward flow, the 1 Sv eastward flow is the northernmost part of the deep northern boundary current, whose totality in the section is about 4 Sv (with the mix of LADCP and SADCP referenced elements) over a 300 km width.

The comparison (Fig. 26b) of LADCP and SADCP based bottom velocities along I9S south of the SADCP failure point indicates an rms difference of 2.7 cm s^{-1}, which we have suggested mainly reflects the less optimal compatibility of the point LADCP profiles with the geostrophic shear than the SADCP data. The tighter station spacings near the northern boundary would tend to lower that rms, but that might be compensated by the shorter horizontal scale of the current near the boundary current. In lieu of any better way to estimate the LADCP horizontal sampling error for this group of stations, we use the 2.7 cm s^{-1} rms from the southern region to estimate a 7 Sv potential sampling error from substituting LADCP referencing for the 6 station pairs northward of the failure point, over their depths, suggests the LADCP-based transport of 16 Sv has an estimated error of 7 Sv from what a SADCP-based estimate would have shown.

Another way to assess validity of this LADCP-based transport is to compare estimated transports for current features where both forms of referencing are available. Table 1 does the comparison for four currents, at the Polar Front and the Subantarctic Front, and the two sides of the cyclonic eddy crossed around 76/47ºS. Generally, the magnitude of the various currents estimated with bottom-referencing underestimates transports compared to the SADCP-referenced or LADCP-referenced magnitudes. The LADCP-referenced transports fall within the indicated error limits for the SADCP values, or would do so if one additionally considers the LADCP transport error (not tabulated) that is always larger than the SADCP transport error.

We are unaware of any moored current measurements extending offshore of the continental slope into deep water south of western Australia. In our earlier work with Hufford it was noted that the LADCP referenced velocity field was consistent with the layering of water masses through the

deep water (Hufford et al., 1997). In particular, the shear evident in the deep density distribution near the northern end of I9S, Fig. 9b, transformed into oppositely signed transports deep and shallow flows. The deep eastward flow carries higher nutrient (e.g., high silicate, Fig. 6B) subtropical gyre-originating deep water into the Great Australian Bight, with maximum speeds near 3500 m at a shear reversal, but remaining eastward all the way to the bottom. The transition to the westward flow of the Flinders current was seen near 2000 m leading to westward flowing intermediate and thermocline water. Westward flow of bottom water is restricted to offshore of the deep northern boundary current.

4.3.2. Transport south of I8S in the southern Princess Elizabeth Trough

As discussed in section 3.2, I8S did not reach all the way south across the Princess Elizabeth Trough. Heywood et al. (1999) reference geostrophic velocities with an SADCP, with the same sort of methodology we use including the use of high accuracy heading determination, and report 45 Sv of westward flow in the southern Trough in a Feb 1993 section, mostly south of I8S's coverage. We therefore append 41 Sv to the southern end of the I8S section, yielding 45 Sv in the westward flow regime within the Princess Elizabeth Trough. A net westward transport of 24 Sv through the Trough results, smaller that the net 34 Sv reported by Heywood et al. (1999). We attribute the difference principally to an eastward 8 Sv transport we estimate over the southern part of the Kerguelen Plateau sampled along I8S, an area north of the area sampled by Heywood et al. (restricted to south from 62ºS). With this 41 Sv adjustment, the total eastward transport through I8S is 186 Sv (159 Sv before the final bias adjustment).

Heywood et al. (1999) defended their estimates from the 1993 data in several ways: the similarity of southbound and northbound SADCP data in 1993 and the similarity of the 1994 data compared to 1993 data. While all but the northernmost of their experiment's six-mooring current meter array had current direction issues, average scalar speeds from the one year records in the southern moorings compared well with the SADCP-referenced geostrophic flows in the westward flow regime and the northern mooring record matched SADCP-reference velocities in the eastern flow regime. In the overlapping latitude range of the central and northern Trough, our section estimates match theirs well.

4.3.3. Transport south of I9S over the continental slope off the Adélie Coast.

The third adjustment occurs at the southern end of I9S, where our sampling ended at about the 2000 m isobath. The adjustment is constructed by first demanding compatibility of the two sections (with Antarctica considered a streamline), and then considering the mass-flux constraint for the totality of I9S, and the convergence constraint for the pair of sections. The SADCP-referenced westward flow regime at the southern end of the section is 33 Sv (final bias), with the southernmost station half way up the continental slope in 2655 m water depth. We require a total westward flow in

the south along 115ºE at least adequate to supply the total westward flow at the southern end of the Princess Elizabeth Trough (45 Sv) plus the contribution (27 Sv) required to support the western boundary current off southern Kerguelen Plateau (whose net 48 Sv has a 21 Sv contribution from eastward flow through the northern Princess Elizabeth Trough). This total flow of 72 Sv requires adding at least 39 Sv south of the southern end of I9S, "uphill" from the 2655 m isobath. Consistency considerations for the circulation within the two layers in the southern half of the Australian–Antarctic Basin lead us to increase that to 76 Sv, corresponding to the addition of 43 Sv south of the southern end of I9S, a value similar to what was needed south of I8S. This yields, using the final bias value, a net eastward transport of 156 Sv between Australia and Antarctica near 115ºE (178 Sv using the initial bias).

The adjustments at the ends of the sections when combined with a final bias adjustment, yields a net 156 Sv eastward flow at 115ºE, which reasonably satisfies the zonal net transport constraint of 145 ± 25 Sv, and a net zonal convergence of -30 Sv, which reasonably matches our constraint of 30 ± 30 Sv. It requires an Antarctic Slope Current of 72 Sv at 115ºE compared to 45 Sv in the Princess Elizabeth Trough.

4.3.4. The final SADCP bias adjustment.

Our initial bias estimate of + 0.5 cm s^{-1}, I9S produces an eastward transport of 219 Sv across I9S before considering the southern adjustment. Compatibility with I8S requires adding a westward 41 Sv, yielding a net transport across 115ºE of 178 Sv, outside our tolerance range of 145 ± 25 Sv. Using the I8S net transport with the initial bias, 159 Sv, then yields a convergence estimate of + 19 Sv, requiring a - 19 Sv (southward) flow that is outside our constraint of 30 ± 30 Sv. One approach would be to append an additional westward flow of 30 Sv south of I9S. This would push the 115ºE net transport down to 145 Sv, and the net convergence to – 14, giving an acceptable 14 Sv northward flow. But that yields a very strong 105 Sv Antarctic Slope Current across 115ºE. While we have not adopted an explicit constraint on that Current (discussed below), that seems too large. The interplay of the Antarctic Slope Current strength, and the zonal transport and zonal convergence constraints are the primary considerations that lead us to iterate the bias from the initial estimate to the final.

A second consideration is revealed in the I8S cul-de-sac region that we used to deduce the initial bias. By design, that initial bias changed the net transport across I8S into the cul-de-sac below neutral density 28.185 (~0.7ºC) of -12.8 Sv (negative is to northwest) to zero. That zero is achieved, however through a balance of a net inflow of the densest waters of the layer and a net outflow of the lighter waters of the layer, this reflects the transformation of those densest waters (entering the cul-de-sac in the deep western boundary current) into the somewhat less dense water flowing eastward beneath the Passage Current waters. In retrospect, why should that transformation necessarily

yield an exact balance at a particular density horizon? When we constructed a consistent regional circulation using that initial bias, we deduced that dense layer flow into the cul-de-sac also occurs through Fawn Trough, and that might include flow in the layer we used for the constraint. So the final bias adjustment relaxed the cul-de-sac constraint, and instead sought a bias that simultaneously satisfies the 115ºE zonal transport constraint (arguably the best known constraint), the net zonal convergence constraint (less tight because it is ad hoc) and yields a more reasonable estimate for the Antarctic Slope Current. We limited the examination of the possibilities to increments of 0.1 cm s^{-1} of bias, and the final bias selected – slightly stronger than the initial estimate – was -0.7 cm s^{-1}. A less negative bias requires a larger Slope Current, to meet the eastward transport constraint, while a more negative bias would reduce that Current – but at the expense of increasing the required strength of northward flow to satisfy the zonal convergence constraint beyond our tolerance limit because that more negative bias shifts the I8S transport higher.

Re-examining the cul-de-sac, we now look at an even denser layer, γ^n = 28.21 kg m^{-3} (~ 0.5°C), the layer whose transports are illustrated in the property sections. This is dense enough that it is unlikely there is appreciable Fawn Trough flow into the cul-de-sac: in Fig. 15 the more uplifted southern station group has 0.5ºC near 2475 m, only about 100 m above the Trough sill depth. For that layer the western boundary current delivers 25.8 Sv into the cul-de-sac, and the meandering flows northward of there give a net flow out of 27.8, for a small residual of 2.0 Sv export from the cul-de-sac, possible indicative of a small Fawn Trough contribution, but not distinguishable from zero. With the initial bias estimate that residual was -1.8 Sv, requiring an upwelling sink, but not a serious imbalance either. That we take as an indication that a small basin-scale constraint like the cul-de-sac is not likely to tighten the bias tuning exercise, and that it is the overall regional constraints that are the most important.

4.4. Discussion of the quality of the transport estimates

Before a discussion of the quantitative circulation field, we discuss a few points about the quality of the transport estimates.

4.4.1. The remaining errors of SADCP referencing and its effect on transport estimates

We believe that the satisfaction of the several overall constraints demonstrates that we have substantially reduced the bias error. Because transport accumulates along a section, even a tiny change in the bias has significant impact on the overall transport constraints. The ±30 Sv tolerance on the constraint of 30 Sv of zonal convergence between I8S and I9S corresponds to about ±0.107 cm s^{-1} bias. An increase/decrease of bias by 0.107 cm s^{-1} increases/decreases the I8S transport by 15.4 Sv and decreases/increases the I9S transport by 14.6 Sv. The addition of a westward flow south of I9S provides an independent means of satisfying the 115ºW transport constraint. Essentially we have reduced the remaining reference adjustment system to a two parameter balancing be-

tween the bias tuning, to achieve reasonable zonal convergence, and strength of westward flow south of I9S to keep the net flow between Antarctica and Australia within tolerance. But there also are limits to how large one and reasonably "set" the Antarctic Slope Current, which we discuss in the next section.

The largest remaining error in the SADCP-reference transport estimation is the ageostrophic error. This error, based on an rms 3 cm s^{-1} everywhere along the sections, accumulates to 52 Sv along I8S and 57 Sv along I9S. If we include a 0.107 cm s^{-1} residual bias error, assumed independent of the ageostrophic error and reflecting the uncertainty of the zonal convergence constraint, then the errors associated with total SADCP-referenced transport become 54 Sv and 58 Sv for I8S and I9S, respectively, dominated by the ageostrophic error, since we have essentially "zeroed out" the bias error through the constraints.

4.4.2. How strong is the Antarctic Slope Current?

The results of the SADCP referencing and the appendage of transports at the southern end of both sections yields a strong westward flow system along the Antarctic continental slope, 45 Sv at the Princess Elizabeth Trough, and 76 Sv at 115°E. This represents a very powerful current, achieved by appending of 41 and 43 Sv to the southern end of each section. We have discussed the I8S justification earlier. For 115ºE we use the Smith and Sandwell (1997) bathymetry for the area south of the southern station along I9S to estimate a required 30 cm s^{-1} average speed to produce the 44 Sv we have appended there. Is that strength to be believed or does it instead represent the accumulation of error that happens because the various other elements are being forced to balance at their central transport values?

A limited form of SADCP referencing has been applied by Bindoff et al. (2000) to a series of eight short meridional hydrographic sections across the continental slope between 80° and 150°E. All began at 63º-63.5ºS, and overlap the southern end of I8S and I9S only by 130 km and 170 km, respectively. For technical reasons, only on-station or near-station SADCP data were available. Optimal mapping (100 km Gaussian correlation length scale) was used to produce a SADCP velocity field at 28.6 m that was used to reference the geostrophic velocities (we note that is a very shallow level for the assumption of geostrophic balance, and contamination by inertial motions will be at its worst near the surface). They noted that the lack of between-station and vertical averaging, and the lack of a vector-based GPS system, would produce less accurate referencing compared to the methods used by Heywood et al. (which are equivalent to those of our procedure). The authors give only limited integral information about transports, breaking each section into two pieces based on the direction of flow at the surface (westward in the southern area and eastward in the northern area).

Bindoff et al. (2000) found westward surface flow in the south of all eight sections, and for this surface flow-defined regime the westward transport ranged from 10 to 55 Sv, with an average of 29

Sv. The surface flow reversed to eastward farther north, and in some sections this regime's referencing to the eastward surface flow produced eastward transport, in others westward transport. Four of their sections, at 104º, 112°, 120° and 128ºE, bracket the location of I9S, and are relatively remote from the eastern and western ends of the Australian–Antarctic Basin. Their westward surface flow regime transports were estimated as westward 28, 30, 29, and 55 Sv (south of 64.1, 65.1, 65.4 and 64.3ºS, respectively), for an average of 36 ± 13 Sv. That regime is located essentially south of the southernmost latitude sampled along I9S, 64.9ºS, and thus is to be compared with the 43 Sv we appended south of I9S. The transports for their eastward surface flow regimes (nominally 63ºS south to the above listed 4 latitudes), which overlap the latitude range (62–64.9ºS) where we measured a westward 31 Sv across I9S, were variable in direction: eastward 10 and 41, and westward 18 and 12 Sv, for an average eastward 5 ± 27 Sv. Their reported total transports across the four sections thus present a confusing picture: three westward, 19, 47 and 67 Sv, and one eastward 11 Sv, for an average of westward 31 ± 34 Sv, to be compared with the part of our estimated 76 Sv that is south of 63ºS, about 60 Sv. While these comparisons are at the edge of the standard deviation envelope of their group of four estimates, the un-assessed errors of their method leave us just reassured that our appended current is not in disagreement with their estimates. The westward surface flow regime was typically 5–20 cm s^{-1}, while the inferred bottom velocities generally were higher and sometimes exceeded 30 or 40 cm s^{-1}. This is also broadly consistent with our estimate of an average 30–40 cm s^{-1} through the estimated cross sectional area south of I9S.

Two more of the Bindoff et al. (2000) sections, at 80° and 94°E, bracket the southern end of I8S and the location of the Heywood et al. (1999) section across the Princess Elizabeth Trough. Here their referencing technique yielded smaller transports in the westward surface flow regime, 16 and 18 Sv, while for the entire area south of 63ºS on the two sections, net westward transports of 22 and 12 Sv were noted. These estimates are smaller than the 34 Sv estimated by Heywood et al. (1999). It may be that the methodology used by Bindoff et al. (2000) to produce the reference surface velocity field systematically underestimates barotropic speeds, that there is a bias introduced because of using a reference level that is to close to the sea surface, or that their published transports for regimes defined by surface flow do not capture the totality of westward flow in the full water column.

There are only sparse current meter measurements along the continental slope for assessing the strength of the Antarctic Slope Current. Nunes Vaz and Lennon (1996) report several current meter moorings in the Prydz Bay area just west of the Princess Elizabeth Trough. All but one of these of these moorings were sited well south inside the Bay, but a single mooring was set in 630 m water depth offshore of the shelf break north of Mawson Station (63ºE), west of the Bay. Its four instruments recorded strong flows, with the 12 month mean of the upper instrument at 127 m reported as

63 cm s^{-1} along the upper continental slope, with very little vertical shear indicated across the four instruments. In the Princess Elizabeth Trough, the Heywood et al. (1999) mooring instruments can be used only for scalar speed. Those speeds were deemed by the authors as consistent with their SADCP referenced velocity field used for their westward 45 Sv estimate. Closer to the eastern end of the Australian–Antarctic Basin, a 140ºE mooring in 2665 m water depth showed a 13 month average westward 16 cm s^{-1} bottom velocity, bottom intensified and diminishing to 5 cm s^{-1} at 1075 m (Fukamachi, Ushio, Takahashi, Oikawa, Furukawa, Yoritaka, Fukuchi, Yamanouchi, Wakatsuchi, Taira & Kitagawa, 2000). To our knowledge these represent the only long time series current measurements in this sector of the Antarctic Slope Current system, and we find them inconclusive as to defining anything but a broad range of measured westward speeds in the Antarctic Slope Current.

We draw no firm conclusion from these estimates of the Slope Current. We feel that the best constrained number is the Princess Elizabeth Trough westward 45 Sv reported by Heywood et al. (1999), because of its use of vector GPS system in its SADCP system, and its application to the shear well below the near-surface ageostrophic domain. Our incorporation of that value combines with eastward flow in the northern Trough and our estimate of western boundary current flow to place a demand for a Slope Current at I9S amounting to 76 Sv. That strength is admissible from the Bindoff et al. (2000) range of estimates, but those cannot be considered well constrained. Relying more on our instincts, after seeing the interplay of transport residuals moving around the various constraints as we converged on a best estimated SADCP bias, it would not surprise us if the Antarctic Slope Current at 115ºE was less strong than 76 Sv, with the residual reflecting the accumulation of errors along the sections, and in the application of other constraints being rolled up into an uncertainty of ± 30 Sv on an Antarctic Slope Current of about 50 Sv.

4.4.3. Summary of estimated section transports, implied convergence, and error.

In conclusion, our error statements for the two sections follow. The stated errors for section transports represent the combination of the ageostrophic errors, likely overestimated, and a contribution corresponding to our estimate of a remaining residual bias uncertainty, ±0.107 cm s^{-1}.

I8S, nominally 89ºE: total transport between Broken Ridge Crest and the Antarctic continental shelf, 186 ± 54 Sv.

I9S, 115ºE: total transport between the continental shelves of Australia and Antarctica, 157 ± 58 Sv.

Zonal convergence 89ºE to 115ºE, 29 ± 83 Sv.

5. Quantification the strength and structure of the regional circulation

We first describe the largest-scale aspects of the system of currents, then discuss dominant individual current elements, and conclude by describing the meridional migration of bottom water through the system.

Fig. 28 shows the plan view of the circulation structure based on the estimates of absolute transport for the two sections (Fig. 27C) and the requirements of Antarctica being a streamline. Transports represent a synoptic snapshot of oceanic conditions during late 1994 through early 1995. Transport schematics are also shown for two γ^n layers: lighter and heavier than 28.15 kg m^{-3} (~1.0ºC), Figs. 29 and 30, respectively. Cumulative and between-station geostrophic transports along I8S and I9S for the denser layer are superimposed on the temperature sections in Fig. 4 to aid in visualizing the estimated dense water circulation.

There is significant mesoscale variability in total transport distribution along both sections (Fig. 27C), mostly manifested by shear and flow reversals spanning one or two station pairs. In contouring the total transport field (Fig. 28) we suppress eddy/meander features weaker than 20 Sv along the sections. The two stronger eddy/meander features along I9S are shown as current rings. One is the ~ 300 km anticyclonic feature near 55ºS discussed in section 3.9, with SADCP-referenced strength of 33 Sv. The other is a more compact cold core cyclonic eddy near 46ºS along I9S (Fig. 4B). This 28 Sv eddy has a diameter of about 150 km, a typical size for cyclonic mesoscale eddies formed during Subantarctic Front meander cutoffs (Savchenko et al., 1978; Morrow, Rintoul, Donguy & Chaigneau, 2004). The strengths of the eddies are estimated as the amplitude of the reversed flow, and both eddies are embedded in eastward flow regimes. Several eddy/meander features along I8S are stronger than 20 Sv, all within the Australian–Antarctic Basin. These are treated as meanders, time-variable in detail but collectively a permanent circulation element, the Crozet–Kerguelen Confluence.

In the transport fields thin contours represent circulation elements less than 10 Sv, while the thick contours indicate the principal axes of various stronger flows. The schematics are quantitatively consistent within ±1 Sv round-off error relative to the computed transports across the sections. On the two layer maps (Figs. 29 & 30) the same eddy/meander features as in the total transport field are retained to the degree that the two layers have congruent circulations. Dashed contours are included in the total transport field representing pathways along which bottom waters from the cyclonic gyre regime intrude into and across the Antarctic Circumpolar Current regime. Without that artifice, the total transport field would be somewhat misleading: the relatively small bottom-water flows would be masked by the larger transports of the total water column. The contouring of the denser layer, Fig. 29, reveals the basis for the bottom water dashed contours on the total transport map. In the following discussion, the error reported includes the ageostrophic and bias contributions as developed in section 4.

5.1 The large-scale circulation in the southeastern Indian Ocean

Within the study domain, the total transport field is dominated by a belt of strong eastward flow with westward flow regimes to its north and south (Fig. 27C). This belt is located where the Antarc-

tic Circumpolar Current flows through the region, but as noted earlier it is something more than that, reflected in the large strength of the estimated eastward flow through the middle of each section. The westward flows compensate the adjacent parts of the eastward flow belt, reducing the net eastward flow for both sections; we will refer to these opposing flows as gyre regimes, anticyclonic to the north and cyclonic to the south. On Fig. 27C three horizontal lines give the southern and northern stream function values as a visual aid in isolating the throughput on each section from gyre circulations to its north and south. A general result, documented next, is that the throughput for both sections is delimited by the Subantarctic and Polar Fronts. That is encouraging, for it was not a requirement of the evolution of the bias adjustments that they would result in alignment of the streamlines with the classical frontal indicators.

Along I9S the flow structure can be split apart into a throughput of 157 ± 30 Sv eastward flow along the Southeast Indian Ridge, with a 38 ± 30 Sv anticyclonic gyre regime to its north in the South Australian Basin, and a 76 ± 26 Sv cyclonic gyre regime to its south in the Australian–Antarctic Basin. The throughput and the eastward flows of the two gyre regimes combine to give a broad belt of east flow of 271 ±47 Sv, split into three substantial branches by the two eddies at 46ºS and 55ºS. It is only the central part of the broad belt that is the true Antarctic Circumpolar Current. Fig. 3 provides a visualization of the stream function field, and the contour color transitions on that figure paint the throughput and gyre transitions, and the contributions for several distinct pathways that we discuss next.

In the north along the I9S section, the 38 Sv anticyclonic regime (yellow on Fig. 3) has two distinct elements. Near Australia is a narrow boundary current regime related to the Flinders Current (Bye, 1972; Veronis, 1973; Hufford et al., 1997; Middleton & Cirano, 2002), but stronger due to the SADCP-referencing than with the more traditional upper ocean reference level. Farther south is an anticyclonic gyre in the Subantarctic Zone first noted in this sector, we believe, by Wyrtki (1971). These two features are separated by an eastward flow. This structure occurs in independent data studies and modeling efforts (Rochford, 1958; Wyrtki, 1962; Wyrtki, 1971; Schodlok & Tomczak, 1997b; Middleton & Cirano, 2002; Middleton & Platov, 2003), with the embedded eastward flow associated with the regional "Subtropical Front." In Fig. 27C the I9S northern boundary stream function value of 157 Sv is encountered three times farther south along I9S (red-yellow transition on Fig. 3), on the two sides of the compact cyclonic eddy near 46ºS, and the third time in the middle of the Subantarctic Front at 48ºS; the latter occurrence we take as the southern boundary of the anticyclonic regime. That 38 Sv regime is predominately a Subantarctic Zone gyre, extending northward from 48ºS to Australia, but mostly, 33 Sv, concentrated between 43º–48ºS. The smaller scale boundary current gyre to its north provides a residual westward 5 Sv. The 38 Sv westward flow across the northern part of I9S provides about 13 Sv directly to the northward flow between Austra-

lia and the Broken Ridge, with the rest of the flow, 25 Sv, extending the Subantarctic Zone gyre westward to and across I8S.

In the south the cyclonic gyre along I9S can be delimited by a similar approach. Westward transport peaks at 76 Sv near 62ºS (Fig. 27C), and the southern boundary value of 0 Sv is encountered once farther north near 57ºS (in the middle of the 4 green contours on Fig. 3). That inferred regime limit may be deceptively far south, for the large eddy/meander along I9S misses by only 5 Sv from wrapping that streamline around the feature to cut and recut the section near 52ºS. Using the classical Polar Front definition (the temperature minimum warming above 2ºC), the Front is encountered three times, on either side of the eddy/meander center at 55ºS, and the last time near the 51ºS; the Front therefore does wrap around the eddy/meander. Essentially the transition from the cyclonic gyre regime to the throughput belt is in the southern part of the Polar Front. Thus the Polar and Subantarctic Fronts can be taken as the regime boundaries between the belt of eastward throughput and the cyclonic domain to its south and the anticyclonic domain to its north.

Taking the southernmost occurrence of 157 Sv near 48ºS and the northernmost occurrence of 0 Sv at 57ºS gives a nominal width of about 1200 km for the belt of eastward flowing throughput (Fig. 3, the red contours and the northern two green contours. Because of the distortion of the eddy/meander near 55ºS, that width is deceptively large, and using instead the most northern Polar Front position as the southern boundary of the belt suggests a width of about 400 km for the bulk of the 157 Sv throughput across I9S.

With somewhat more complexity than for I9S we can look along I8S for the regime boundaries between the southern cyclonic gyre, the throughput delivered to I9S, 157 Sv, the Subantarctic Zone anticyclone, and the excess flow through that section, 29 Sv, that ultimately passes northward between I8S and Australia. Working northward from the southern boundary stream function of 0 Sv (Fig. 27C) stream function diminishes to -45 Sv in the middle of the Princess Elizabeth Trough, then increases to -24 Sv over the southern Kerguelen platform. This can be interpreted as a 45 Sv extension of the I9S cyclonic gyre's southern limb through the Trough into the Weddell–Enderby Basin, with 21 Sv returning eastward in the northern Trough (the blue and purple contours on Fig. 3).

From the resulting local maximum of -24 Sv, the stream function diminishes northward to its most negative value of -72 Sv across the western boundary current, a value for the maximum cyclonic gyre strength not appreciably different from that at I9S, -76 Sv, by construction (I9S is required to supply the net westward flows through the Princess Elizabeth Trough and the western boundary current). Our estimates indicate that 27 Sv of the 48 Sv western boundary current transport off the southern platform of the Kerguelen Plateau is directly delivered from I9S, and 21 Sv indirectly from the projection of part of the gyre through the Princess Elizabeth Trough. The stream function crosses zero three times northward from the -72 Sv minimum, in the first meanders of the Crozet–

Kerguelen Confluence (captured in Fig. 3 by tracing the middle of the group of four green contours). The most northern zero crossing is at station 56 in the southern part of the strongest band of south-east flow, 100 Sv (Fig. 28), which on the section plots (Figs. 4–9) is the southernmost Polar Front indicator in the section. The next meander to the north is totally water from the Passage (the red meandering contours on Fig. 3). The zero stream function for the depth-integrated flow traces up-stream to the 38 Sv Fawn Trough Current in this transport construction (the middle of the group of four green contours in Fig. 4), further indication of the cyclonic gyre regime's penetration westward past Kerguelen Plateau. We estimate that 24 Sv of the Fawn Trough Current is associated with the cyclonic gyre, with the -72 Sv stream function minimum formed by the direct 27 Sv flow from I9S, the retroflection of 21 Sv of the 45 Sv westward flow through the Princess Elizabeth Trough, and the remainder of that flow recirculation over a longer pathway in the Weddell Enderby Basin to return through the Fawn Trough. The other 14 Sv of estimated flow through Fawn Trough we associate with the throughput south of Australia, and also, given the closure of the cyclonic gyre suggested by the above sums, with the southernmost elements of circumpolar flow through Drake Passage.

Most (143 Sv) of the 157 Sv throughput across I9S is attributed to the circumpolar flow passing north of Kerguelen through the Kerguelen–St. Paul Island Passage (red contours on Fig.3). With the cyclonic regime across I8S delimited, continuing northward from that zero stream function locates the 157 Sv stream function (corresponding to the Australian boundary value) in the middle of the Subantarctic Front near 43ºS (red-yellow transition, Fig. 3). Thus, at I8S as at I9S, the throughput ultimately passing south of Australia is bracketed by the enhanced Polar Front in the south and the Subantarctic Front to the north. The stream function continues to rise northward along I8S from 157 Sv to 189 Sv, with the excess (yellow contours on Figure 3 including purple contour denoting return flow from the Tasman Basin) defining a Subantarctic Zone anticyclone, whose 32 ± 17 Sv westward return flow that is essentially the same strength as the westward flow across northern I9S. The "ex-cess" eastward flow across I8S is recirculated back westward, including a substantial element that first crosses I9S before retroflecting to return westward south of Australia.

North of the westward return flow of the Subantarctic Zone anticyclone is a belt of eastward flow across I8, 36 ±25 Sv. This northern belt of eastward flow includes a surprisingly substantial 6 Sv contribution below ~ 3500 m in the denser layer, Fig. 29. The rest, 30 Sv we interpret as mostly (22 Sv) coming northward from the Subantarctic Zone anticyclone within the South Australian Basin, with a smaller contribution, 8 Sv, from the Crozet Basin passing north of St. Paul Island. Most, 33 Sv, of the 36 Sv eastward flow turns north into the eastern subtropical gyre, partially, 17 Sv, returning westward across the northern end of the section, and partially, 16 Sv, flowing north between the Broken Ridge and Australia where it combines with 13 Sv turning north from the westward flow

across I9S to provide the net 29 Sv export into the subtropical gyre between the two sections. All this is in the structure of the yellow contours on Fig. 3.

The finding that the regional throughput is bounded by the Subantarctic and Polar Fronts is perhaps not surprising, as that fits the traditional image of the Antarctic Circumpolar Current thus delimited. We note that this alignment of the fronts was not an imposed constraint, but is what follows from adjusting the bias to satisfy the budgeting constraints discussed in section 4. Without those adjustments the estimated flows between the two fronts for the two sections would not match, and the circumpolar throughput belt would itself require a large meridional convergence would into the belt between the sections.

5.2 The dominant current elements

We next detail several specific circulation elements and their implications. In the discussion, when appropriate, a feature's transport is followed by an estimated error that represents the ageostrophic error combined with the residual bias error. In parentheses following that will be two additional transports, the transport using the deepest common level, and the transport using LADCP-reference. These will enable the recognition that the SADCP reference generally strengthens the transports and illustrate the relatively consistency between the two forms of ADCP references. When a transport is estimated for locations other than along I8S and I9S, it will be given without an error.

5.2.1. Flow through Kerguelen–St. Paul Island Passage

The estimated net flow across I8S is 186 ± 54 Sv. This is hypothesized as achieved mostly by a concentration of eastward flow through the Kerguelen–St. Paul Island Passage, where a concentration of fronts is recognized (section 3.5). Working northward from Antarctica, the identified net source/sink flows west of the section are the net westward 24 Sv through the Princess Elizabeth Trough, and the net 38 Sv eastward flow estimated for the Fawn Trough (which will be discussed below, section 5.2.4). These combine to give a 14 Sv net eastward flow between Kerguelen Island and Antarctica. This leaves 172 Sv of the net flow across I8S to be accounted for sources in the Crozet Basin passing north of Kerguelen Island. We posit that is achieved by a powerful 181 Sv eastward transport through the Kerguelen–St. Paul Passage, partially compensated by a small 9 Sv westward residual of a anticyclonic exchange flow across the saddle between the St. Paul outcrop on the Southeast Indian Ridge and the Ninety East and Broken Ridges. This is an area where smoothed circulation diagrams show mid-depth (1000–3000 db surfaces) anticyclonic circulation with the maximum steric height over the saddle (Wyrtki, 1971; Reid, 2003). It is possible that some part of the eastward 181 Sv we have placed at the Passage may pass northward of St. Paul Island. We have limited flow there to 8 Sv based on published level of no motion transport estimates (Park et

al., 1993; Stramma & Lutjeharms, 1997) and consistent with the distribution of potential vorticity (McCartney, 1982; Toole & Warren, 1993; McCarthy & Talley, 1999).

The inferred 181 Sv flow through the Kerguelen–St. Paul Island Passage is considerably larger than previously estimated transports from the only two extant sections across the Passage: Park et al. (1991; 1993) report 99 and 106 Sv based on a bottom (3600 m or shallower) level of no motion. Is such transport enhancement at the Passage plausible? A bottom velocity of 2.5–2.7 cm s^{-1} applied to the entire span of the Passage of those sections would provide the necessary boost. Alternatively, noting that most of the bottom-referenced transport is at the compressed band of fronts in the southern Passage, restricting the barotropic flow to that regime (a 200 km band over the deeper part of the Passage) would require about 11–12 cm s^{-1} bottom velocity.

We know of no SADCP or LADCP referenced hydrographic sections in the Passage. Gille (2003) estimated the full Southern Ocean circulation utilizing ALACE float displacement vectors, objectively mapped, to estimate a reference velocity field (nominal 900 m) for climatological average hydrography. The float data in our domain are from the same time frame as the I8S/I9S sections (indeed, most were launched during that cruise. The smoothing inherent in her method limits expectations on comparison with SADCP-referenced synoptic sections, but the results are encouraging. Her Fig. 5 plots as a function of longitude the maximum eastward speed at 900 m and the bottom speed beneath that location, from 1º meridional bins for the smoothed fields. At the longitude of the Passage, where the 1987 and 1991 section data by Park et al. (1991, 1993) are the only significant hydrography in the hydrographic climatology, both speeds are at their circumpolar maximum, 19 cm s^{-1} at 900 m, and 11 cm s^{-1} at the bottom (around 3500 m at the Passage). The 900 m extrema is consistent with this Passage's compression of fronts, while the inference of strong bottom speeds at the sill depth supports the requirements of our estimated large eastward transport.

We further consider the demand for substantial eastward transport and bottom velocity in the Passage from two indirect perspectives. First, downstream of the Passage in sections I8S and I9S, what sort of transport enhancement is associated with the flow between the fronts that emerge from the Passage? Second, the flow through the Passage comes from the Crozet Basin, a much deeper area than the Passage sill. What are typical velocities within the approaching flow at depths near 3500 m?

The Subantarctic Front dominants the compressed frontal group within the Passage (section 3.5). At other circumpolar locations to the east, the enhancement of transport by bottom velocity at this front has been noted. Donohue et al. (2001) tabulated bottom velocities for 10 synoptic crossings of the Front in the South Pacific, deduced by the SADCP referencing method used here. The average bottom speed (normal to sections) was 5.9 cm s^{-1} for a range of bottom depths from 2700 to 5300 m (average 4180 m). In I8S and I9S the SADCP-inferred bottom velocities are routinely several cm s^{-1}

in the belts of eastward flow (Fig. 26); we report in Table 2. For the Subantarctic Front the 3200 db speeds are 8.5 and 1.5 cm s^{-1} for I8S and I9S, respectively.

The transport enhancement required in the Passage is about a factor of 80%. Along I8S stations 27–48 define a belt of eastward flow over the Southeast Indian Ridge with average depth 3380 m. The SADCP-referenced transport of 152 Sv for the group is 70 Sv greater than the bottom-referenced value. Farther east, along I9S stations 124–110 define a similar belt of eastward flow over the Ridge, with average depth 3750 m. Its 188 Sv SADCP-referenced transport is enhanced by 58 Sv over the bottom-referenced value. Thus the enhancement factor required at the Passage is not out of line with our estimates downstream for areas where the current is over relatively shallow topography.

Looking west from the Passage, we expect that the approaching deep flow above the sill depth is carried into the passage with its 3400 m transport undiminished rather than decelerating to zero at sill depth in the Passage. In Park et al.'s (1993) SUZIL section near 60ºE in 4500-5000 water well west of the sill, the front spans about 300 km. Using bottom referencing for this 1991 data, the average 3400 m speed normal to the section for that group is 2.9 cm s^{-1}, accounting for 31 Sv in the flow above 3400 m. We expect that this section too should exhibit eastward bottom velocities, increasing the 3400 m speed above that due to the bottom-referenced shear alone. Gille's (2003) estimates, mentioned above, indicate a maximum bottom velocity of 4 cm s^{-1} in the jet near 60ºE, which would add 43 Sv to the frontal group transport above 3400 m in addition to the 31 Sv due to the shear between the bottom and 400 m.

The bottom velocities we estimate at the Passage imply a small but significant eastward transport of dense water through the Passage. At the frontal group of stations in the Passage (e.g. Fig. 17), about 350 km width, the average thickness of water denser than γ^n = 28.15 kg m^{-3} is about 250 m, and a bottom velocity of 2–12 cm s^{-1}, corresponding to the two alternative approaches to the Passage barotropic flow discussed above, would support an eastward transport of 2–6 Sv in that layer. We choose to represent this eastward dense transport as 4 Sv, with the comment that it falls in the warmest part of the dense layer, between 1ºC and the coldest temperature observed in stations near the sill, slightly above 0.7ºC.

Signatures attributable to the deeper flow through the Passage are evident in the property distributions for I8S and I9S. In the Crozet Basin a minimum CFC-11 coincides with the salinity maximum that is the core of the North Atlantic Deep Water. That minimum has concentrations < 0.06 pmol kg^{-1} south of the Polar Front and that diminish northward to <0.04 pmol kg^{-1} at the Polar Front and to < 0.02 pmol kg^{-1} farther north around the Subantarctic Front (in the mid-1993 data reported by Boswell & Smythe-Wright, 2002). Beneath that minimum only a small increase in CFC-11 was observed, to ~ 0.08–0.1 pmol kg^{-1} in the bottom water, as this area is far from the Weddell Gyre

sources for CFC's (Haine, Watson, Liddicoat & Dickson, 1998). With eastward advection carrying such structure eastward, we infer that in the silled Passage at the time of I8S (1.5 years later), the CFC-11 minimum in the compressed band of Fronts would be < 0.02-0.04 pmol kg^{-1}, and the coldest water passing eastward over the sill at 0.7ºC would be only slightly higher, ~ 0.04-0.06 pmol kg^{-1}. In the property sections for I8S and I9S the eastward extension of the salinity maximum (Fig. 5) through the Passage is visible between the Polar and Subantarctic Fronts, with some penetration into the anticyclonic gyre regime in the Subantarctic Zone. The associated CFC-11 minimum is evident (Fig. 7) indicative of Crozet Basin influences rather than the Kerguelen western boundary current, which has higher CFC-11 concentrations. South of the crest of the Southeast Indian Ridge along I8S, in the vertical the minimum character is enhanced through the intrusion of the western boundary current waters beneath the Passage waters, elevating the deeper CFC concentration above levels that could be obtained by advection of any deep water present west of the Passage in the Crozet Basin. On both I8S and I9S the CFC minimum weakens towards the Polar Front, which is the pattern observed in the Crozet Basin. But the values are higher than explainable by pure advection, and likely represent a lateral mixing influence across the Polar Front and Crozet–Kerguelen Confluence with the western boundary current waters. We conclude that this CFC-11 minimum layer is an advective feature enabled by eastward velocity at the sill depth of the Passage.

5.2.2. Flow along and across the Southeast Indian Ridge

In this subsection, we discuss how the eastward flow emerging from the Kerguelen–St. Paul Island Passage negotiates the Southeast Indian Ridge. In the total transport field construction of Fig. 28, we have indicated the Passage flow strength as 181 Sv, based on assuming there is only a limited flow (8 Sv) into the South Australian Basin to the north of St. Paul Island. In the 1987 and 1991 sections across the Passage (Park et al., 1991; 1993) the Subantarctic Front is the central element of the compressed set of fronts, near 46ºS. That front is at essentially the same latitude on I8S as in the Passage. The crest of the Southeast Indian Ridge has swept south from near 41ºS to near 45ºS, and part of the eastward flow through the Passage has crossed over to the north flank of the Ridge. But a substantial part has curved somewhat southwards following the southern flank of the Ridge. The result is that the concentrated flow at the Kerguelen–St. Paul Island Passage, about 350 km wide (Park et al., 1991; 1993), has diverged to about 1300 km width at I8S. For a quantitative discussion of this we focus on the lighter layer, Fig. 30, where the estimated Passage flow is 177 Sv, since the denser layer circulation is dominated by southern sources. In that lighter layer between the Passage and I8S, about 53 Sv crosses the Ridge Crest, with about 124 Sv still south of the crest. An additional 10 Sv eastward flow north of the crest represents anticyclonic recirculation within the Subantarctic Zone closing east of the Passage.

Between I8S and I9S the Ridge crest descends from 2900 m to 3300 m, and sweeps farther south from 45ºS to 50ºS. The continued eastward orientation of the flow leads to more crossing-over of the Ridge crest. At I9S we estimate that about 129 Sv of the 177 Sv Passage-originating light layer flow is north of the Ridge crest with 76 Sv having crossed over between the two sections. Only about 48 Sv is still south of the crest, and most of that, 40 Sv, is immediately south of the crest at I9S, delimited by the reversed flow of the large cyclonic meander/eddy to its south. The remaining 8 Sv passes south of that feature.

Because the Southeast Indian Ridge to the east of I9S ultimately turns southeast to the Balleny Islands off the continental slope of Antarctica (near 165ºE), the throughput across I9S remaining south of the Ridge ultimately must cross the Ridge. WOCE section SR3 (Figs. 20 & 32) enables a exploration of how that last stage of crossing over occurs, but a limited one because of the lack of absolute velocity measurements for much of that section. Phillips and Rintoul (2002) combined moored current and temperature data from an array on the north flank of the Ridge (average water depth 3800 m) with the SR3 hydrographic section data to produce an estimate for the transport for part of the mean synoptic Subantarctic Front near 50.5ºS: a net frontal transport of 116 ± 10 Sv. This represents the sum of estimated flow above the deepest current-meter sampling level, 3320 db (3265 m), and transports below that level determined by assuming deeper speeds equal to the 3320 db speed at each position across the front. That deeper flow amounts to only 1 Sv, colder than about 1ºC (Phillips, personal communication, 2004). They estimate that at this location 14% of the total transport is attributable to the bottom velocity (3265 m). We relate their transport estimate to our I9S estimate by using the criterion they developed for delimiting the segment of the current that their estimate applies to: in the south, 2.9ºC in situ temperature at 780 dbar, and in the north the change of sign of shear from eastward to westward. I9S has a cyclonic eddy in the middle of the band defined by these limits, which we choose to ignore by reporting the net eastward transport from the flow reversal at station 128 to stations 115 or 114 between which their temperature criterion occurs: 87.9 ± 24.6 Sv or 95.9 ± 25.3 Sv. Going one station farther south to 113, the station at the Ridge crest, changes the estimate to 134.7 ± 26.0 Sv, a large change because along I9S their temperature indicator occurs in the northern part of a very strong front near the Ridge crest. We thus find reasonable agreement between their long-duration current measurements, and out SADCP-referenced synoptic section.

Approaching this somewhat differently, in the less dense layer we found that at I9S all but 48 Sv of the 177 Sv from the Passage has crossed over the ridge. Is it possible that the rest of this eastward flow, 48 Sv, ends up north of the Ridge at SR3? Phillips and Rintoul estimated that the limited span of their array means that their transport estimate of 116 Sv represented only 65% the total transport by missing transport on the southern side of the frontal system (based on comparisons

with the bottom-referenced transports for the SR3 repeat sections). Scaling up their 116 Sv absolute transport by that amount yields 178 Sv (which will probably include a few Sv in the dense layer). This suggests that the residual 48 Sv of Passage flow in the lighter layer, still south of the Ridge at I9S, crosses over the Ridge between I9S and SR3. Consistent with this conclusion is the positioning of the Polar Front for the two sections. Along I9S, as noted above, the Polar Front indicators delimit the southern edge of the Passage flow, with the principal Front position between stations 113–112. In the SR3 section shown in Fig. 20 (occupied at the same time as I9S), the Front is at the Ridge crest (and south of the moored array); it is generally co-located in the various SR3 repeats.

The altimeter data of Fig. 19a suggests that the crossing of the Southeast Indian Ridge by the Passage flow involves pathways that are relatively stable for significant longitudinal segments of the Ridge. West of the Passage sea surface height variance is high for the front group approaching the Passage over the deep water of the Crozet Basin, but diminishes into the Passage, with only a weak tongue projecting eastward from the Passage sill. Along and west of I8S, the sea surface height variance is concentrated at the meanders of the Crozet–Kerguelen Confluence, at and south of the Polar Front indicators in Fig. 4a. There is no axis of high variance following the Subantarctic Front from the Passage to its position north of the crest of the Ridge along I8S suggesting relative stationarity of that path. A relative longitudinal minimum in SSH variance is found near 105ºE, with a band of higher variance growing eastward from there on the north side of the Southeast Indian Ridge in the Subantarctic zone. This evolves into a more extensive patch over the Australian–Antarctic Discordance in the area we infer the last stage of crossing over of the Ridge by the Passage flow occurs.

5.2.3. Westward recirculation south of Australia

North of the belt of eastward flow across I9S we estimate a total water column westward flow of 38 Sv, forming the anticyclonic regime. This reflects an unknown combination of recirculation within the eastern South Australian Basin (west of SR3 or Tasmania) and on a longer zonal scale penetrating beyond Tasmania. Rintoul and Bullister (1999), using deepest common level referencing for a 1991 SR3 repeat, estimated a westward 37 Sv westward flow to the south of Tasmania, with a 137 Sv belt of eastward flow to its south between the Subantarctic and Polar Fronts. Rintoul and Sokolov (2001) using a variable reference level (bottom-referenced for most of section, shallow-referenced over the Antarctic continental slope) indicated a six-repeat average of 30 Sv westward flow to the north of a 142 Sv eastward flow between the Fronts. They attributed 22 Sv of this to local Subantarctic Zone recirculation, with the other 8 Sv differentiated as recirculating through the Tasman Basin by its water mass characteristics. The January 1995 SR3 repeat, synoptic with I9S, recorded the largest net transport of 158 Sv, close to our I9S absolute transport estimate of 157 Sv, but probably fortuitous given the referencing differences. In that occupation they found a much

stronger Subantarctic Zone recirculation, 50 Sv, some 12 Sv larger than we estimate at I9S. There is a baroclinic expression for that strengthened recirculation: the maximum thermocline depth, which marks the shear reversal for the baroclinic flow of the recirculation, was about 150 m deeper than along I9S. That defines southward shear between the two sections, and thus a convergence into the eastward belt from the north that intensifies the Subantarctic Zone recirculation eastward from I9S. We have included this in our Fig. 3 circulation schematic as representing the circulation during this time period, although we cannot claim that this eastward intensification of the anticyclone generally occurs

The westward regime south of Tasmania has recently attracted attention as a pathway between the southern South Pacific Ocean and the South Indian Ocean (Rintoul & Sokolov, 2001; Speich & Blanke, 2001; Speich, Blanke, de Vries, Drijfhout, Döös, Ganachaud & Marsh, 2002), with part of that flow coming from a distant origin rather than a locally compact recirculation from the eastward flow south of Tasmania. We have not attempted to parse out of the water mass characteristics at the northern end of I9S to determine the fraction of the recirculation with a more distant origin that the South Australian Basin. Instead, for Fig. 3 we have used the proportions indicated by Rintoul and Sokolov for the 6-section mean, 8 Sv of the average 30, or about 25% linking on longer scale with the South Pacific circulation versus 75% recirculating near Tasmania.

5.2.4. The collision of the western boundary and Fawn Trough currents east of Kerguelen Plateau

The western boundary current off the southern Kerguelen Plateau carries a northwest transport of 48.1 ± 6.3 Sv (0.4, 53.2). This boundary current is dominated by a 32.3 Sv ± 3.7 Sv (0.3, 33.6) transport in the layer denser than γ^n = 28.15 kg m^{-3} (about 1ºC). North of the boundary current, 86.3 ± 17.5 Sv (27.0, 37.5) flows back southeastward through the section, less predominately in the denser layer 45.1 ± 11.1 Sv (8.7, 14.0). This we identify as a retroflection of the western boundary current, with augmentation of its transport. We hypothesize a 38 Sv Fawn Trough Current, with 13 Sv in the dense layer, as the source of this augmentation, ruling out the Kerguelen–St. Paul Passage as the source for two reasons. First, it would require a convoluted pathway southeast from the Kerguelen–St. Paul Island Passage and there is little potential for significant flow out of the Passage in the dense layer. Second, the Fawn Trough pathway is more likely, given its proximity and the presence west of the Trough of waters of the correct properties above sill depth (Fig. 15). This augmentation of the western boundary current by the Fawn Trough Current represents the first stage of the progressive Crozet–Kerguelen Confluence. The offshore turning current carries the combined flow eastward across I8S and may reflect the result of the collision with the Fawn Trough Current or merely reflect a topographic steering of the bottom-intensified western boundary current by the Chun Spur (Fig. 14).

Is a large (38 Sv) transport through Fawn Trough plausible? Sparrow et al. (1996) using a bottom level of no motion and climatological data estimated that the southern branch of the Polar Front represented the core of a 65 Sv eastward transport at 50–60ºE (Fig. 13). The southern branch of the Polar Front as mapped by Sparrow et al. (1996) and Holliday and Read (1998) passes through a hydrographic section along 62ºE from the 1994 ANTARES II expedition (upper ocean characteristics discussed by Park, Charriaud & Fieux, 1998; full water-column data obtained from NODC, 2000). Deep-water isotherms uplift about 700 km across the Front, indicative of a substantial eastward shear. Using a near-bottom level (4687 db, 4594 m) of no motion we estimate 39 Sv eastward total transport for the station pair bracketing the front, with 35 Sv above 2650 m, the sill depth of Fawn Trough. A bottom velocity beneath the front would augment this by about 3 Sv per 1 cm/sec added speed and per 100 km width. Using the average profiles and standard deviations for the area west of Fawn Trough (Figs. 14 and 15) the bottom level of no motion transport is 33.8±9.8 Sv with 30.1±9.5 Sv above 2650 m, again with the possibility of significant augmentation through bottom velocity. Thus there is plenty of eastward transport associated with the southern concentration of flow in the Crozet Basin. We hypothesize that the Fawn Trough Front marks an axis of deep-reaching flow that brings cold deep waters into the Australian–Antarctic Basin at colder temperatures than through the Passage north of Kerguelen.

Precisely characterizing the waters that might flow east across the 2650 m sill of Fawn Trough is difficult, for stations deeper than 1000 m are very scarce around Kerguelen Plateau. We earlier illustrated stations from immediately west of Fawn Trough (Figs. 14 and 15). On average the southern group shows 800 m thickness between γ^n = 28.15 kg m^{-3} and 2650 m, while the northern group has about 110 m. We assume that this layer flows through the Fawn Trough, but even denser water may flow east from the area south of the station group, where there is rather dense water on the flanks of the southern platform of Kerguelen Plateau (e.g. Fig. 9A), including data over the western flank and Banzare Bank. The bottom-referenced total water-column transport estimate at 62ºE from the ANTARES II data was 39 Sv, which includes 3 Sv in the layer denser than γ^n = 28.15 kg m^{-3} but above the Fawn Trough sill depth. The 21–39 Sv range of transport above sill depth from the average stations of Fig. 15 supports a similar few Sv of dense flow. Farther west, at 30ºE Park et al. (2001) used a form of on-station SADCP referencing for a section southward from 54ºS. Eastward bottom velocities of several cm s^{-1} were estimated in the eastward flow regimes. Ultimately, the absence of synoptic station pairs near the sill, and lack of reference speed precludes knowing whether our estimate of 13 Sv dense transport through Fawn Trough is reasonable.

With γ^n = 28.15 kg m^{-3} typically between 1500 and 2500 m west of the southern Kerguelen Plateau, there is a considerable cross sectional area available for flow across the southern Plateau in our lighter layer (the Fawn Trough spans about 400 km at 1500 m depth). While the dense layer

flow will be somewhat bathymetrically confined to the Fawn Trough, the lighter layer need not be a narrow current. Surface temperature and XBT data described by Holliday and Read (1998) do, however, exhibit a frontal character at the Trough, so we choose to represent the total and upper layer eastward flow across the plateau as focused at the Trough in Figs. 28, 30 & 3.

5.2.5. The Crozet–Kerguelen Confluence meander field

The energetic meandering observed along I8S in the Australian–Antarctic Basin is the Crozet–Kerguelen Confluence. The Fawn Trough Current emerges from the Crozet Basin and meets the southern Kerguelen western boundary current, then they merge progressively with the Antarctic Circumpolar Current which has entered the basin via the Kerguelen–St. Paul Island Passage. The eastward turning of the 86 Sv combined flow of western boundary and Fawn Trough currents after their collision is thus the initiation of the meandering Crozet–Kerguelen Confluence.

Our interpretation is that there is a continuation of western boundary current flow off the part of Kerguelen Plateau north of Chun Spur, fed by the return meander of part, 44.8 Sv ± 7.8 Sv (10.3, 28.4), of the combined Fawn Trough and western boundary current flows. That northwestward return retains a strong contribution from the denser layer, 23.3 ± 4.8 Sv (1.8, 13.0). This retroflects southeastward somewhere north of Chun Spur but south of the Gallieni Spur (inferred from the coldest deep waters of this current not being observed northwest of Gallieni Spur in the Passage). It is at this point that the first encounter with waters emerging from the Kerguelen–St. Paul Passage occurs. There is one more cycle of northwest and southeast flow before the Confluence system and the Passage flow complete their crossing of the I8S section. In Fig. 19A, in the western part of the Australian–Antarctic Basin the strongest sea surface height variance is near the eastern flank of the Kerguelen Plateau, west of I8S, north of the Fawn Trough and Chun Spur, but south of the Gallieni Spur in the southern Passage. This is consistent with our schematic's placement of the principal collision of the Passage flow with the western boundary current.

Hydrographic data west of I8S north of Chun Spur along the eastern slope of Kerguelen Plateau is extremely sparse, so there is very little information to guide the regional circulation interpretation. There is a three-station Eltanin group on the east flank of northern Kerguelen Plateau near 51ºS (Fig. 14). Characteristics at these three stations suggest a southern origin consistent with a retroflecting western boundary current having carried the Fawn Trough current waters back to the boundary north of the Spur. The three Eltanin profiles, Fig. 18, show that above 2500 m the temperature – depth relations are bracketed by the profiles from west of Fawn Trough (Fig. 15, overplotted also on Fig. 18). This is consistent with the Fawn Trough Current waters becoming the onshore side of the western boundary current system. Waters below 2500 m in the Eltanin group are colder that the coldest waters observed at the Kerguelen–St. Paul Island Passage sill area (blue curves, Fig. 18), precluding a northern source. Coldest waters flowing through Fawn Trough are

probably warmer than at least 0.3ºC (Fig. 15), and the deeper two of the three Eltanin stations show waters colder than that, indicating the influence of the colder waters present in the deep western boundary current farther south intruding beneath the Fawn Trough Current waters and continuing to be present farther north along the boundary. We therefore retain a western boundary current character to our contoured fields (Figs. 3, note the green contours passing Chun Spur and approaching Gallieni Spur before turning back southeast, 28–30).

In all these meanders of the Crozet–Kerguelen Confluence, deep waters are found that are colder than the estimated sill depth in the Kerguelen–St. Paul Island Passage, indicative of the progressive northward intrusion of the western boundary current and Fawn Trough waters beneath the waters flowing eastward through the Passage. To some degree all of these meanders could be represented with elements of compact eddy recirculation. But I8S in the Australian–Antarctic Basin is more than a cross section of eddies, for as can be seen in Fig. 27 there is a steady gain of eastward transport marching from south to north from the western boundary current, each northwestward current element's strength is weaker than that of the preceding southeastward current element (Table 2). The meandering of a progressive confluence seems the better representation than a field of eddies. Within the confluence the major eastward flow branches are near 56º, 54º and 49ºS.

There are two shifts in the structure of the flow part way through the series of meanders. In the south the dense layer flow generally is in the same direction as the lighter layer, as it is over the upper flank of the southeast Indian Ridge (stations shallower that 4000 m). In between, a single group of stations shows opposing light (southeast) and dense (northwest) flow, stations 48-52 (Table 2). The property sections (Figs. 4–9) show that these stations define the main Polar Front crossings along I8S, and are where the most extensive northward monotonic descent of the γ^n = 28.15 kg m^{-3} surface is observed at about 900 m. The temperature section (Fig. 4A) includes the dense layer transport distribution and reveals the westward bottom flow in the eastward shear regime. It is interesting that the only example of opposing flows in the two layers occurs at the enhanced Polar Front, which, as discussed in section 3.7, is the spot where the dynamic height values suggest the transition from the Kerguelen–St. Paul Passage Waters to the western boundary current regime. In the transport diagrams we have portrayed this circulation anomaly consistently in the three views: a columnar 36 Sv northwest flow separated from a 89 Sv columnar southeast flow farther north by the counterflow group, where 27 Sv lighter layer water flows southeast undercut by 13 Sv denser water flowing northwest, for a net flow of 14 Sv southeast. The counterflow group also is where the highest potential vorticity is found below γ^n = 28.15 kg m^{-3}, which is consistent with the concept that the feature results from the interaction of the dense waters from the south with their first encounter with the densest waters emerging from the Passage into the Basin. While the "details" of the meanders encountered on I8S are undoubtedly synoptic, our analysis of other data in section 3.7.4 sug-

gests it may be typical: the elevated potential vorticity is a feature of the regional climatology extending eastward along the Ridge from this area, which includes other data besides I8S.

The second shift in structure occurs in the same area of the section, beside and linked to the counterflow structural anomaly, and is an area of recirculating dense flow. In the columnar northwest flow adjacent (stations 52–54) to the south of the counterflow group, there is northwest flowing dense water that rather that retroflecting north and east, turns south and east in a closed recirculation cell. Again this might be taken merely as a synoptic detail, but referring again to the sections we note that because the γ^n = 28.15 kg m^{-3} surface north of this feature plunges by 900 m, and the flank of the Ridge is simultaneously rising steeply, there certainly would be a potential vorticity constraint on a northward turn, were the system behaving with purely advective potential vorticity conservation following such a flow. According to our estimates, of the total 25 Sv flowing northeast across the section in the dense layer at this area, 11 Sv turns north beneath the Passage Current, and 14 Sv turns south in the recirculation cell. How the system self-determines the degree of intrusion of the dense water under the Passage waters and the mixing between the layers is an interesting question, but beyond the scope of this paper.

The meandering pathway of the Confluence leads to the intrusion of the cold dense water of the western boundary current and the Fawn Trough Front beneath the light waters entering the Australian–Antarctic Basin through the Kerguelen–St. Paul Island Passage. Table 2 gives the entire sequence of total transports for the Confluence meander system, and the contributions to transport in two denser layers, the Fig. 29 mapped layer $\gamma^n \geq 28.15$ kg m^{-3} layer (≤ 1.0ºC) and a somewhat denser one. Transports are given in both in Sv and as percentage of the total to illustrate its progressively diminishing contribution northward along the section. The $\gamma^n \geq 28.21$ kg m^{-3} layer (≤ 0.7ºC) is selected to preclude any contribution from the flow through the Passage and illustrates the penetration of dense circulation beneath the Passage flow until the layer is laterally truncated by the shoaling flank of the Southeast Indian Ridge near 49ºS (Fig. 9a). The $\gamma^n \geq 28.15$ kg m^{-3} layer (≤ 1.0 ºC) shows similar activity and penetration, to 46ºS. In the transport field for the $\gamma^n \geq 28.15$ kg m^{-3} layer (≤ 1.0ºC) (Fig. 29), 4 Sv of dense water from the south extends all the way to the northeastern corner of the cul-de-sac, east of the Passage sill, and near the southern mouth of the Geelvinck Fracture Zone. This is dominated by $\gamma^n \geq 28.21$ kg m^{-3} water, which undercuts the somewhat lighter waters flowing out of the Kerguelen–St. Paul Island Passage, and accounts for the crossing flow paths in Figs. 3 & 29. Again, this is the point of initiation of the potential vorticity maximum layer described in section 3.7.4.

5.2.6. The connection between the cyclonic gyres of the Weddell–Enderby and Australian–Antarctic Basins

At I9S, the cyclonic circulation is a strong circulation feature with 76 Sv total water-column transport. I8S indicates that there is only partial closure of the gyre in the western Australian–Antarctic Basin, with about 35 Sv turning north and back east: 8 Sv in the Basin interior, 27 Sv directly flowing into the western boundary current. The rest (45 Sv) is inferred as looping through the Weddell–Enderby Basin – before turning northward and returning eastward. The 21 Sv eastward flow in the northern Princess Elizabeth Trough may represent a compact scale retroflection of part of the 45 Sv (Smith, Zhaoqian, Kerry & Wright, 1984; Nunes Vaz & Lennon, 1996; Heywood et al., 1999). The other 24 Sv ultimately returns through the Fawn Trough, possibly representing a larger scale bridge linking cyclonic gyres of the basins west and east of Kerguelen Plateau.

The full water-column circulation in the Weddell–Enderby Basin is well known as a large cyclonic gyre (Deacon, 1976; 1979; Gordon, Martinson & Taylor, 1981), with the Weddell–Scotia Confluence being its boundary with the Antarctic Circumpolar Current flow through the Drake Passage (Deacon & Moorey, 1975; Deacon & Foster, 1977; Patterson & Sievers, 1980). The Australian–Antarctic Basin cyclonic gyre and its Crozet–Kerguelen Confluence is an analogous system. Together the two systems represent a large elongated cyclonic gyre partially interrupted by Kerguelen Plateau, but linked by the 45 Sv within the westward-flowing Antarctic Slope Current in the southern Princess Elizabeth Trough and the compensating eastward flows over the southern Kerguelen Plateau (northern Princess Elizabeth Trough and Fawn Trough). We believe this is an essentially new concept. In 2001, the Southern Ocean's subpolar domain was summarized as having only two substantial cyclonic gyres south of the Antarctic Circumpolar Current, the Weddell Gyre and the Ross Sea Gyre (Figure 4.6.1 in Rintoul, Hughes & Olbers, 2001); while in 2003 Reid (2003) mapped circulation as predominately eastward in the Australian–Antarctic Basin, with little discernable westward flow in the south, and with only weak basin-wide meridional flow in the abyss. The nearly circumpolar aspect of the Antarctic Slope Current has long been recognized (the east wind drift of Deacon, 1937) and was emphasized and detailed in a synthesis (Whitworth III et al., 1998), but without taking "the next step to point out the interconnection between gyres" (personal communication, T. Whitworth, 2005).

Most estimates for the transport intensity of the Weddell Gyre have been determined by using a deepest common level reference. At the Greenwich Meridian, Whitworth and Nowlin (1987) estimated a 17 Sv intensity using a level of no motion at the bottom, but commented that this could be a "considerable underestimate," noting Carmack and Foster's (1975) 97 Sv estimate from 10–30ºW using current-meter referencing. In the latter study, 69 Sv was estimated in the temperature class < 0.0ºC, wholly within our denser than γ^n = 28.15 kg m^{-3} layer. The probability that the gyre transport has been underestimated using a deepest common level is high: Fig. 33 illustrates the baroclinic transport with a bottom level of no motion for I9S, compared with the additive barotropic transport that the SADCP referencing requires. We therefore report on Weddell gyre transport estimates

where direct-velocity measurements have constrained the referencing. Reid (1989) indicated a Weddell gyre strength of only between 20 and 30 Sv in his synthesis treatment of the South Atlantic, and his 2003 paper on the Indian Ocean sector shows a 20 Sv strength at 30ºE. These estimates are weaker that the estimates based on direct velocity referencing.

At the Greenwich Meridian, Schröder and Fahrbach (1999) applied SADCP referencing to a 1996 section to estimate the eastward and westward gyre limbs as 61 and 66 Sv, respectively. This section, and other repeats in earlier years with no SADCP data, had less than half those values as baroclinic estimates with bottom level of no motion. Klatt, Fahrbach, Hoppema and Rohardt (2005) update this work using a much more substantial data set including long time-averages moored current measurements, estimating a westward 56 Sv and eastward 45 Sv gyre limbs at the Greenwich Meridian, indicating that the difference of 11 Sv represented the escape of waters from the gyre into the southern part of the Antarctic Circumpolar Current west of the section. As in the Australian–Antarctic Basin, the northern limb of the gyre flow is in the eastward belt of the circumpolar flow. At the Greenwich Meridian the westward flowing limb strength estimate is 30% smaller that along I9S. We are unaware of any measurements between the Greenwich Meridian and the Antarctic Peninsula (60ºW) that would quantify the gyre strength towards the western boundary, although the Carmack and Foster (1975) estimate of 97 Sv might indicate a western intensification of the gyre.

Closer to Kerguelen, Park and Gamberoni (1995) suggested the Weddell Gyre might extend eastward to 60ºE. Park et al. (2001) applied SADCP referencing to a 1996 section along 30ºE. There they found no westward flowing southern limb in the baroclinic transport relative to a bottom level of no motion. SADCP referencing strengthened the eastward flowing limb and revealed the westward flowing limb, together a 43 Sv gyre, similar to our inference of the strength of the linkage of the circulations west and east of the Kerguelen Plateau. Their westward flow regime like ours is an eastward shear regime transformed to westward flow by the barotropic component.

The picture of cyclonic flow south of the Antarctic Circumpolar Current has evolved with our inference of a 45 Sv "bridge" between the Weddell–Enderby cyclonic gyre and the Australian–Antarctic Basin cyclonic gyre. A very elongated gyre has been revealed, extending from the Antarctic Peninsula in the west near 50ºW eastward to somewhere east of 155ºE, spanning at least 10,000 km with two intensity centers where the transports peak in each basin, with a neck at the longitude of Kerguelen Plateau where the transport bridge is about half the strength of the center east of Kerguelen, and perhaps more than half that of the center west of Kerguelen.

5.2.7. The zonal overturning and the eastward closure of the cyclonic gyre

The estimated circulation in the dense layer (Fig. 29) implies a net light to dense layer transformation east of I9S: the 157 Sv total transport between Australia and Antarctica has a 11 Sv zonal overturning superimposed. This is most directly interpreted as an estimate of the bottom water for-

mation east of the section, and we can construct a scenario for the eastward cyclonic gyre closure as follows. South of the Southeast Indian Ridge along I9S in the deep layer, the 63 Sv westward flow of the Antarctic Slope Current is partly supplied by closing the gyre flow by southward turning of the eastward flow north and south of the anticyclonic eddy (37 + 15 Sv) and partly by the transformation of 11 Sv of the eastward flow of the lighter layer somewhere east of I9S. In the lighter layer, there is only a 13 Sv estimated westward flow in the Antarctic Slope Current, which is then supported by a southward turning of 13 Sv from the 44 Sv eastward flow south of the eddy. Thus we infer that of that 44 Sv eastward flow, 13 recirculates directly in the cyclonic gyre, and 11 indirectly (transformed down into the dense layer). With the deduction that 24 Sv of the I9S light layer flow is tied up with the cyclonic gyre, the net light layer flow northward of that 24 Sv is 157 Sv, which is the throughput transport in that layer.

Thus the characterization of the total transport as a 38 Sv anticyclonic regime, a 157 Sv throughput, and a 76 Sv cyclonic regime can be recast in the two layer framework. The light layer has a 32 Sv anticyclonic regime, a 157 Sv throughput regime, and a 24 Sv cyclonic regime with, somewhere to the east, a loss of 11 Sv through transformation to dense water diminishing its westward limb. The dense layer has a 6 Sv anticyclonic regime in the north, no throughput regime, and a 52 Sv cyclonic regime with, somewhere to the east, a gain of 11 Sv through transformation from light layer water boosting its westward limb.

To what degree does the cyclonic circulation regime east of I9S close within the Australian–Antarctic Basin? The SR3 and P11A sections (Fig.32) cross the eastern part of the Australian–Antarctic Basin (Fig. 1) and are well placed to address the eastern closure of the gyre. The multiple occupations of SR3 enable an estimation of mean baroclinic transports, an advantage over the one-time snapshots of I8S an I9S. Unfortunately the SR3 underway SADCP data could not be used to reference those baroclinic fields. The long-duration moored array (Phillips & Rintoul, 2000; 2002) along this line was placed north of the crest of the Southeast Indian Ridge, enabling the absolute transport estimates discussed in the preceding section, but not helping sort out absolute circulation south of the Ridge.

There is some indirect evidence in SR3 that the deep cyclonic gyre extends eastward through the Australian–Antarctic Basin to the SR3 longitude and beyond, possibly with diminished strength. SR3 shares the following characteristics with I9S: strong eastward baroclinic shear in a broad belt south of the Polar Front and within that shear domain, a water mass transition in the south that on I9S marked the shift from westward to eastward flow. To compare the I9S and SR3 absolute transports requires a direct-velocity reference along SR3. We have shown that the traditional bottom level of no motion within the I9S belt of eastward shear underestimates the intensity of the eastward flow there, 113 Sv using SADCP referencing and only 96 Sv using bottom reference (Fig. 34). Addition-

ally, a surface reference applied south of the water-mass transition along the Antarctic shelf underestimates the westward flow there, 33 Sv using SADCP referencing and only 14 Sv using a surface reference. We note that Rintoul and Bullister (1999) and Rintoul and Sokolov (2001) discuss the need for an off-the-bottom level of no motion along the Antarctic shelf. The traditional level of no motion reference techniques yield a weaker cyclonic gyre – or no gyre at all.

We can compare the sections by applying the same reference scheme with the caveat that we are not calculating the absolute flow field. Along I9S we found a reversal from eastward to westward absolute flow within the regime of eastward baroclinic shear, with a transition in water-mass characteristics at the same location (Figs. 6b, 12, & 34). The SR3 sections contain a similar water-mass transition within the eastward baroclinic shear regime. We take this transition on the 1994 SR3 section to be the point where the absolute flow switches from eastward to westward. Between the two flow reversals the I9S bottom referenced transports are larger for I9S than SR3, 68 Sv versus 47 Sv. This indicates a weaker baroclinic transport for the eastward limb of the gyre, but not necessarily a weaker absolute transport. The eastward flow regime by surface referencing is stronger on SR3, but that section reached to the shelfbreak as opposed to the mid-continental shelf terminus of I9S. Surface referencing works reasonably well for most of the southern regime, but at the water-mass transition it fails because there is a westward barotropic transport of 19 Sv.

The baroclinic structure south of the crest of the Southeast Indian Ridge along P11A resembles I9S and SR3: neutral surfaces reach shallowest levels at the Ridge crest, then reverse slope south of the crest, before reversing again to rise towards Antarctica (Fig. 32). We believe this reflects the same pattern of eastward flow north of the crest, westward flow south of the crest, eastward flow to the south of that, and presumably the regime shift to westward flow on the continental slope. Note that the minimum depths of the neutral surfaces at the Ridge crest in P11A are distinctly less than along SR3, indicating a northward geostrophic shear between the two sections. With a bottom-reference this transforms to northward flow, as diagrammed on Fig. 3. Consistent with that pattern, there is a distinctly larger bottom-referenced eastward transport (Fig. 35) north of the crest along P11A (159 Sv) than along SR3 (131 Sv). Without absolute referencing we can only guess at the cross-ridge transport, subject to the overall constraints to the circulation pattern and amplitude from I8S and I9S; we use an estimate of 30 Sv in the schematic of Fig. 3.

Farther south, with the uncertainty of the strength of westward flow in the southern parts of SR3 and P11A, where the regime shift and I9S ADCP data indicate a dominance of barotropic flow, we have made a fairly arbitrary partition of the fate for the remainder of the eastward flow across I9S associated with the cyclonic gyre. We turn about 25 Sv southwards onto the continental slope between I9S and SR3, and 10 Sv between SR3 and P11A as a partial closure of the cyclonic gyre within the eastern Australian–Antarctic Basin. This yields a residual projection of the cyclonic gyre east-

ward into the central South Pacific in the Ross Sea sector: we indicate 40 Sv westward flow along the Antarctic continental slope, suggesting that, as with the Princess Elizabeth Trough, the cyclonic gyre bridges to the adjacent basin in the South Pacific. On Fig. 3 this means that the two purple and three of the four green contours exiting across the eastern edge of the map ultimately turn southwards east of 150ºE, then return westward to the Australian–Antarctic Basin.

5.2.8. The connection between the cyclonic gyre of the Australian–Antarctic Basin and the Ross Gyre

The next basin to the east of the Australian-Antarctic Basin is the domain of the Ross Gyre, usually depicted as a compact cyclonic gyre tucked into the Ross Sea Antarctic embayment (e.g., Rintoul et al., 2001). Gouretski (1999) has reviewed the regional hydrography and estimated geostrophic flow for the Ross Gyre, using all available hydrographic stations circa 1997 and also using a synoptic survey from 1985–1986 along the crest and north and south flanks of the Pacific–Antarctic Ridge. Deep referenced dynamic height reveals that the belt of strong eastward flow north of the Ridge along P11A, remains aligned with the Ridge eastward to about 150ºW, where one by one dynamic contours turn southwards across the Ridge. These are familiar patterns from earlier studies with sparser data coverage (Gordon & Bye, 1972; Gordon et al., 1978; Gordon & Molinelli, 1982; Olbers et al., 1992). Many of these contours ultimately turn back eastward after this southward offset, projecting eastward above the Amundsen Abyssal Plain; but with some flow turning westward along the Antarctic slope. Only weak gradients are present in the far south area attributed to the Ross Gyre, and this area is bounded in the north by the belt of strong eastward flow along the Ridge, and the east by the baroclinic southward flow east of 150ºE just mentioned.

Gouretski (1999) estimates the belt of eastward flow as 140–160 Sv between 175ºW and 150ºW – his smaller values near 110ºW we interpret as reflecting the presence of the Campbell Plateau south of New Zealand where bottom referencing underestimates flow (Stanton & Morris, 2004). West of the area of baroclinic southward flow, bottom referencing shows no westward flow at all west of 170ºE, and east of there a maximum of only 8 Sv westward flow near 150ºE, there being so little shear over the continental slope. This is a very weak Ross Gyre estimate, and we hypothesize that it reflects the same issues as in the Australian–Antarctic Basin, namely the probability of substantial barotropic flows transforming that weak shear regime to significant westward transport. By the same token, the impression that all the southward baroclinic flow east of 150ºW turns eastward probably is incorrect, and some of that flow may turn back westward along the continental slope, with the westward barotropic flow canceling the eastward baroclinic shear. A study of the South Pacific circulation by Reid (1997) indicated a cyclonic Ross gyre exceeding 20 Sv south of the Antarctic Circumpolar Current, confined to east of the Balleny Islands and west of 90ºW. As for his 2003 treatment of the Australian–Antarctic Basin circulation and (1989) treatment of the South Atlantic, we

suggest that his methodology does not capture and represent the barotropic flows that dominate the regional cyclonic circulations.

To our knowledge, the only large-scale circulation estimates for the southwestern South Pacific south of the Pacific–Antarctic Ridge that use absolute velocity constraints are those reported by Koshlyakov and colleagues (Koshlyakov & Sazhina, 1995; Koshlyakov, Sazhina & Gol'din, 2001). They reference hydrography using SADCP data. Their section is land to land across the South Pacific near 67ºS, enabling bias adjustment to bring the total flow into the closed domain to zero. Unfortunately, the 480 km western boundary crossing (near 165ºE) does not have SADCP, and a mid-depth level of no motion is used instead. This looks like a doubtful choice to us, for while it results in westward bottom-water flow, it causes a considerable eastward flow above that. Significantly, the main section, with SADCP referencing, has top to bottom southward flow, with southward bottom velocity, between 160ºW and 110ºW. Their velocity section indicates an average southward speed of 1 to 2 cm/sec, which gives a rough transport range of 98 to 196 Sv (their tables do not give the geography of the transports in and out of the domain giving only a total inflow of 137 Sv). These large numbers combined with the meridional orientation of deep referenced dynamic height contours in the same longitude leads us to conjecture that the eastern closure of the cyclonic gyre occurs with this southward flow belt between 160ºW and 110ºW followed by westward turning of a fraction of it along the continental slope, with the remainder turning eastward across the South pacific as the southern part of the Antarctic Circumpolar Current. Given our summary quantitative circulation schematic, Fig 3, for consistency, we would estimate that 40 Sv of this southward flow turns west in the southern Ross Gyre and bridges back to the Australian–Antarctic Basin along the Adélie Coast.

5.3. The flow of bottom water from the Australian–Antarctic Basin to the South Australian Basin

The bottom-water transport field is depicted in Fig. 29. A powerful cyclonic circulation dominates this bottom-water layer in the southern Australian–Antarctic Basin, south of 58–60°S. In the northern part of the Basin, flow is weaker and dense water intrudes into the Antarctic Circumpolar Current regime, being found beneath the waters emanating from the Kerguelen–St. Paul Island Passage. This intrusion is tied to the meanders in the Crozet–Kerguelen Confluence. From that intrusion two pathways across the Southeast Indian Ridge are identified, a small leak through the Geelvinck Fracture Zone, and a significant eastward flow through I9S positioned to crossover the Southeast Indian Ridge through the Australian–Antarctic Discordance just east of the section.

5.3.1. Hypothesized northward dense water flow through the Geelvinck Fracture Zone

This deduced bottom-water flow towards the sill of Kerguelen Plateau–St Paul Island Passage partly explains an unexpected aspect of the I8S transport field. In I8S the SADCP referenced transports north of the Southeast Indian Ridge show a 6 Sv net *eastward* transport in the dense layer,

requiring a dense water source to the west. Measurements of water characteristics near the saddle between the Broken and Southeast Indian Ridges do not reveal waters indicative a Mid-Indian Ocean Basin source this dense (Reid, 2003). Looking south, there are two possible sources, the densest waters flowing into the Kerguelen–St. Paul Island Passage from the Crozet Basin, and the waters from the western boundary current system east of Kerguelen Plateau that intrude northwest to the Passage sill area. The southwestward projection of the southeast wall of the Geelvinck Fracture Zone wall from the Ridge to the Kerguelen Plateau actually seems to form the sill between the Ridge and Kerguelen Plateau, with the bathymetry database indicating it is numerously interrupted at the 3400 m contour (Fig. 16).

We hypothesize that the 4 Sv eastward bottom flow we estimate in the Passage immediately west of the Passage sill splits with 2 Sv flowing east and 2 Sv diverted northeast through the Fracture Zone to contribute to the 6 Sv eastward deep transport that we estimate north of the Ridge. The rest (4 Sv) of that eastward transport we indicate as originating from the Australian–Antarctic Basin side of the sill, deduced because the coldest waters flowing eastward north of the Ridge are in the range 0.64–0.70ºC, slightly colder than the coldest waters west of the sill. We would expect that these waters enter the Fracture Zone at colder temperatures and are warmed through vertical mixing before exiting in the north – the fracture zone is about 600 km long at 3400 m depth. In the dense layer schematic, Fig. 29, the combination of these two dense water deliveries requires artificially "crossing" streamlines to represent flow path differences within the dense layer, rather than dicing up the layer into separate circulation schematics for temperature subdivisions within the layer.

As support for this notion of flow through the Geelvinck Fracture Zone, Fig. 31 shows density–depth and temperature–depth plots of three groups of stations (positions on Fig. 16). One is just west of the sill in the Kerguelen Plateau–St Paul Island Passage, and is the northern part of the 1991 section (Fig. 17) reported by (Park et al., 1993); the maximum depths of these stations, 3250–3650 m, bracket the sill depth to their east. The other two groups, from 1972 Eltanin data and I8S, are stations in the same depth range along the southern flank of the Southeast Indian Ridge east of the mouth of the Geelvinck Fracture Zone. The plots indicate two features of note. First, east of the sill the northward intrusion of cold dense water from the south has penetrated up the flank of the Ridge so that bottom temperatures are distinctly colder than west of the sill, cold enough to provide the sought-for bottom-water characteristics in western part of the South Australian Basin. In particular note the 1.0ºC isotherm typically between 3000 and 3200 m, well above the blocking depth of the wall projection of the Geelvinck wall across the Passage. Second, there is a substantial zonal density gradient along the Ridge in this bathymetric depth range. This is part of a full-water-column density gradient that at shallower levels is the geostrophic shear signature of a cross-Ridge flow component above the Ridge crest. Recall that part of the flow through the Kerguelen Plateau–St Paul Island

Passage crosses the Ridge crest before reaching I9S (discussed in section 5.2.2). For the Geelvinck Fracture Zone, whose sill depth is similar to that of the Kerguelen Plateau–St Paul Island Passage, and much deeper than the Ridge crest, this density gradient crosses the mouth of the Fracture Zone. It is a northward shear that below the nominal Ridge crest depth could indicate geostrophic flow towards the Fracture Zone – and through it. We have not found any deep data nearer to or within the Geelvinck Fracture Zone to better establish conditions.

5.3.2. Escape of dense water out of the cyclonic gyre in the Australian–Antarctic Basin

The deep water transport evolution within the Crozet–Kerguelen Confluence reveals the progressive descent and intrusion of dense waters of southern origin beneath lighter waters principally from the Crozet Basin (sections 5.2.4 & 5.2.5). This culminates with the counter-flowing layers southeast of the Kerguelen–St. Paul Island Passage. Of the 63 Sv westward flow of dense water in the southern limb of the cyclonic gyre, 34 Sv turns north east of Kerguelen and is boosted by 22 Sv from eastward flows through the Princess Elizabeth Trough (7 Sv), the Fawn Trough (13 Sv) and the Kerguelen–St. Paul Island Passage (2 Sv). Of that combined 56 Sv only about 37 Sv flows back eastward across I9S within the eastward flow concentration near 60ºS. We estimate (section 5.3.1) 4 Sv escapes through the Geelvinck Fracture Zone. The other 15 Sv is "deeply submerged beneath the Antarctic Circumpolar Current north of the large eddy/meander. An estimate of the fraction of that dense water that has completed its escape from the cyclonic gyre by I9S is made by locating the zero of the total transport stream function: as noted before it lies immediately south of the eddy/meander between stations 103–104. Interpolating the zero, we find the integral southwards across the depth integrated "gyre" has a net westward 31 Sv and a net eastward 31 Sv dense flow. Thus we infer that west of I9S 31 Sv of dense flow has intruded under 31 Sv of light flow along the zero stream function pathway marking the cyclonic gyre of the total transport.

The Fawn Trough Current and the counterflow in the Princess Elizabeth Trough account for some of that net dense layer export from the barotropic cyclonic gyre: along I8S the first zero of the total transport stream function northward from Antarctica falls between stations 61–62, in the eastward current that results from the Fawn Trough and western boundary currents' collision. Again interpolating to the zero, we find a net westward 18 Sv dense layer flow and a net eastward 18 Sv light layer flow. Thus 18 Sv of the total 31 Sv exchange reflects exchange flow between the Australian–Antarctic and Weddell–Enderby Basins within the total transport cyclonic gyre system linking the two basins. Along I9S the zero stream function meanders back west and returns east between stations 45–55, and the exchange rises from 18 to 23 Sv. An additional 9 Sv exchange across the zero of the total transport stream function is inferred to occur between the sections to elevate the escape of dense water from the cyclonic gyre from to the 31 Sv estimated at I9S.

What is the fate of the dense water that has escaped the total transport cyclonic gyre into the domain of the circumpolar throughput? As noted in the preceding section, there is a net export of 2 Sv dense water into the Geelvinck Fracture Zone from the northwest corner of the Australian–Antarctic Basin, leaving 29 Sv to be accounted for. We find 14 Sv of it passing south of the eddy/meander feature along I9S and the other 15 in the strong eastward current just south of the Southeast Indian Ridge crest.

Our inference is that although that 29 Sv of dense layer is at I9S north of the zero stream function of the total transport field, it ultimately returns into the cyclonic gyre, either within the Australian–Antarctic Basin, or more distantly after crossing over to the South Australian Basin and flowing to the South Pacific. The explanation for this odd result lies our use of $\gamma^n \geq 28.15$ kg m^{-3} as our dense layer, which as it turns out masks some of the differences in circulation for the coldest waters within that layer. This lead to the artifice of crossing streamlines in the northwest corner of the Australian–Antarctic Basin in Fig. 29, and to a second such feature we indicate in the Australian–Antarctic Discordance area of the figure immediately east of I9S. For the dense layer as a whole, north of the Ridge the east–west flows cancel, and with no net flow, there is no requirement for flow from south of the Ridge to turn north across the Discordance and back west through the northern I9S within the South Australian Basin, although it might crossover and flow east north of the Ridge towards SR3. In Figs 4 and 9 the temperature and neutral density sections show a considerable area of water colder than 0.5ºC and $\gamma^n \geq 28.15$ kg m^{-3} well north of the Ridge crest that can only have gotten there by exactly that sort of retroflecting turn through the Australian–Antarctic Discordance. Our SADCP referencing of I9S gives a net westward flow of 4 Sv for this area of the section, and immediately south of the Ridge there is an ample 9 Sv eastward transport this dense between the crest and the eddy Meander feature farther south, well positioned to cross the Ridge at the Australian–Antarctic Discordance. North of the crest somewhat less dense water, $28.21 \geq \gamma^n \geq 28.15$ kg m^{-3} compensates that westward flow with a 4 Sv net eastward flow, accounting for the zero net flow for the full layer. We represent this in Fig. 29 with crossing streamlines to the east of I9S feeding the denser water (dashed contour) from the concentrated eastward flow regime just south of the crest to where we find its strongest westward flow south of Australia, crossing under the not so dense water (dotted contour) where its eastward flow is most concentrated immediately north of the Ridge crest. We include a similar representation in the overall schematic of Fig. 3. The net 6 Sv export of dense layer flow into the Perth Basin we estimate from the zonal convergence represents the 4 Sv of water colder that 0.5ºC flowing west through I9S and turning north into the Perth Basin, and a north-turning 2 Sv of the 6 Sv flow from the Geelvinck Fracture Zone waters, which in the western part of the South Australian Basin is all warmer than 0.5ºC and in the $28.21 \geq \gamma^n \geq 28.15$ kg m^{-3} range. Its other 4 Sv flows along the northern flank of the Ridge and across I9S. The most direct

estimate for the deep flow into the Perth Basin is the recent one by Sloyan (2006) using a WOCE current meter array, an annual average 4.4–5.8 Sv northward flow below γ^n = 28.1 kg m^{-3}, with around half of that, 2.0–2.9 Sv, being very dense, $\gamma^n \geq 28.2$ kg m^{-3}.

Along I9S, the South Australian Basin deepens to greater than 5300 m depth in the northern portion of the Basin. The eastward shoaling of the South Australian Basin topography from I9S to SR3 probably limits the amount of bottom water denser than γ^n = 28.15 kg m^{-3} flowing across SR3. The sill depth between the Tasman Rise and the Southeast Indian Ridge is around 4150 m. The γ^n = 28.21 kg m^{-3} surface does not reach that sill, Fig. 32, but south of the Ridge there is a considerable thickness of water that dense. We surmise that only the 4 Sv retroflection of that dense water across the Discordance described above occurs and that the other 5 Sv flowing east through I9S south of the Ridge may remain south of the Ridge. But since the coldest waters north of the Discordance are significantly warmer than those delivered to the rough topography of the sill (Fig. 24), we could invoke diapycnal processes and assert that some additional part of the $\gamma^n \geq 28.21$ kg m^{-3} water turns across the Discordance and flows east to SR3, warming above 0.5ºC en route. This would represent another internal evolution within the $\gamma^n \geq 28.15$ kg m^{-3} layer. That layer retains a typical thickness of 500 m along the northern flank of the Southeast Indian Ridge, present throughout the eastward shear regime, but attenuated in the westward shear regime near Tasmania, Fig. 32. For that layer if the full 15 Sv still south of the Ridge crest along I9S crosses over, the eastward flow immediately north of the Ridge eastward of the Discordance would total 21 Sv. We estimate only 6 Sv recirculating back west farther north along I9S. The remainder, ~ 15 Sv, then would represent a net export to the Tasman Basin north of the Ridge. Phillips and Rintoul's current-meter based estimates include only 1 Sv of water this cold (Phillips, personal communication, 2004), so if this flow exists it would fall in the deeper region between their array and Tasman Rise (Fig. 32).

While the densest waters of the South Australian Basin are blocked by the sill south of Tasmania from entering the Tasman Basin, P11 (Fig. 32) shows a considerable area denser than γ^n = 28.21 kg m^{-3} indicating that there is dense water flowing over the Southeast Indian Ridge in the southeastern corner. The Ridge crest is rather deep there, > 2500 m, and that neutral surface lies some 1000 m above the crest. The absence of water this dense north of the Ridge along SR3 precludes an east-west flow through the area between the Ridge and Tasmania.

6. Conclusions

ADCP measurements reveal a surprisingly vigorous circulation in the Australian sector of the Southern Ocean. Traditionally, Southern Ocean transport estimates are made with a deepest common level applied to geostrophic shears. Generally, this yields transports comparable to measured transport at Drake Passage – or in the case of the Australian sector the Drake Passage transport plus a compensation for the Indonesian throughflow. The ADCP data from two sections south and south-

west of Australia show that the deepest common level referencing underestimates the eastward transport elements and misses westward transport elements.

Here are the principal circulation elements that largely shape the circulation field that we have mapped on Fig. 3:

A strong cyclonic gyre is revealed south of the belt of eastward transport attributable to the Antarctic Circumpolar Current. The gyre's eastward limb is parallel to the Circumpolar Current, and is part of a belt of eastward transport that reaches 271 ± 49 Sv south of western Australia, significantly larger, by more than 120 Sv, than the combined Drake Passage and Indonesian throughflow compensation. The opposing limb of the cyclonic gyre is a 76 ± 26 Sv westward flowing Antarctic Slope Current. To the north of the eastern transport belt 38 ± 30 Sv flows west as part of the an Indian Ocean Subantarctic Zone recirculation gyre. The resulting net flow south of Australia is 157 ± 58 Sv, a number similar to deepest common level referenced net transport of 180 Sv (provided an allowance is made for the missed westward transport of the Antarctic Slope Current unsampled south of the section). But the resulting circulation fields are very different because that approach significantly underestimates the eastward flow strength in the cyclonic gyre and underestimates or even reverses the westward flow in the far south.

The cyclonic gyre partially closes with northward flow in a western boundary current off the east coast of Kerguelen Plateau. That current's initial transport, 48 ±6 Sv near 58ºS, is boosted by 38 Sv of eastward transport through the Fawn Trough, which bisects the Plateau near 56ºS. The combined flow, 86 ±18 Sv encounters the Antarctic Circumpolar Current and other eastward flowing waters (total 181 Sv) that enter the Australian–Antarctic Basin through the Kerguelen–St Paul Island Passage north of Kerguelen Plateau. That encounter is an energetic Crozet–Kerguelen Confluence that meanders northeast from 54ºS.

The cyclonic gyre's closure within the Australian–Antarctic Basin is only about 40% of the maximum gyre transport. The other 60% of the transport is linked to the Weddell Gyre west of Kerguelen Plateau. That gyre may approach 100 Sv amplitude, although the most recent best estimate is 56 ±8 Sv (Klatt et al., 2005). Together the two gyres represent an elongated cyclonic system with two transport centers, one in each basin, and with a connecting bridge of 60% of the maximum strength, comprised of a westward flow over the Antarctic continental slope in the southern Princess Elizabeth Trough, and eastward transports in the northern Princess Elizabeth Trough and through the Fawn Trough. The cyclonic gyre appears to be only partly diminished in the eastern Australian–Antarctic Basin, by our interpretation of sections near 140ºE and 160ºE, and is inferred as having a projection into the Ross Gyre of the Pacific sector of the Southern Ocean perhaps reaching 40 Sv.

Dense bottom water is carried around the cyclonic gyre within the Australian–Antarctic Basin. Along the Crozet–Kerguelen Confluence the bottom water is folded under the lighter Antarctic Circumpolar Current waters flowing through the Kerguelen–St. Paul Island Passage, an interaction producing a vertical mixing signature in the potential vorticity distribution. Bottom water escapes the Australian–Antarctic Basin by two pathways, the long recognized pathway across the Southeast Indian Ridge at the Australian–Antarctic Discordance, where a transport of 4 Sv is estimated to cross-over the Ridge to flow northwest to the Perth Basin, and a 6 Sv flow hypothesized through the Geelvinck Fracture Zone which is a narrow passage penetrating the Ridge Northeast of Kerguelen Island, with 2 Sv of that flow delivered to the Perth Basin.

The least well determined/ observed parts of the system are the westward flow along the Antarctic continental slope, the separation point and other structural aspects of the western boundary current system off the Kerguelen Plateau, the speculated northward dense flow through the Geelvinck Fracture Zone, the structure an amplitude of flows crossing the Southeast Indian Ridge at the Antarctic Discordance and the nature of the eastward closure of the cyclonic gyre.

Acknowledgments

The analysis by MSM and KAD reported here was supported by the National Science Foundation under grants OCE 0118410 and OCE 0117601, respectively. The efforts of the many participants in the cruises we described and interpret here are gratefully acknowledged, particularly MSM's co-chief scientist Tom Whitworth on the long arduous I8S/I9S expedition, Eric Firing for his careful work on its ADCP and LADCP datasets which have proved to be the key to unlocking the regional circulation, Captain Paul Howland and the fine crew of the R/V Knorr, and the WHOI CTD operations team lead by Marshall Swartz and Laura Goepfert with water sample process ably done by Joseph Jennings, George Knapp, and Toshiko Turner. Gwyneth Packard (né Hufford) helped considerably on the cruise and with the first stages of the interpretation. This is contribution number 11368 of the Woods Hole Oceanographic Institution.

References

Agra, C. & Nof, D. (1993). Collision and separation of boundary currents. *Deep-Sea Research, Part I*, *40*, 2259-2282.

Belkin, I. M. & Gordon, A. L. (1996). Southern Ocean fronts from the Greenwich meridian to Tasmania. *Journal of Geophysical Research*, *101*, 3675-3696.

Bindoff, N. L., Rosenberg, M. A. & Warner, M. J. (2000). On the circulation and water masses over the Antarctic continental slope and rise between 80 and 150ºE. *Deep-Sea Research II*, *47*, 2299-2326.

Boswell, S. M. & Smythe-Wright, D. (2002). The tracer signature of Antarctic Bottom Water and its spread in the Southwest Indian Ocean: Part I, CFC-derived translation rate and topographic control around the Southwest Indian Ridge and the Conrad Rise. *Deep-Sea Research. Part 1: Oceanographic Research Papers 49 (3): pp. 555-573; Pergamon, Oxford, International; 61 refs.*: International.

Bye, J. A. T. (1972). Oceanic circulation South of Australia. In: Ed. D. E. Hayes, *Antarctic Oceanology II: The Australian-New Zealand Sector*. *Antarctic Research Series Vol. 19*, (pp. 95-100). American Geophysical Union: Washington DC.

Callahan, J. E. (1971). Velocity structure and flux of the Antarctic Circumpolar Current south of Australia. *Journal of Geophysical Research*, *76*, 5859-5864.

Carmack, E. C. (1973). Silicate and potential temperature in the deep and bottom waters of the western Weddell Sea. *Deep Sea Research*, *20*, 927-932.

Carmack, E. C. & Foster, T. D. (1975). On the flow of water out of the Weddell Sea. *Deep-Sea Research*, *22*, 711-724.

Cunningham, S. A., Alderson, S. G., King, B. A. & Brandon, M. A. (2003). Transport and variability of the Antarctic Circumpolar Current in Drake Passage. *Journal of Geophysical Research C: Oceans*, *108*, SOV 11-1 - 11-17.

Deacon, G. E. R. (1937). The hydrology of the Southern Ocean. *Cambridge University Press*, *15*, 1-124, ill. maps, plates.

Deacon, G. E. R. (1976). Cyclonic circulation in the Weddell Sea. *Deep-Sea Research*, *23*, 125-126.

Deacon, G. E. R. (1979). Weddell gyre. *Deep-Sea Research*, *26*, 981-995.

Deacon, G. E. R. & Foster, T. D. (1977). Boundary region between the Weddell Sea and Drake Passage currents. *Deep-Sea Research*, *24*, 505-510.

Deacon, G. E. R. & Moorey, J. A. (1975). Boundary region between currents from the Weddell Sea and Drake Passage. *Deep-Sea Research*, *22*, 265-268.

Dengler, M., Fischer, J., Quadfasel, D. & Schott, F. (2002). Abyssal circulation in the Somali Basin. *Deep-Sea Research Part II: Topical Studies in Oceanography*, *49*, 1297-1322.

Dezileau, L., Bareille, G., Reyss, J. L. & Lemoine, F. (2000). Evidence for strong sediment redistribution by bottom currents along the southeast Indian ridge. *Deep-Sea Research*, *47*, 1899-1936.

Donohue, K. A., Firing, E. & Chen, S. (2001). Absolute geostrophic velocity within the Subantarctic Front in the Pacific Ocean. *Journal of Geophysical Research*, *106*, 19,869-19,882.

Donohue, K. A., Hufford, G. E. & McCartney, M. S. (1999). Sources and transport of the deep western boundary current east of the Kerguelen Plateau. *Geophysical Research Letters*, *26*, 851-854.

Ducet, N., Le Traon, P. Y. & Reverdin, G. (2000). Global high-resolution mapping of ocean circulation from TOPEX/Poseidon and ERS-1 and -2. *Journal of Geophysical Research*, *105*, 19,477-19,498.

Edmond, J. M., Jacobs, S. S., Gordon, A. L., Mantyla, A. W. & Weiss, R. F. (1979). Water column anomalies in dissolved silica over opaline pelagic sediments and the origin of the deep silica maximum. *Journal of Geophysical Research*, *84*, 7809-7826.

Egbert, G. D. (1997). Tidal data inversion: Interpolation and inference. *Progress In Oceanography*, *40*, 53-80.

Egbert, G. D., Bennett, A. F. & Foreman, M. G. G. (1994). TOPEX/POSEIDON tides estimated using a global inverse model. *Journal of Geophysical Research*, *99*, 24,821-24,852.

Fine, R. A. (1993). Circulation of Antarctic intermediate water in the South Indian Ocean. *Deep-Sea Research I*, *40*, 2021-2042.

Fine, R. A., Maillet, K. A., Sullivan, K. F. & Willey, D. (2001). Circulation and ventilation flux of the Pacific Ocean. *Journal of Geophysical Research C: Oceans*, *106*, 22159-22178.

Fischer, J. & Visbeck, M. (1993). Deep velocity profiling with self-contained ADCPs. *Journal of Atmospheric & Oceanic Technology*, *10*, 764-773.

Frew, R. D., Heywood, K. J. & Dennis, P. F. (1995). Oxygen isotope study of water masses in the Princess Elizabeth Trough, Antarctica. *Marine Chemistry*, *49*, 141-153.

Fukamachi, Y., Ushio, S., Takahashi, A., Oikawa, K., Furukawa, T., Yoritaka, H., Fukuchi, M., Yamanouchi, T., Wakatsuchi, M., Taira, K. & Kitagawa, S. (2000). Seasonal variability of bottom water properties off Adelie Land, Antarctica. *Journal of Geophysical Research C: Oceans*, *105*, 6531-6540.

Ganachaud, A. (2003). Large-scale mass transports, water mass formation, and diffusivities estimated from World Ocean Circulation Experiment (WOCE) hydrographic data. *Journal of Geophysical Research 108*, 6-1 - 6-24.

Ganachaud, A., Wunsch, C., Marotzke, J. & Toole, J. (2000). Meridional overturning and large-scale circulation of the Indian Ocean. *Journal of Geophysical Research 105*, 26117-26134.

Garrett, C. & Munk, W. H. (1972). Space-time scales of internal waves. *Geophysical Fluid Dynamics*, *3*, 225-264.

GEBCO (2005). Gazetteer of Undersea Feature Names - December 2005. http://www.ngdc.noaa.gov/mgg/gebco/). IHO-IOC.

Gille, S. T. (2003). Float observations of the Southern Ocean. Part I: Estimating mean fields, bottom velocities, and topographic steering. *Journal of Physical Oceanography*, *33*, 1167-1181.

Gordon, A. L. (2001). Interocean Exchange. In: Eds. G. Siedler, J. Church & J. Gould, *Ocean circulation and climate; observing and modelling the global ocean*. *International Geophysics Series Vol. 77*, (pp. 303-314). Academic Press: San Diego-San Francisco-New York-Boston-London-Sydney-Tokyo.

Gordon, A. L. & Bye, J. A. T. (1972). Surface dynamic topography of Antarctic waters. *Journal of Geophysical Research*, *77*, 5,993-5,999.

Gordon, A. L., Martinson, D. G. & Taylor, H. W. (1981). The wind-driven circulation in the Weddell-Enderby Basin. *Deep-Sea Research*, *28*, 151-163.

Gordon, A. L., Molinelli, E. & Baker, T. (1978). Large-scale relative dynamic topography of the Southern Ocean. *Journal of Geophysical Research*, *83*, 3,023-3,032.

Gordon, A. L. & Molinelli, E. J. (1982). Southern Ocean Atlas. *Columbia University Press*, 11 pp., 233 plates.

Gordon, A. L. & Tchernia, P. (1972). Waters of the continental margin off the Adélie Coast Antarctic. In: Ed. D. E. Hayes, *Antarctic Oceanology II: The Australian-New Zealand Sector*. *Antarctic Research Series Vol. 19*, (pp. 59-69). American Geophysical Society: Washington DC.

Gouretski, V. (1999). The large-scale thermohaline circulation of the Ross Sea. In: Eds. G. Spezie & G. M. R. Manzella, *Oceanography of the Ross Sea, Antarctica.*, (pp. 77-100). Springer-Verlag: Milan, Italy.

Gouretski, V. & Jancke, K. (1998). A new climatology for the World Ocean. *WHP SAC Technical Report*). WOCE Special Analysis Centre, Max Planck Institute: Hamburg, Germany.

Hacker, P., Firing, E., Wilson, W. D. & Molinari, R. (1996). Direct observations of the current structure east of the Bahamas. *Geophysical Research Letters*, *23*, 1127-1130.

Haine, T. W. N., Watson, A. J., Liddicoat, M. I. & Dickson, R. R. (1998). The flow of Antarctic bottom water to the southwest Indian Ocean estimated using CFCs. *Journal of Geophysical Research 103*, 27,637-27,653.

Hall, M. M., Joyce, T. M., Pickart, R. S., Smethie, W. M. & Torres, D. J. (2004). Zonal Circulation across 52°W in the North Atlantic. *Journal of Geophysical Research*, *109*, doi:10.1029/2003JC002103.

Heywood, K. J., Sparrow, M. D., Brown, J. & Dickson, R. R. (1999). Frontal structure and Antarctic Bottom Water flow through the Princess Elizabeth Trough, Antarctica. *Deep-Sea Research 46*, 1181-1200.

Holliday, N. P. & Read, J. F. (1998). Surface oceanic fronts between Africa and Antarctica. *Deep-Sea Research 45*, 217-238.

Houtz, R. E., Hayes, D. E. & Markl, R. G. (1977). Kerguelen Plateau bathymetry, sediment distribution and crustal structure. *Marine Geology*, *15*, 95-130.

Hufford, G. E., McCartney, M. S. & Donohue, K. A. (1997). Northern boundary currents and adjacent recirculations off southwestern Australia. *Geophysical Research Letters*, *24*, 2797-2800.

Jackett, D. R. & McDougall, T. J. (1997). A neutral density variable for the world's oceans. *Journal of Physical Oceanography*, *27*, 237-263.

Joyce, T. M. (1989). On In Situ "Calibration" of Shipboard ADCPs. *Journal of Atmospheric and Oceanic Technology*, *6*, 169-172.

Joyce, T. M., Hernandez-Guerra, A. & Smethie, W. M. (2001). Zonal Circulation in the NW Atlantic and Carribbean from a meridional World Ocean Circulation Experiment hydrographic section at 66°W. *Journal of Geophysical Research*, *106*, 22095 - 22113.

Kennett, J. P. & Watkins, N. D. (1976). Regional deep-sea dynamic processes recorded by late Cenozoic sediments of the southeastern Indian Ocean. *Geological Society of America Bulletin*, *87*, 321-339.

King, B. A. & Cooper, E. B. (1993). Comparison of ship's heading determined from an array of GPS antennas with heading from conventional gyrocompass measurements. *Deep-Sea Research I*, *40*, 2207-2216.

Klatt, O., Fahrbach, E., Hoppema, M. & Rohardt, G. (2005). The transport of the Weddell Gyre across the Prime Meridian. *Deep Sea Research Part II: Topical Studies in Oceanography*, *52*, 513-528.

Kobayashi, T. & Suga, T. (2006). The Indian Ocean HydroBase: A high-quality climatological dataset for the Indian Ocean. *Progress In Oceanography*, *68*, 75-114.

Kolla, V., Henderson, L., Sullivan, L. & Biscaye, P. E. (1978). Recent sedimentation in the Southeast Indian Ocean with special reference to the effects of Antarctic Bottom Water circulation. *Marine Geology*, *27*, 1-7.

Kolla, V., Sullivan, L., Streeter, S. S. & Langseth, M. G. (1976). Spreading of Antarctic Bottom Water and its effects on the floor of the Indian Ocean inferred from bottom-water potential temperature, turbidity, and sea-floor photography. *Marine Geology*, *21*, 171-189.

Koshlyakov, M. N. & Sazhina, T. G. (1995). Meridional Volume and Heat Transport in the Pacific Sector of the Antarctic. *International WOCE Newsletter*, *18*, 3-6.

Koshlyakov, M. N., Sazhina, T. G. & Gol'din, A. Y. (2001). Pacific Antarctic cell of the Global oceanic conveyer. *Izvestiya - Atmospheric and Ocean Physics*, *37*, 482-489.

Le Traon, P. Y. & Dibarboure, G. (1999). Mesoscale mapping capabilities of multiple-satellite altimeter missions. *Journal of Atmospheric and Oceanic Technology*, *16*, 1208-1223.

Lebedev, I. & Nof, D. (1996). The drifting confluence zone. *Journal of Physical Oceanography*, *26*, 2429-2448.

Lebedev, I. & Nof, D. (1997). Collision of boundary currents: beyond a steady state. *Deep-Sea Research, Part I*, *44*, 771-791.

Levitus, S. & Boyer, T. (1994). World Ocean Atlas 1994. *Technical Report NOAA*, 201.

Lozier, M. S., McCartney, M. S. & Owens, W. B. (1994). Anomalous anomalies in averaged hydrographic data. *Journal of Physical Oceanography*, *24*, 2624-2638.

Lozier, M. S., Owens, W. B. & Curry, R. G. (1995). The climatology of the North Atlantic. *Progress In Oceanography*, *36*, 1-44.

Macdonald, A. M. (1998). The global ocean circulation: a hydrographic estimate and regional analysis. *Progress In Oceanography*, *41*, 281-382.

Mantyla, A. W. & Reid, J. L. (1995). On the origins of deep and bottom waters of the Indian Ocean. *Journal of Geophysical Research*, *100*, 2417-2439.

McCarthy, M. C. & Talley, L. D. (1999). Three-dimensional isoneutral potential vorticity structure in the Indian Ocean. *Journal of Geophysical Research 104*, 13,251-13,267.

McCartney, M. S. (1976). The interaction of zonal currents with topography and applications to the Southern Ocean. *Deep-Sea Research*, *23*, 413-427.

McCartney, M. S. (1977). Subantarctic mode water. *A Voyage of Discovery, Supplement to Deep-Sea Research*, *George Deacon 70th Anniversary Volume*, 103-119.

McCartney, M. S. (1982). The subtropical recirculation of mode waters. *Journal of Marine Research*, *Supplement to 40*, 427-464.

Middleton, J. F. & Cirano, M. (2002). A northern boundary current along Australia's southern shelves: The Flinders Current. *Journal of Geophysical Research 107*, 12-1 - 12-11.

Middleton, J. F. & Platov, G. (2003). The mean summertime circulation along Australia's southern shelves: A numerical study. *Journal of Physical Oceanography*, *33*, 2270-2287.

Morrow, R., Rintoul, S. R., Donguy, J. R. & Chaigneau, A. (2004). Cold-core anomalies at the subantarctic front, south of Tasmania. *Deep-Sea Research Part I: Oceanographic Research Papers*, *51*, 1417-1440.

NODC (1998). *World Ocean Database 1998*. *World Ocean Database 1998*. NOAA National Oceanographic Data Center's Ocean Climate Laboratory: Silver Spring, MD.

NODC (2000). Online World Ocean Database 1998, (pp. no). NOAA National Oceanographic Data Center's Climate Laboratory: Silver Spring, MD.

Nunes Vaz, R. A. & Lennon, G. W. (1996). Physical oceanography of the Prydz Bay region of Antarctic waters. *Deep-Sea Research, Part I*, *43*, 603-641.

Olbers, D., Gouretski, V., Seiß, G. & Schröter, J. (1992). Hydrographic atlas of the Southern Ocean. *Bremerhaven, Germany. Alfred Wegener Institute, 1992, xvii, 82 plates (including 12 in pocket), maps; 62 cm*). Alfred Wegener Institute.

Orsi, A. H., Johnson, G. C. & Bullister, J. L. (1999). Circulation, mixing, and production of Antarctic Bottom Water. *Progress In Oceanography*, *43*, 55-109.

Orsi, A. H., Whitworth III, T. & Nowlin, W. D., Jr. (1995). On the meridional extent and fronts of the Antarctic Circumpolar Current. *Deep-Sea Research I*, *42*, 641-673.

Park, Y. H., Charriaud, E., Craneguy, P. & Kartavtseff, A. (2001). Fronts, transport, and Weddell Gyre at 30ºE between Africa and Antartica. *Journal of Geophysical Research 106*, 2857-2879.

Park, Y.-H., Charriaud, E. & Fieux, M. (1998). Thermohaline structure of the Antarctic Surface Water/Winter Water in the Indian sector of the Southern Ocean. *Journal of Marine Systems*, *17*, 5-23.

Park, Y. H. & Gamberoni, L. (1995). Large-scale circulation and its variability in the south Indian Ocean from TOPEX/POSEIDON altimetry. *Journal of Geophysical Research*, *100*, 24,911-24,929.

Park, Y. H. & Gamberoni, L. (1997). Cross-frontal exchange of Antarctic Intermediate Water and Antarctic Bottom Water in the Crozet Basin. *Deep-Sea Research II*, *44*, 963-986.

Park, Y.-H., Gamberoni, L. & Charriaud, E. (1991). Frontal structure and transport of the Antarctic Circumpolar Current in the south Indian Ocean sector, 40-80°E. *Marine Chemistry*, *35*, 45 - 62.

Park, Y.-H., Gamberoni, L. & Charriaud, E. (1993). Frontal structure, water masses, and circulation in the Crozet Basin. *Journal of Geophysical Research*, *98*, 12,361-12,385.

Park, Y. H., Leboucher, V., Pollard, R. T. & Read, J. F. (2002). A quasi-synoptic view of the frontal circulation in the Crozet Basin during the Antares-4 cruise. *Deep-Sea Research II*, *49*, 1823-1842.

Patterson, S. L. & Sievers, H. A. (1980). Weddell-Scotia confluence. *Journal of Physical Oceanography*, *10*, 1584-1610.

Phillips, H. E. & Rintoul, S. R. (2000). Eddy variability and energetics from direct current measurements in the Antarctic Circumpolar Current south of Australia. *Journal of Physical Oceanography*, *30*, 3050-3076.

Phillips, H. E. & Rintoul, S. R. (2002). A mean synoptic view of the Subantarctic Front south of Australia. *Journal of Physical Oceanography*, *32*, 1536-1553.

Pollard, R. & Read, J. (1989). A Method for Calibrating Shipmounted Acoustic Doppler Profilers and the Limitations of Gyro Compasses. *Journal of Atmospheric and Oceanic Technology*, *6*, 859-865.

Pollard, R. T., Lucas, M. I. & Read, J. F. (2002). Physical controls on biogeochemical zonation in the Southern Ocean. *Deep-Sea Research II*, *49*, 3289-3305.

Pollard, R. T. & Read, J. F. (2001). Circulation pathways and transports of the Southern Ocean in the vicinity of the Southwest Indian Ridge. *Journal of Geophysical Research-Oceans*, *106*, 2881-2898.

Polzin, K. L. & Firing, E. (1997). Estimates of diapycnal mixing using LADCP and CTD data from 18S. *International WOCE Newsletter*, *29*, 39-42.

Read, J. F. & Pollard, R. T. (1993). Structure and transport of the Antarctic Circumpolar Current and Agulhas return current at 40°S. *Journal of Geophysical Research*, *98*, 12281-12295.

Reid, J. L. (1989). On the total geostrophic circulation of the South Atlantic Ocean: flow patterns, tracers and transports. *Progress In Oceanography*, *23*, 149-244.

Reid, J. L. (1997). On the total geostrophic circulation of the Pacific Ocean: Flow patterns, tracers, and transports. *Progress In Oceanography*, *39*, 263-283.

Reid, J. L. (2003). On the total geostrophic circulation of the Indian Ocean: Flow patterns, tracers, and transports. *Progress In Oceanography*, *56*, 137-186.

Rintoul, S. R. (1998). On the origin and influence of Adélie land bottom water. In: Eds. S. Jacobs & R. Weiss, *Ocean, Ice and Atmosphere: Interactions at the Antarctic Continental Margin*. *Antarctic Research Series Vol. 75*, (pp. 151-171). American Geophysical Union: Washington DC.

Rintoul, S. R. & Bullister, J. L. (1999). A late winter hydrographic section from Tasmania to Antarctica. *Deep-Sea Research I*, *46*, 1417-1454.

Rintoul, S. R., Hughes, C. W. & Olbers, D. (2001). The Antarctic Circumpolar Current system. In: Eds. G. Siedler, J. Church & J. Gould, *Ocean circulation and climate; observing and modelling the global ocean*. *International Geophysics Series Vol. 77*, (pp. 271-302). Academic Press: San Diego-San Francisco-New York-Boston-London-Sydney-Tokyo.

Rintoul, S. R. & Sokolov, S. (2001). Baroclinic transport variability of the Antarctic Circumpolar Current south of Australia (WOCE Repeat Section SR3). *Journal of Geophysical Research 106*, 2815-2832.

Robbins, P. E. & Toole, J. M. (1997). The dissolved silica budget as a constraint on the meridional overturning circulation of the Indian Ocean. *Deep-Sea Research I*, *44*, 879-906.

Rochford, D. J. (1958). Characteristics and flow paths of the intermediate depth waters of the southeast Indian Ocean. *Journal of Marine Research*, *17*, 483-504.

Rodman, M. R. & Gordon, A. L. (1982). Southern ocean bottom water of the Australian-New Zealand sector. *Journal of Geophysical Research*, *87*, 5771-5778.

Savchenko, V. G., Emery, W. G. & Vladimirov, O. A. (1978). A cyclonic eddy in the Antarctic Circumpolar Current south of Australia. *Journal of Physical Oceanography*, *8*, 825-837.

Schmitz, W. J., Jr. (1995). On the interbasin-scale thermohaline circulation. *Reviews of Geophysics*, *33*, 151-173.

Schmitz, W. J., Jr. (1996). *On the World Ocean Circulation. Volume II: the Pacific and Indian Oceans/a global update*. *Technical Report*. Woods Hole Oceanographic Institution: Woods Hole MA.

Schodlok, M. P. & Tomczak, M. (1997a). The circulation in the South Australian Basin during FR10/94. *FIAMS*, *56*, 1-31.

Schodlok, M. P. & Tomczak, M. (1997b). The circulation south of Australia derived from an inverse model. *Geophysical Research Letters*, *24*, 2781-2784.

Schodlok, M. P., Tomczak, M. & White, N. (1997). Deep sections through the South Australian Basin and across the Australian-Antarctic discordance. *Geophysical Research Letters*, *24*, 2785-2788.

Schröder, M. & Fahrbach, E. (1999). On the structure and the transport of the eastern Weddell Gyre. *Deep-Sea Research II*, *46*, 501-527.

Sloyan, B. M. (2005). Spatial variability of mixing in the Southern Ocean. *Geophysical Research Letters*, *32*, L18603.

Sloyan, B. M. (2006). Antarctic Bottom and Circumpolar Deep Water circulation in the eastern Indian Ocean. *Journal of Geophysical Research*, *111*, doi:10.1029/2005JC003011.

Sloyan, B. M. & Rintoul, S. R. (2001a). Circulation, renewal, and modification of antarctic mode and intermediate water. *Journal of Physical Oceanography*, *31*, 1005-1030.

Sloyan, B. M. & Rintoul, S. R. (2001b). The Southern Ocean limb of the global deep overturning circulation. *Journal of Physical Oceanography*, *31*, 143-173.

Smith, N. R., Zhaoqian, D., Kerry, K. R. & Wright, S. (1984). Water masses and circulation in the region of Prydz Bay, Antarctica. *Deep Sea Research Part A. Oceanographic Research Papers*, *31*, 1121-1147.

Smith, W. H. F. & Sandwell, D. T. (1997). Global sea floor topography from satellite altimetry and ship depth soundings. *Science*, *277*, 1956-1962.

Sokolov, S. & Rintoul, S. R. (2002). Structure of Southern Ocean fronts at 140°E. *Journal of Marine Systems*, *37*, 151-184.

Sparrow, M. D., Heywood, K. J., Brown, J. & Stevens, D. P. (1996). Current structure of the south Indian Ocean. *Journal of Geophysical Research*, *101*, 6377-6391.

Speer, K. G. & Forbes, A. (1994). A deep western boundary current in the South Indian Basin. *Deep-Sea Research I*, *41*, 1289-1303.

Speich, S. & Blanke, B. (2001). Warm and cold water routes of an O.G.C.M. thermohaline conveyor belt. *Geophysical Research Letters*, *28*, 311-314.

Speich, S., Blanke, B., de Vries, P., Drijfhout, S., Döös, K., Ganachaud, A. & Marsh, R. (2002). Tasman leakage: A new route in the global ocean conveyor belt. *Geophysical Research Letters*, *29*, 55-1 - 55-4.

Stanton, B. R. & Morris, M. Y. (2004). Direct velocity measurements in the Subantarctic front and over Campbell Plateau, southeast of New Zealand. *Journal of Geophysical Research 109*, C01028 1-11.

Stramma, L. & Lutjeharms, J. R. E. (1997). The flow field of the subtropical gyre of the South Indian Ocean. *Journal of Geophysical Research*, *102*, 5513-5530.

Talley, L. D. & Baringer, M. O. (1997). Preliminary results from WOCE hydrographic sections at 80ºE and 32ºS in the central Indian Ocean. *Geophysical Research Letters*, *24*, 2789-2792.

Talley, L. D. & Sprintall, J. (2005). Deep expression of the Indonesian Throughflow: Indonesian Intermediate Water in the South Equatorial Current. *Journal of Geophysical Research C: Oceans*, *110*, 1-30 Article Number C10009.

Tchernia, P. (1974). Étude de la dérive antarctique est-ouest au moyen d'icebergs suivis par le satellite Eole. *Comptes Rendus de l'Academie de Sciences - Serie B*, *278*, 667--674.

Tchernia, P. & Jeannin, P. F. (1980). Observations on the Antarctic East Wind Drift using tabular icebergs tracked by satellite Nimbus F (1975-1977). *Deep-Sea Research*, *27*, 467-474.

Toole, J. M. & Warren, B. A. (1993). A hydrographic section across the subtropical South Indian Ocean. *Deep-Sea Research I*, *40*, 1973-2019.

Veronis, G. (1973). Model of World Ocean circulation: 1. Wind-driven, two-layer. *Journal of Marine Research*, *31*, 228-288.

Warren, B. A. (1981). Deep circulation of the world oceans. *Evolution of Physical Oceanography*, 6-41.

Warren, B. A. & Johnson, G. C. (2002). The overflows across the Ninetyeast Ridge. *Deep-Sea Research II*, *49*, 1423-1439.

Whitworth III, T., Orsi, A. H., Kim, S. J. & Nowlin Jr, W. D. (1998). Water masses and mixing near the Antarctic Slope Front. In: Eds. S. Jacobs & R. Weiss, *Antarctic Research Series*. *Vol. 75*, (pp. 1-27). American Geophysical Union.

Whitworth, T. (2002). Two modes of bottom water in the Australian-Antarctic Basin. *Geophysical Research Letters*, *29*, 17-1-17-3.

Whitworth, T., III (1983). Monitoring the transport of the Antarctic Circumpolar Current at Drake Passage. *Journal of Physical Oceanography*, *13*, 2045-2057.

Whitworth, T., III & Nowlin, W. D., Jr. (1987). Water masses and currents of the Southern Ocean at the Greenwich Meridian. *Journal of Geophysical Research*, *92*, 6462-6476.

Wyrtki, K. (1962). Geopotential topographies and associated circulation in the south-eastern Indian Ocean. *Australian Journal of Marine and Freshwater Research*, *13*, 1-17.

Wyrtki, K. (1971). *Ocean Atlas of the International Indian Ocean Experiment*. National Science Foundation: Washington DC.

Yaremchuk, M., Bindoff, N. L., Schröter, J., Nechaev, D. & Rintoul, S. R. (2001). On the zonal and meridional circulation and ocean transports between Tasmania and Antarctica. *Journal of Geophysical Research 106*, 2795-2814.

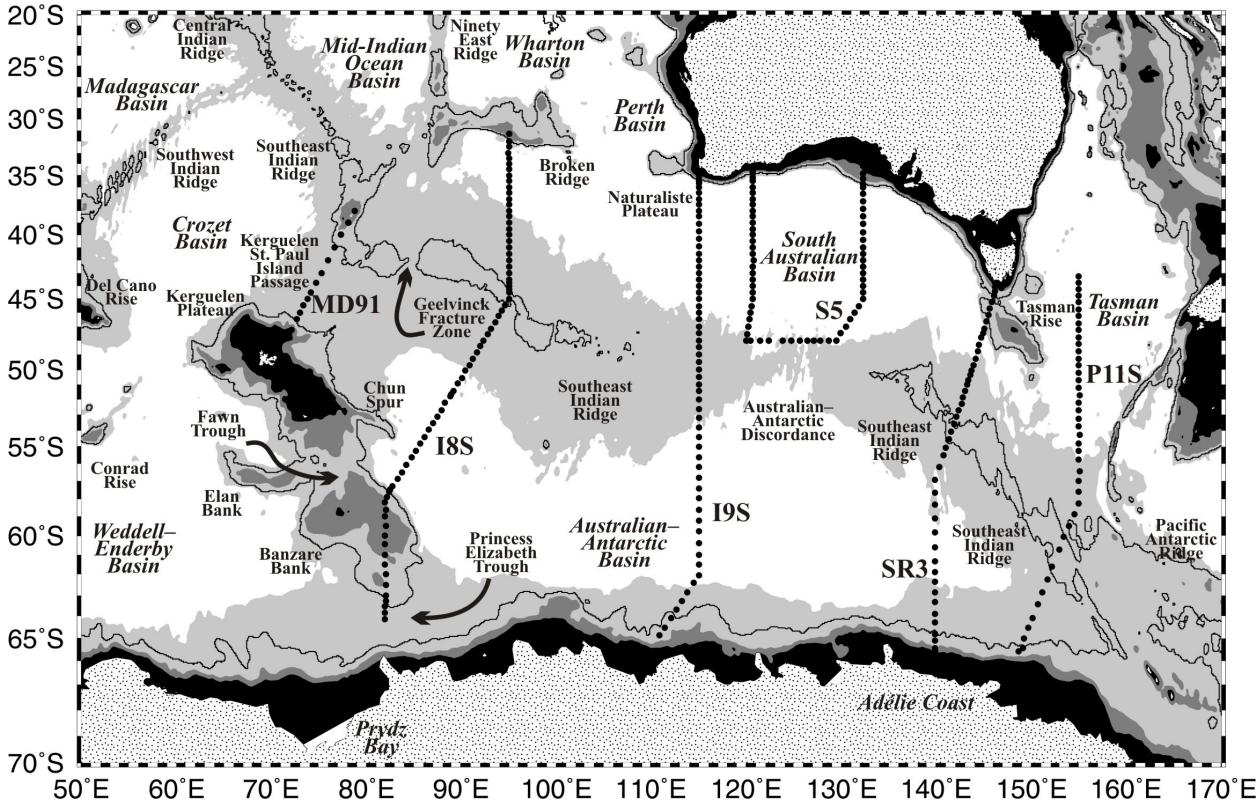

Fig. 1. Southeast Indian Ocean topographic features using names from GEBCO (2005) except for the "Kerguelen Plateau-St. Paul Island Passage." Bathymetry derives from Smith and Sandwell (1997) and is smoothed at 50 km scale for clarity. Black indicates depths < 1000 m, shading changes at 1000, 2000 and 4000 m depths, white shades indicate depths > 4000 m, and there is a single contour at 3000 m. Land and permanent ice are stippled white. Station locations are shown for the six primary section datasets used in the study. I8S, I9S, SR3, and S5 were occupied from late 1994 through early 1995, P11A hydrographic casts were taken in austral spring 1993, and MD91 was conducted in early 1991.

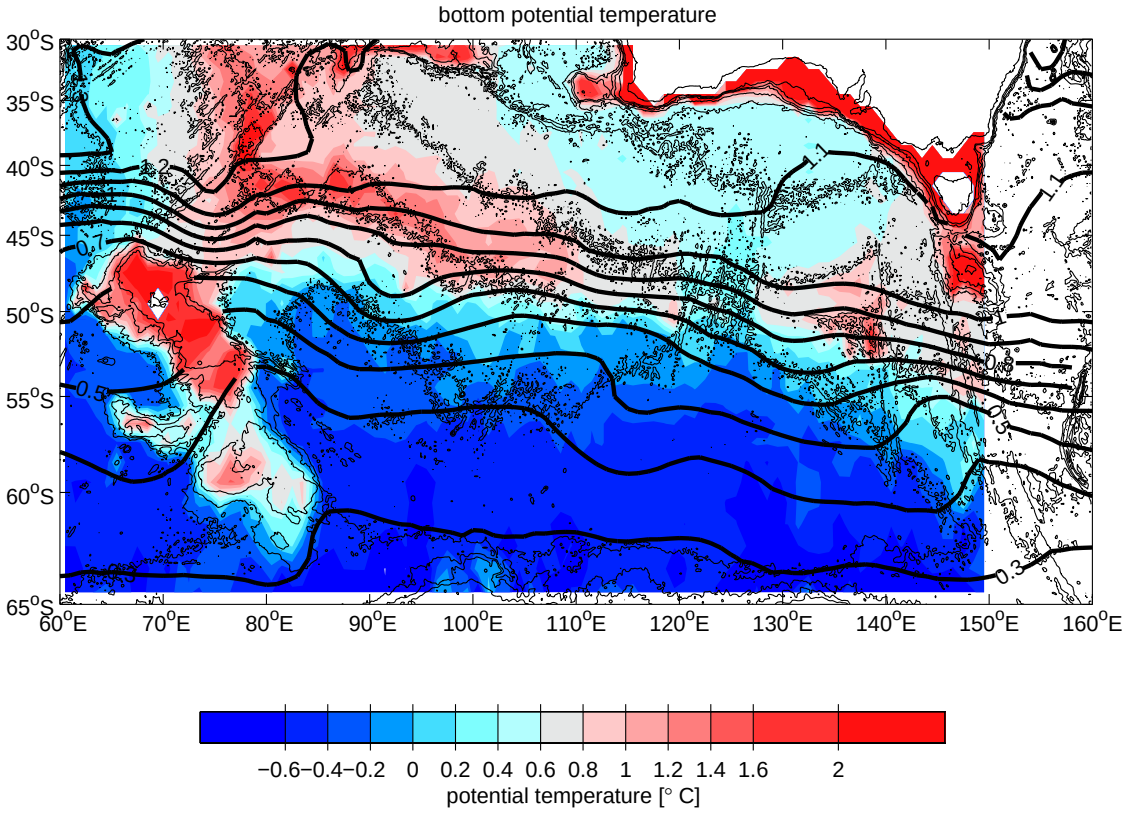

Fig. 2. Contours of dynamic height values at 100 db referenced to 1000 db, calculated from the Gouretski and Jancke (1998) climatology superimposed upon near bottom temperature from Hydrobase (Lozier et al., 1995) courtesy of R. Curry. Dynamic height contours range from 0.3-1.4 dyn m with a contour interval of 0.1 dyn m. Bottom temperature contours are 0.2°C.

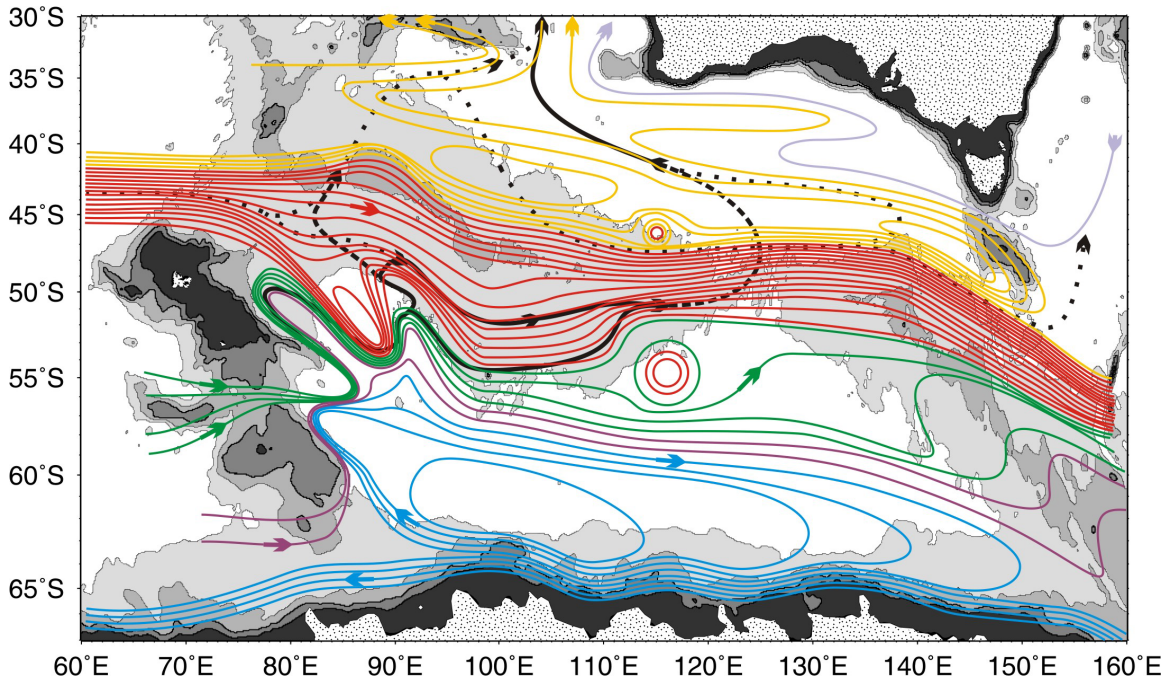

Fig. 3. A schematic of the basin-scale total (depth-integral) transport field, with 10 Sv contour intervals, based on the transport estimates developed in this study. In the following we list our estimated transports for selected elements, with the errors discussed in the text. Blue contours include the westward flow of the Antarctic Slope Current (maximum 76 Sv), the southern limb of a cyclonic gyre. Part of the cyclonic gyre (blue, 35 Sv) returns eastward as cyclonic recirculation within the Australian–Antarctic Basin, and part as recirculation that has looped through the Weddell–Enderby Basin: purple contours (21 Sv) in the northern Princess Elizabeth Trough and two of the four green contours (24 Sv) passing through the Fawn Trough. The middle of the green contour group marks the boundary between the cyclonic gyre domain and the Antarctic Circumpolar Current throughput domain (157 Sv), which has 14 Sv through Fawn Trough and 143 Sv through the Kerguelen–St. Paul Island Passage. The three inflows from the west and the western boundary current of the cyclonic recirculation gyre form the energetic Crozet–Kerguelen Confluence east of Kerguelen Plateau. The northern boundary of the 157 Sv throughput domain is the red to yellow transition in the Kerguelen–St. Paul Island Passage, and we estimate a total eastward flow of 181 Sv through the Passage. North of St. Paul Island an additional 8 Sv lops through the domain. North of that throughput boundary, yellow contours denote an anticyclonic circulation in the Subantarctic Zone and the subtropics (as strong as 50 Sv near Tasmania, but around 36–38 Sv in the I8S/I9S sections). The violet contour represents a return from the Tasman Sea westward to the southeast Indian Ocean that compensates for a limited penetration (drawn as 10 Sv, but perhaps 20 or 30 Sv depending on the degree of non-locality of the Subantarctic recirculation near Tasmania) of the anticyclonic domain past Tasmania. The black curves denote pathways (not strengths) along which the bottom waters (< 1.0°C) that submerge beneath lighter waters in the Confluence escape the Australian–Antarctic Basin to cross the Southeast Indian Ridge. Note these cold bottom waters include a contribution from the Crozet Basin. The dashed black contours show the delivery of waters colder than 0.7ºC to the Geelvinck Fracture Zone and across the Australian–Antarctic Discordance, which undercuts waters between 1.0 and 0.7ºC (dotted contours). These two paths contribute 2 Sv and 4 Sv, respectively to the 6 Sv estimated transport of water colder than 1ºC into the Perth Basin.

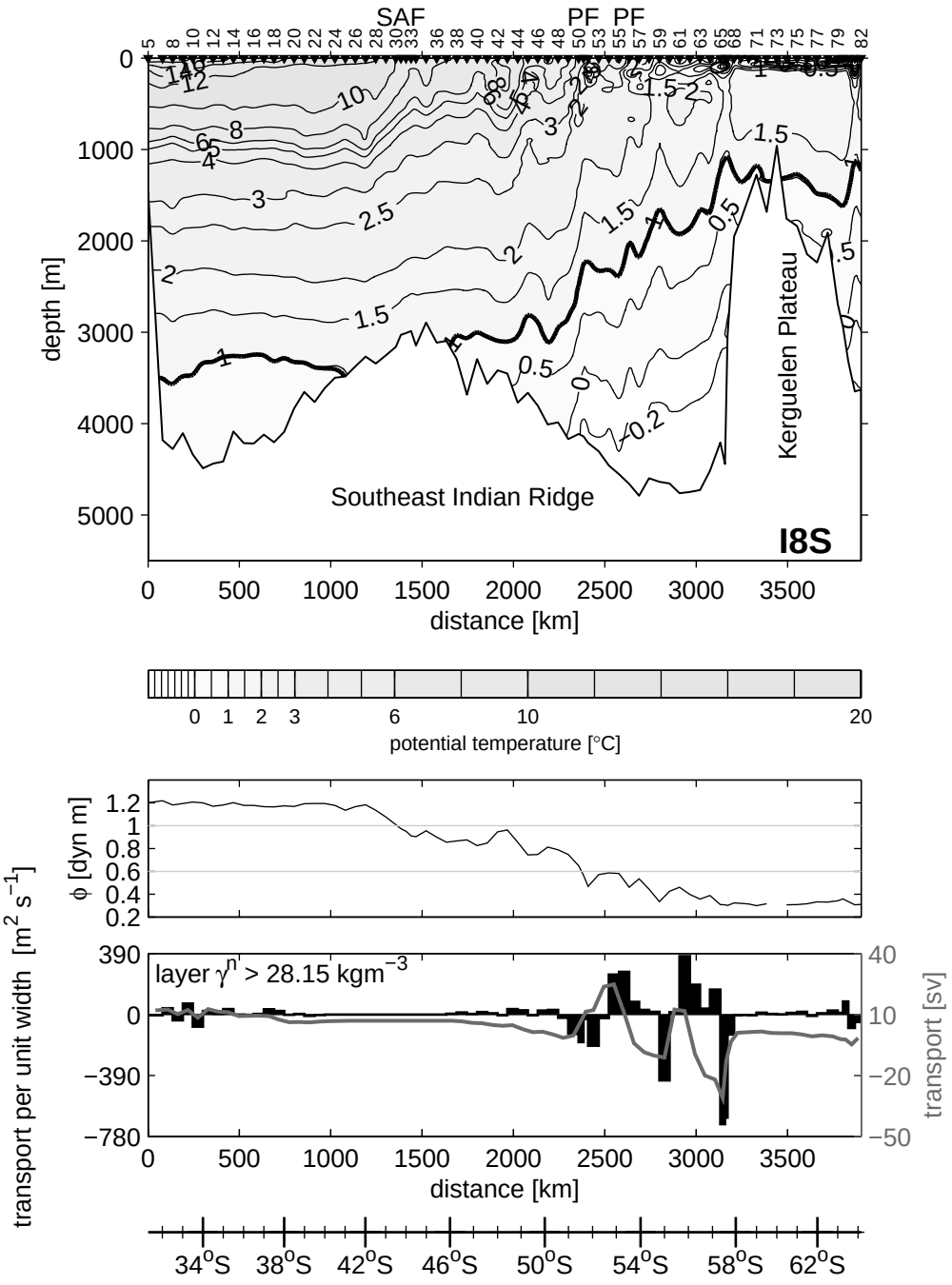

Fig. 4A. I8S Upper panel: Distribution of potential temperature in ºC. Solid line is the neutral density $\gamma^n = 28.15$ kg m^{-3} isopleth. Station numbers and positions and location of the Subantarctic Front, SAF, and Polar Front, PF, are indicated at the top of each panel. Middle panel: Dynamic height values at 100 db referenced to 1000 db in dynamic meters. Bottom panel: SADCP-referenced geostrophic transports below neutral density, $\gamma^n = 28.15$ kg m^{-3}. Cumulative (between-station) volume transport in Sv integrated from north to south shown with grey line (black bars). Station pair transports are per unit area so that the area of the bar reflects the transport. Positive is eastward.

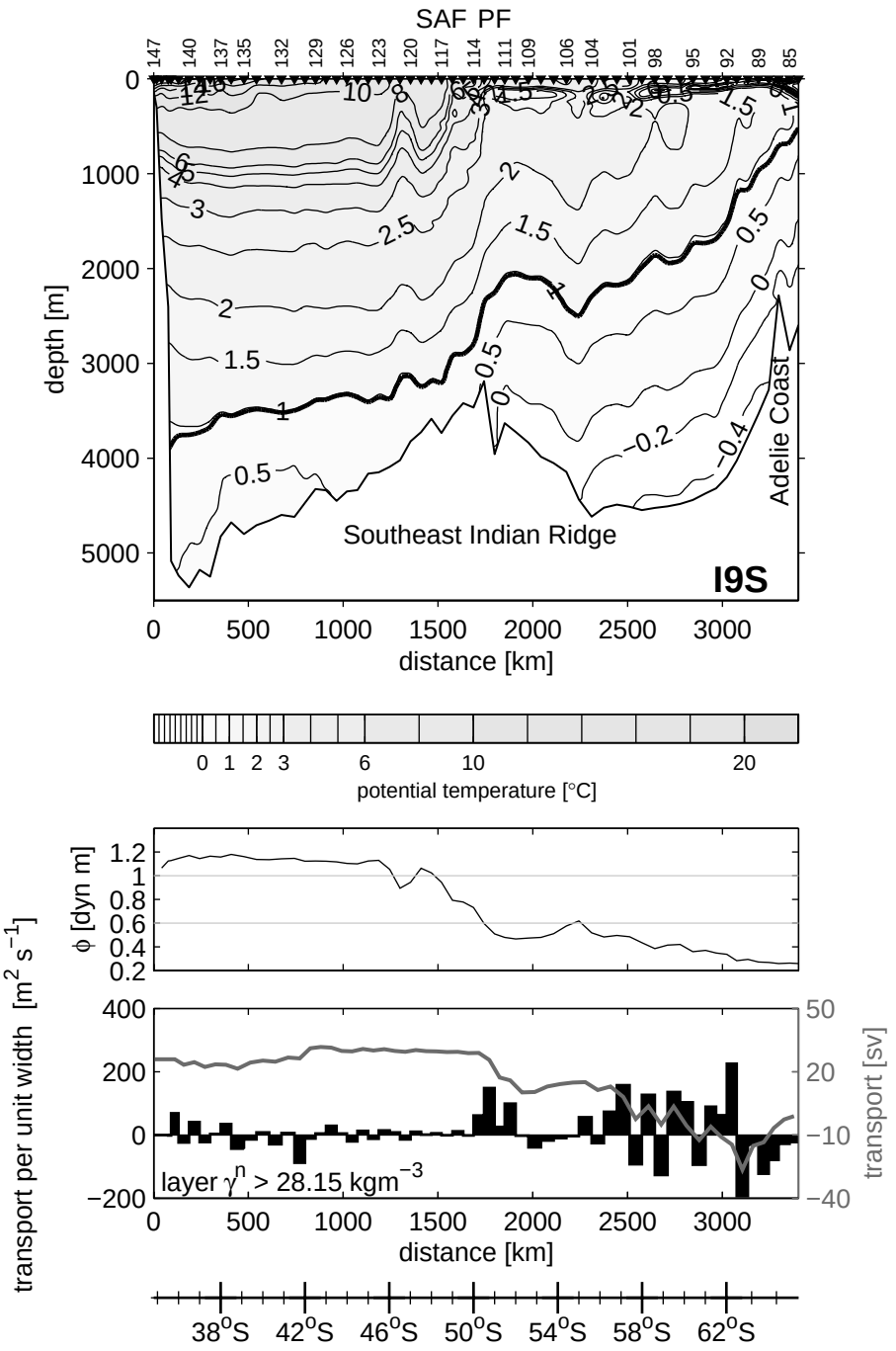

Fig. 4B. I9S Upper panel: Distribution of potential temperature in ºC. Solid line is the neutral density $\gamma^n = 28.15$ kg m^{-3} isopleth. Station numbers and positions and location of the Subantarctic Front, SAF, and Polar Front, PF, are indicated at the top of each panel. Middle panel: Dynamic height values at 100 db referenced to 1000 db in dynamic meters. Bottom panel: SADCP-referenced geostrophic transports below neutral density, $\gamma^n = 28.15$ kg m^{-3}. Cumulative (between-station) volume transport in Sv integrated from north to south shown with grey line (black bars). Station pair transports are per unit area so that the area of the bar reflects the transport. Positive is eastward. LADCP-referencing is used northward of station 140.

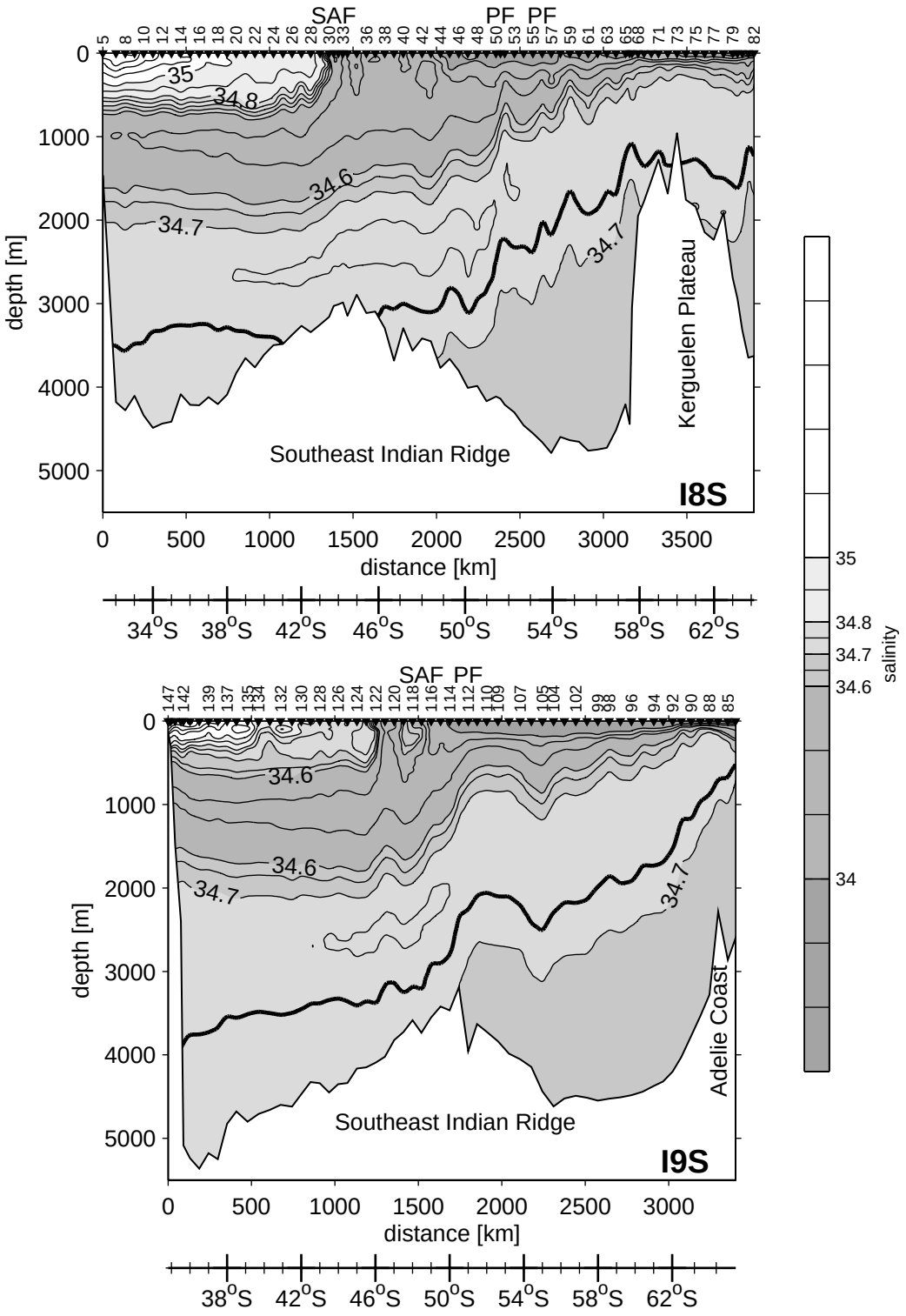

Fig. 5. Distribution of salinity, upper panel I8S, lower panel I9S. Solid line is the neutral density $\gamma^n = 28.15$ kg m^{-3} isopleth.

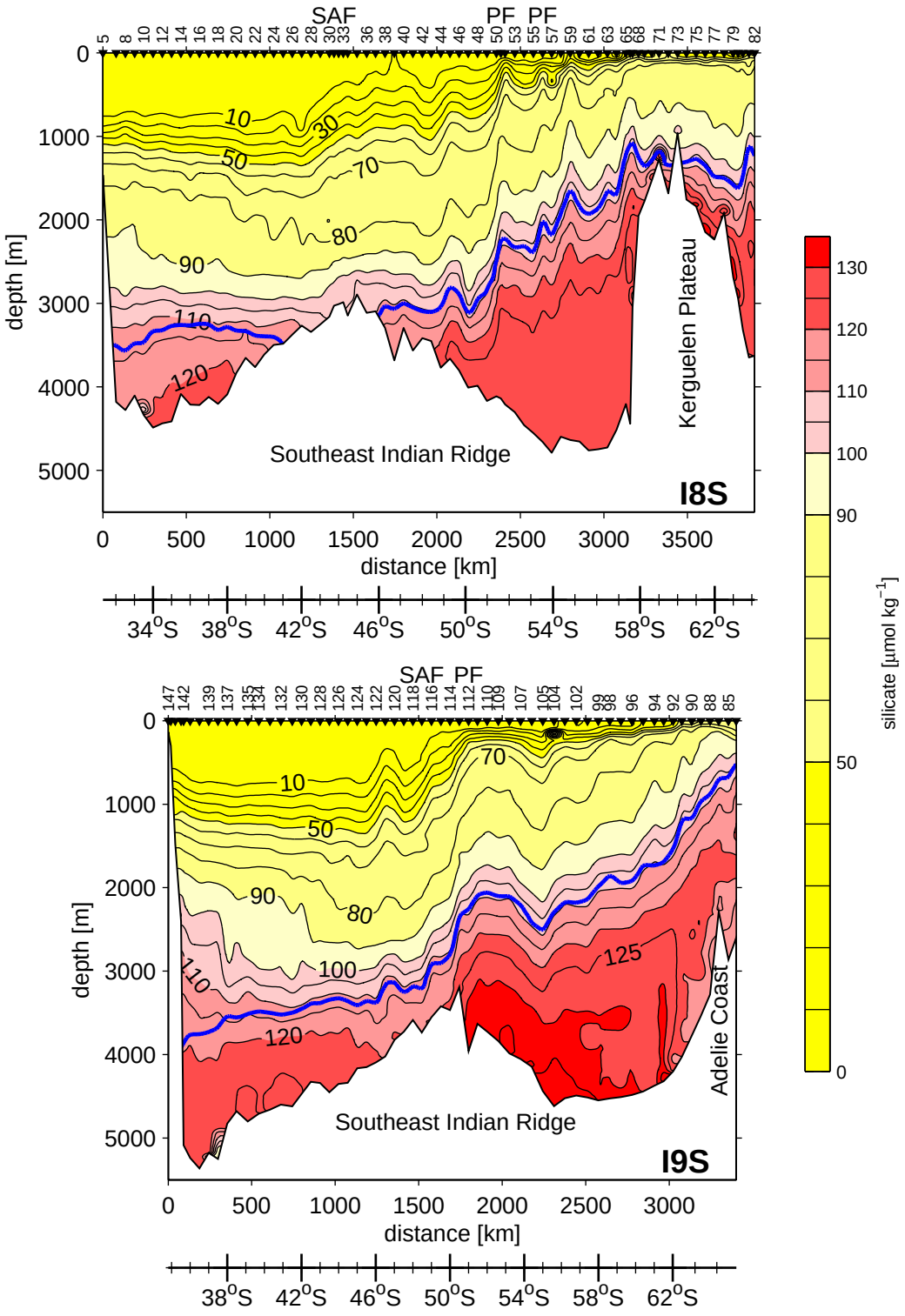

Fig. 6. Distribution of silicate in µmol kg^{-1}, upper panel I8S, lower panel I9S. Solid thick blue line is the neutral density $\gamma^n = 28.15$ kg m^{-3} isopleth.

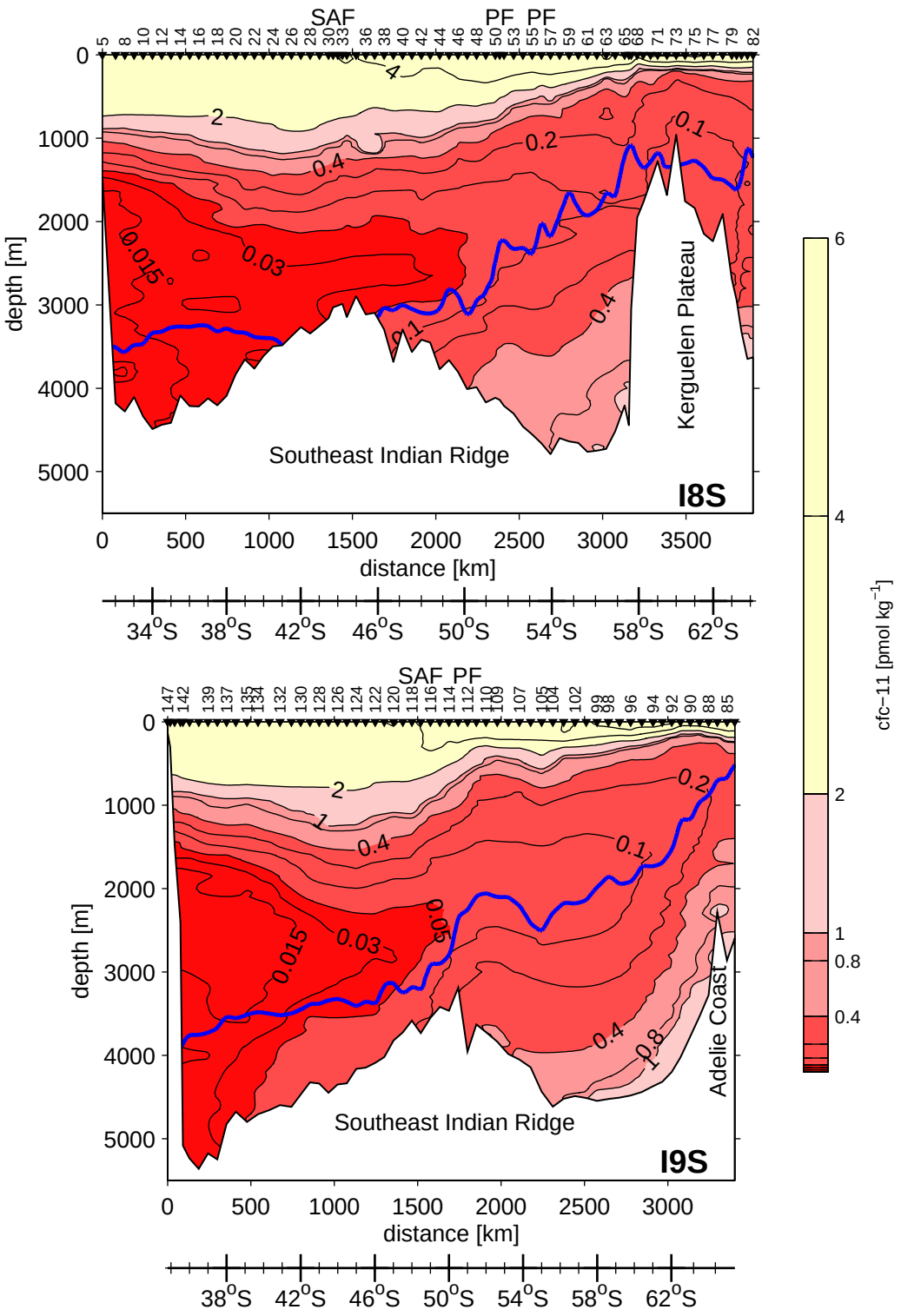

Fig. 7. Distribution of CFC-11 in pmol kg^{-1}, upper panel I8S, lower panel I9S. Solid thick blue line is the neutral density $\gamma^n = 28.15$ kg m^{-3} isopleth.

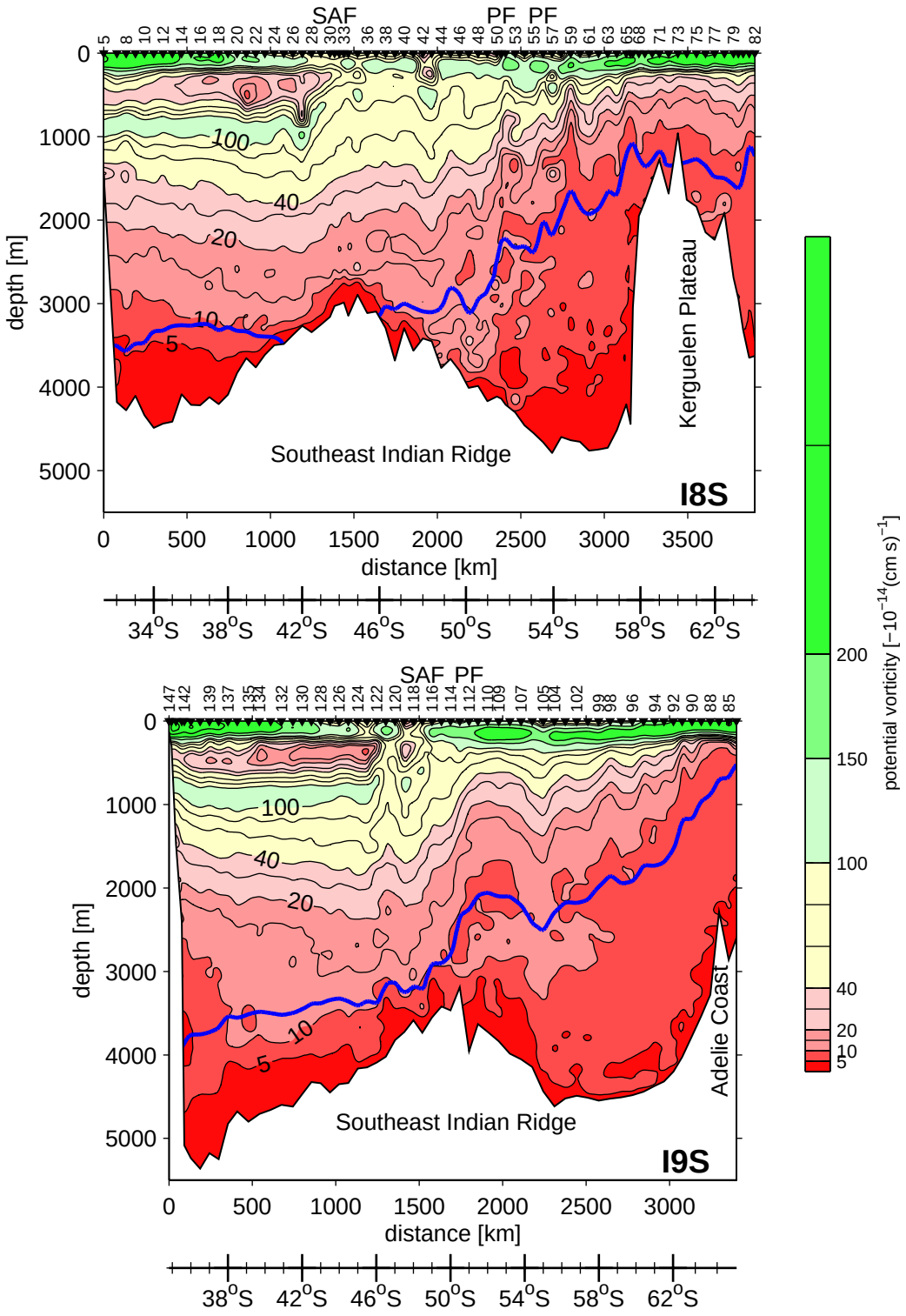

Fig. 8. Distribution of potential vorticity in 10^{-14} (cm s)$^{-1}$, upper panel I8S, lower panel I9S. Solid thick blue line is the neutral density $\gamma^n = 28.15$ kg m^{-3} isopleth.

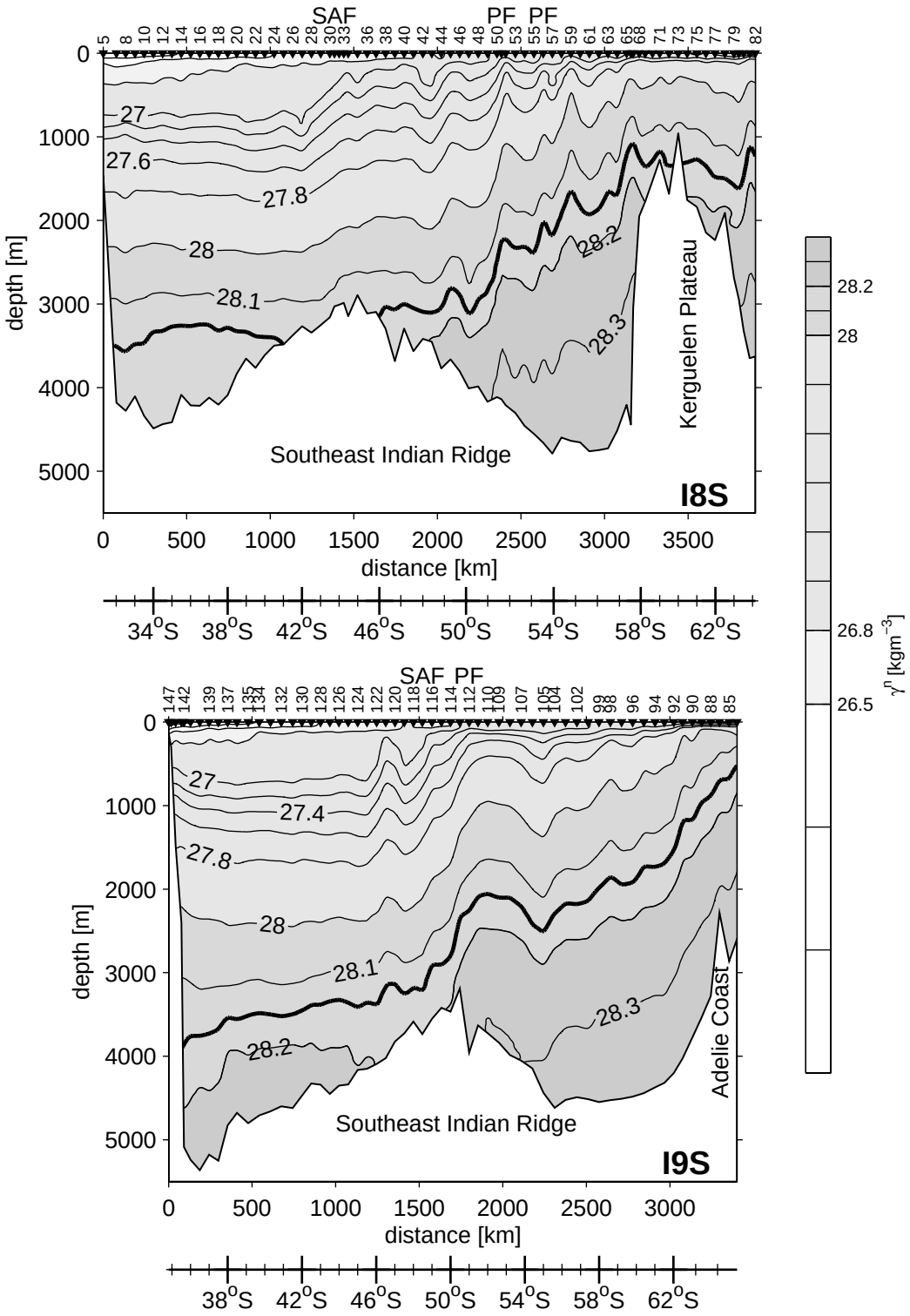

Fig. 9. Profiles of neutral density, γ^n, in kg m^{-3}, upper panel I8S, lower panel I9S. Solid thick line is the neutral density $\gamma^n = 28.15$ kg m^{-3} isopleth.

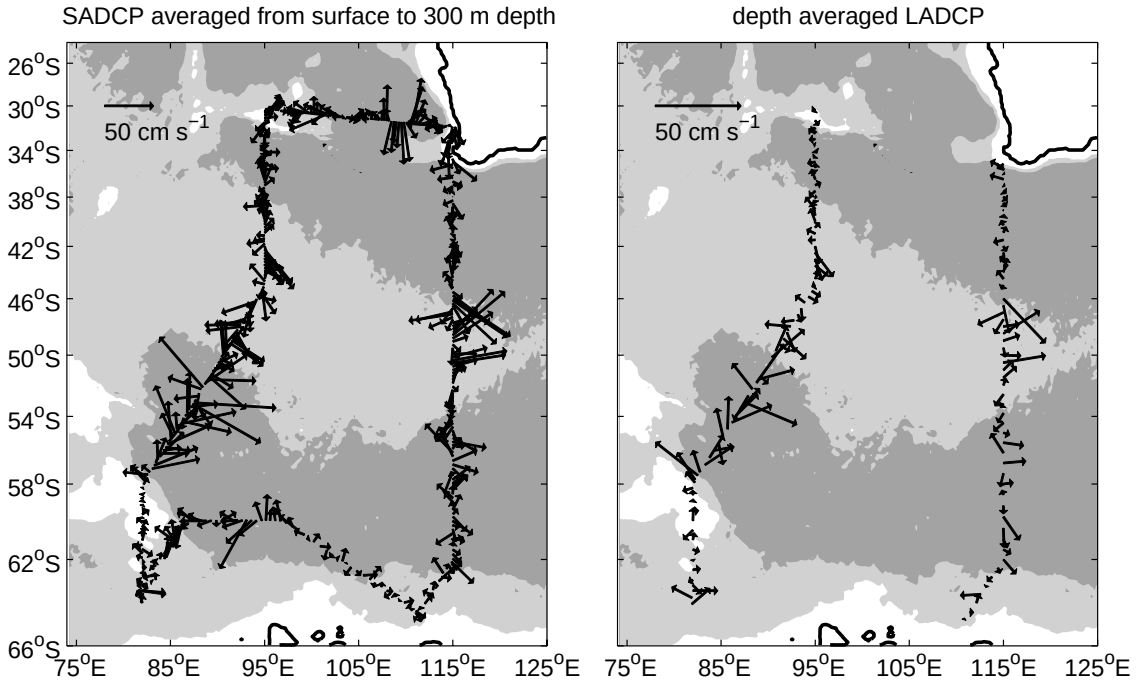

Fig. 10. Strong correspondence between near-surface velocity from the SADCP (left) and depth-averaged velocity from the LADCP (right) reflects the tendency for equivalent barotropic structure in this region. Depths greater than 2000 m are shaded every 2000 m.

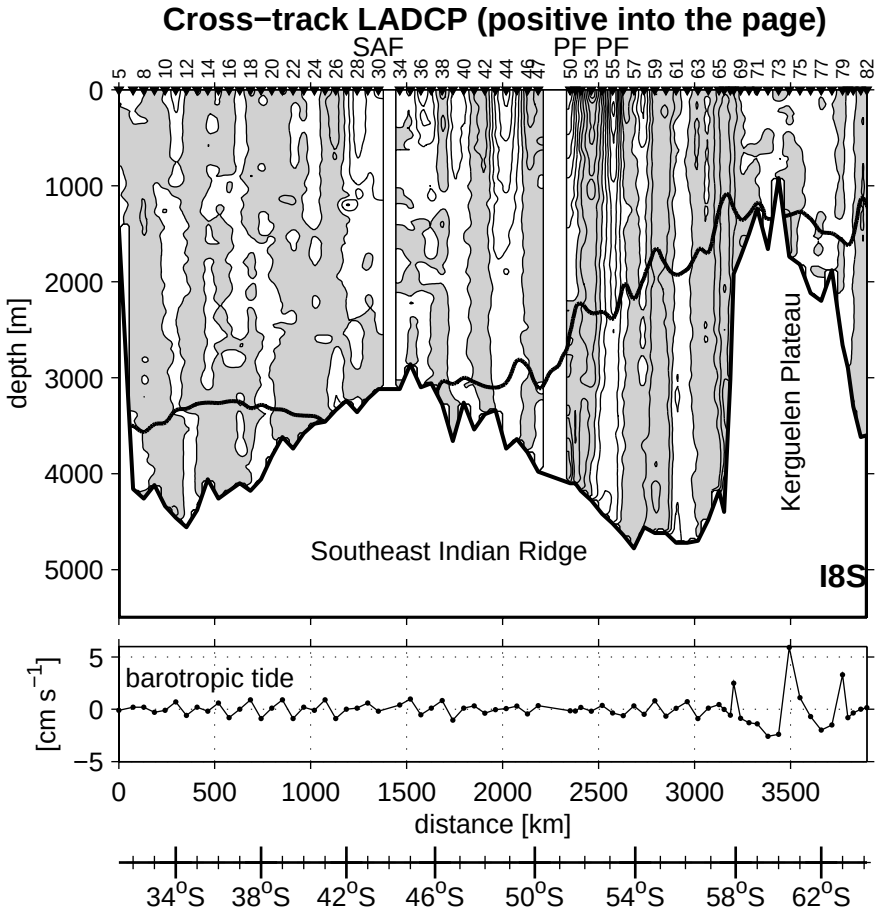

Fig. 11A. I8S Upper panels: Detided cross-track LADCP velocity profiles show deep reaching fronts and eddies. The contour interval is 10 cms^{-1}. Negative flow is shaded and to the west. No LADCP data at stations 6 and 32 because the instrument stopped recording during the upcast. No LADCP data for stations 31,33,48, and 49 because the small rosette was used in the hydrographic casts. 2. Lower panels: The predicted cross-track barotropic tide that has been removed from the LADCP profiles; it is weak except near Kerguelen Plateau.

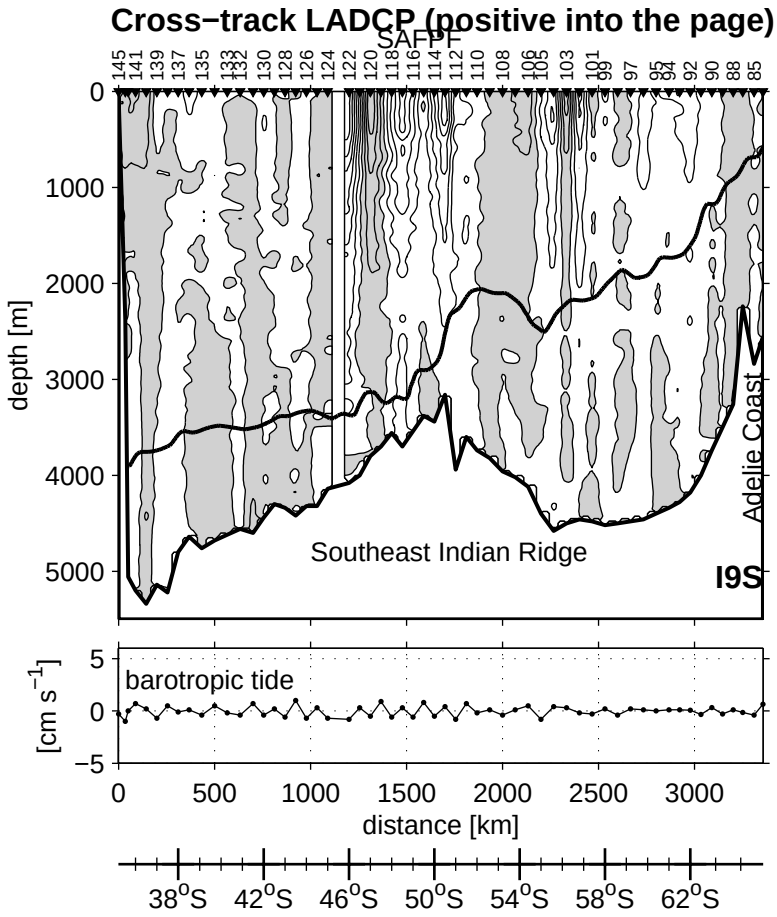

Fig. 11B. I9S Upper panels: Detided cross-track LADCP velocity profiles show deep reaching fronts and eddies. The contour interval is 10 cms^{-1}. Negative flow is shaded and to the west. Lower panels: The predicted cross-track barotropic tide that has been removed from the LADCP.

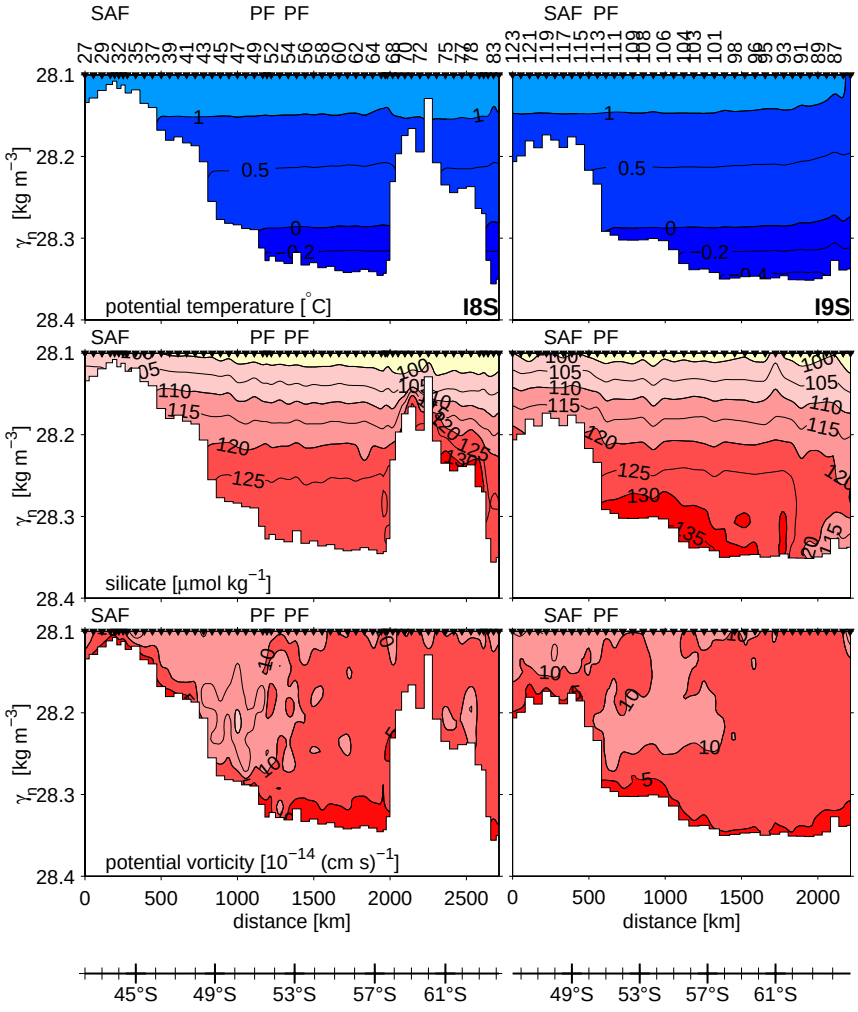

Fig. 12. Deep- and bottom-water properties contoured with neutral density, γ^n, as the vertical coordinate for I8S (left) and I9S (right). Potential temperature (top panels) silicate (middle panels) and potential vorticity (bottom panels). Station numbers and positions and location of the Subantarctic Front, SAF, and Polar Front, PF, are indicated at the top of each panel.

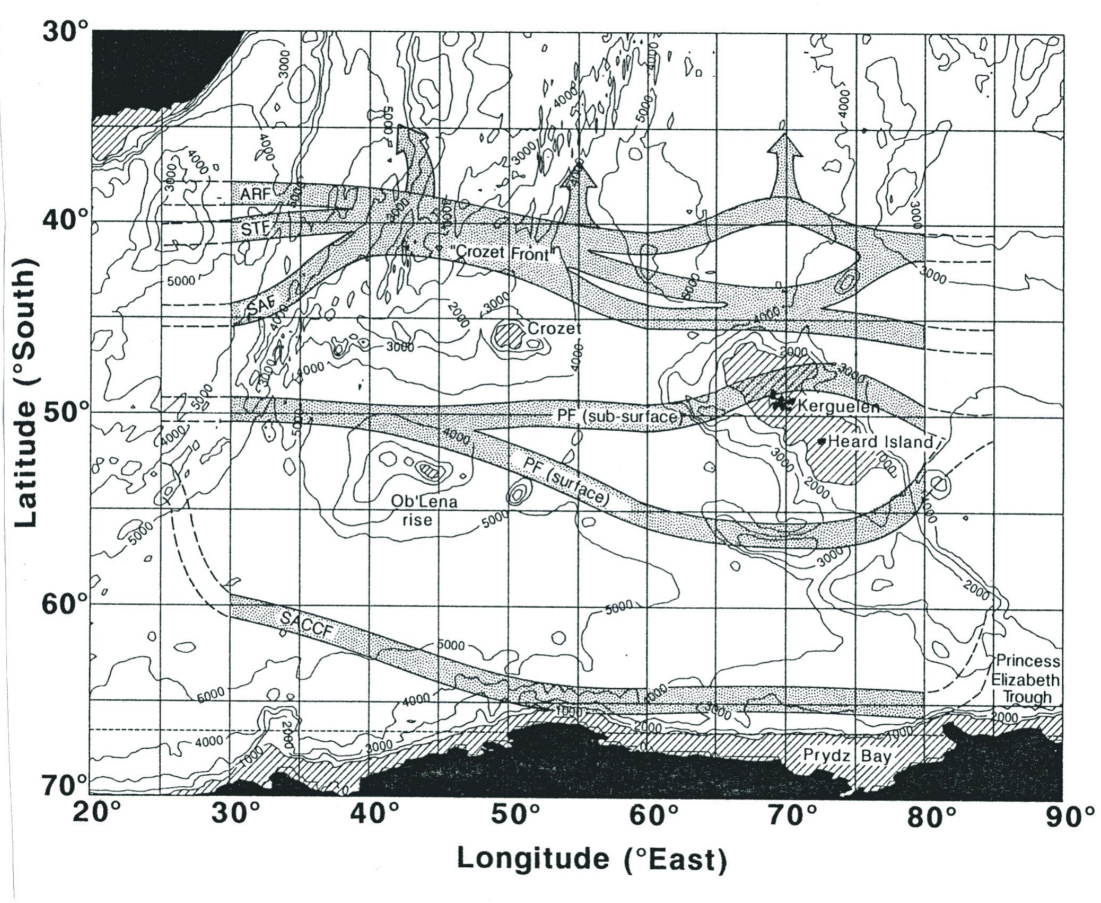

Fig. 13. Fronts in the central Indian Ocean sector of the Southern Ocean from Sparrow et al. (1996) Agulhas Retroflection Front (ARF), Subtropical Front (STF), and the Subantarctic Front merge to form the Crozet Front. The Polar Front (PF) is indicated by surface and sub-surface definitions. The subsurface Polar Front flows north of Kerguelen while the surface Polar Front transits through Fawn Trough. Finally, the Southern Antarctic Circumpolar Current Front (SACCF) flows south of Kerguelen Plateau.

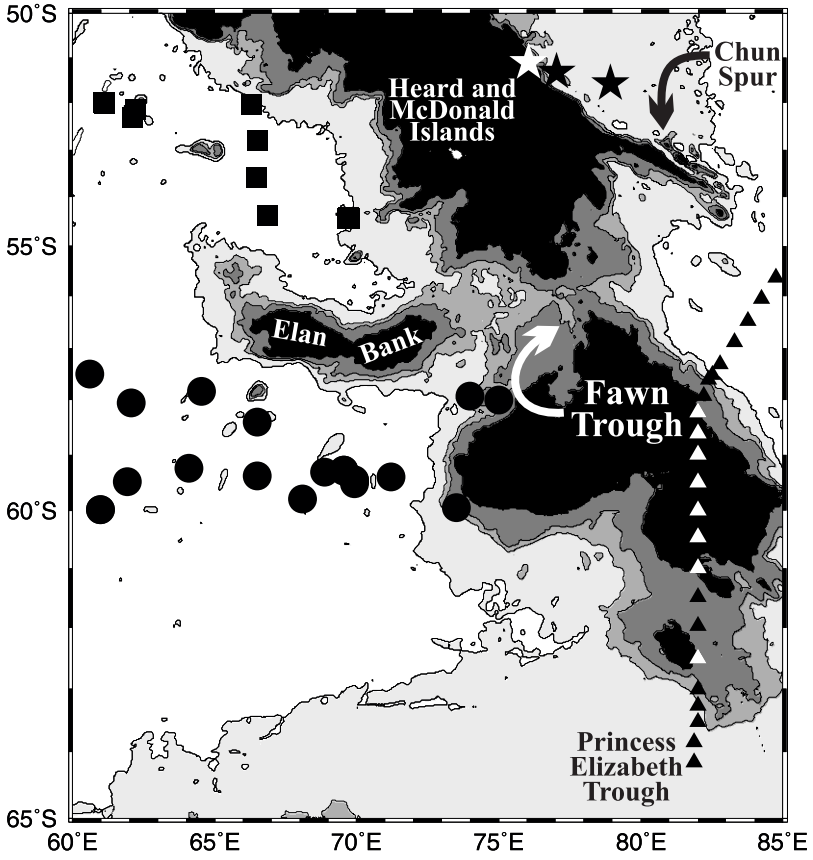

Fig. 14. Topography of the central Kerguelen Plateau (Smith and Sandwell, 1997) with black indicating depths less than 2000 m, shade breaks and contour intervals occur at 2000, 2600, 3000 and 4000 m depths, with white shading indicating either depths greater than 4000 m depth or land. The 2600 m value is chosen to highlight the apparent sill depth. Symbols: squares and circles are the two station groups used to form average profiles in Fig. 15; triangles are the southwestern I8S stations; and stars are USNS Eltanin stations used in Fig. 15 and 18.

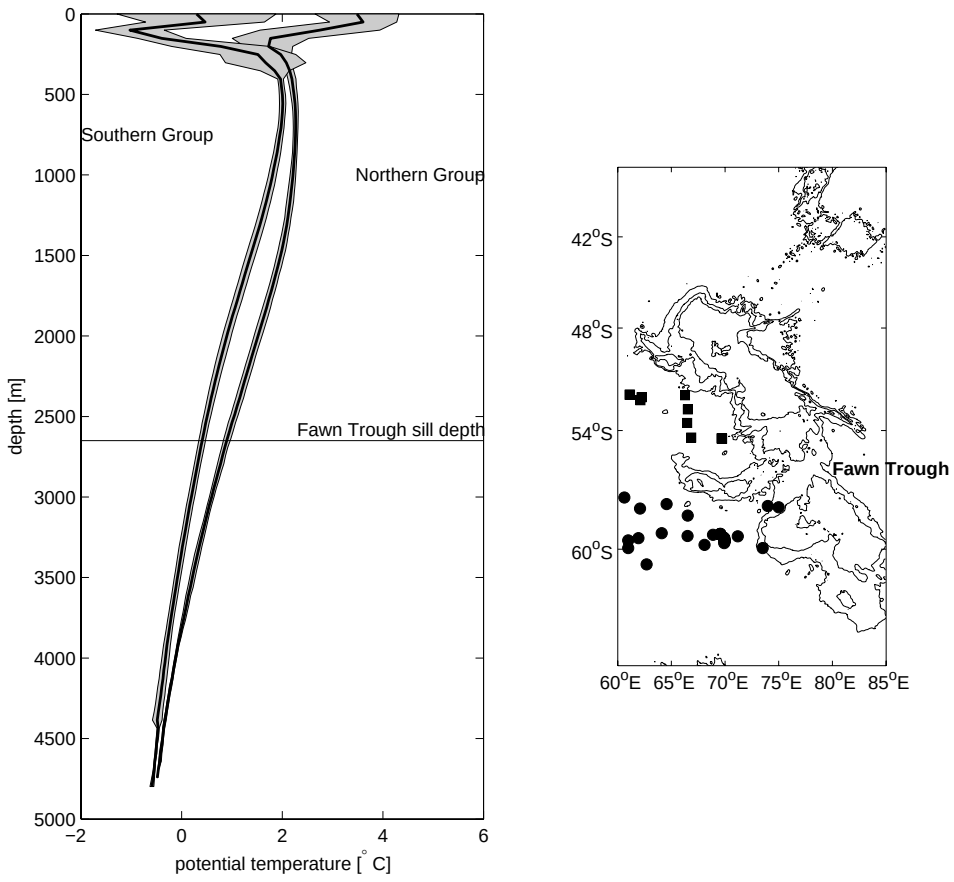

Fig. 15. Left panel: Average potential temperature profiles in °C with standard deviation envelopes for two station groups west of Fawn Trough. Right panel: Bathymetry from Smith and Sandwell (1997) contoured every 1000 m depth with squares and circles representing northern and southern station groups, respectively. The northern group is the warmer profile. Below the temperature maximum isotherms in the southern group are considerable uplifted compared to the northern group, indicative of deep reaching geostrophic shear at this front. A deep reference level would lead to eastward flow that could pass through Fawn Trough.

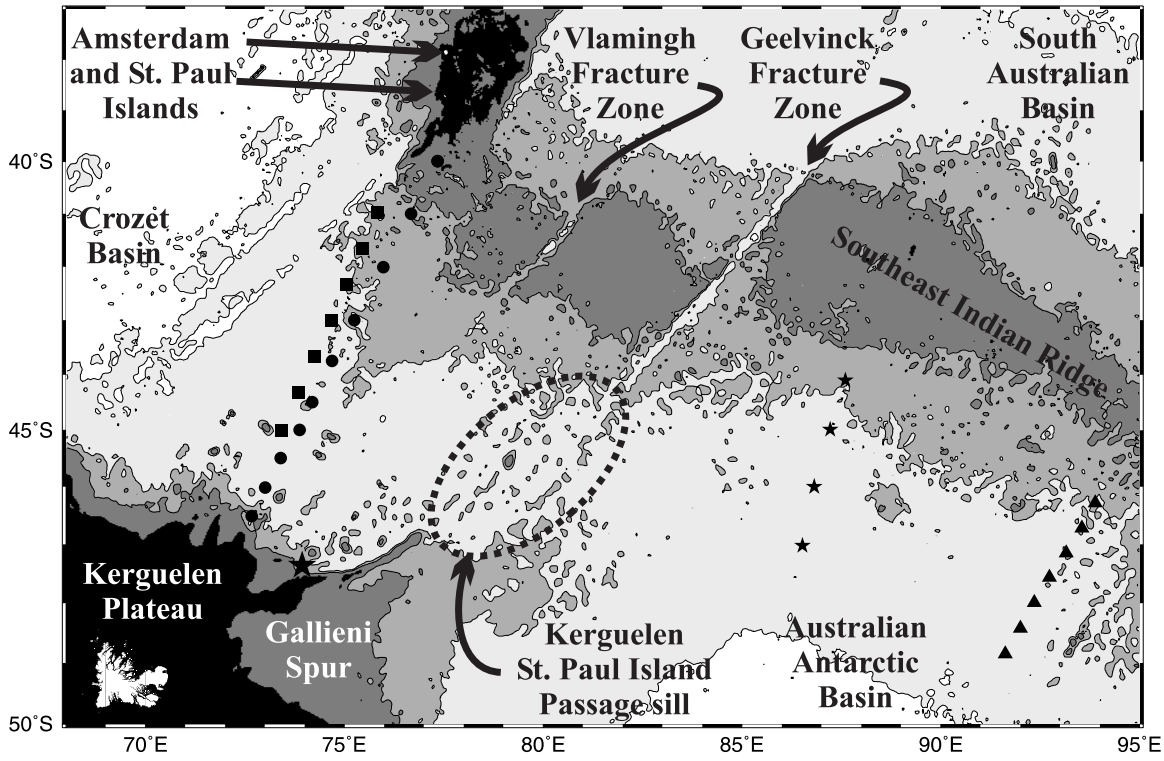

Fig. 16. Topography of the Kerguelen–St Paul Island Passage region (Smith and Sandwell, 1997) with black indicating depths less than 2000 m, shade breaks and contours occur at 2000, 3000, 3400 and 4000 m depths, with white indicating either depths greater than 4000 m or land. The 3400 m contour is chossen to highlight the apparent sill depth. Symbols: squares and circles are 1987 and 1991 stations discussed by Park et al. (1991; 1993); triangles are I8S stations and stars are USNS Eltanin stations. Hydrographic station data are plotted in Figs. 17 and 31.

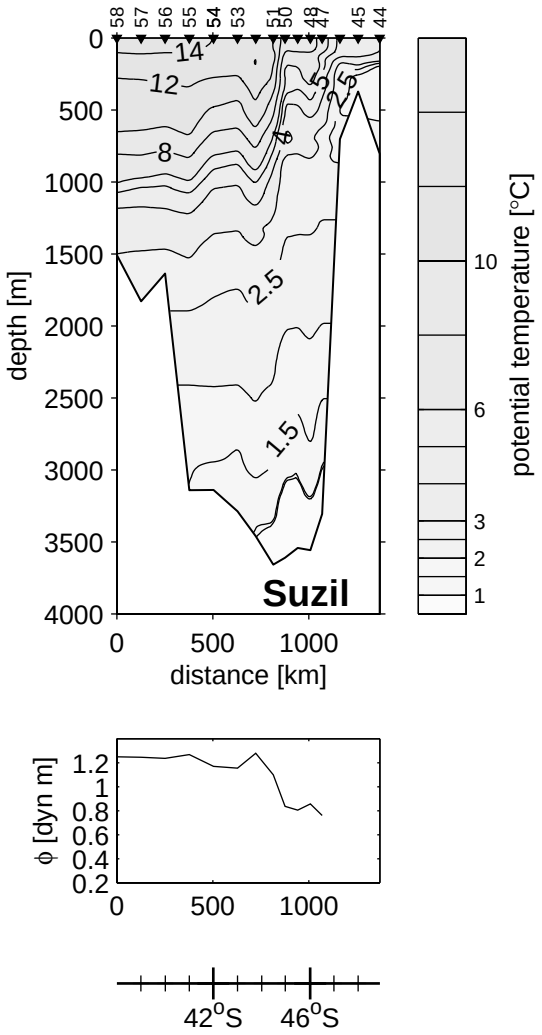

Fig. 17. Upper panel: Distribution of potential temperature in ºC for the section across the Kerguelen–St Paul Island Passage discussed by Park et al. (1993), station positions labeled MD91 in Fig. 1 and plotted with circles in Fig. 16. Solid line is the neutral density $\gamma^n = 28.15$ kg m^{-3} isopleth which is nearly coincident with 1.0°C. The coldest observed bottom water in the section was 0.73°C at 3620 m. The Passage sill lies east of the section and is between 3300 and 3400 m. Lower panel: Dynamic height values at 100 db referenced to 1000 db in dynamic meters.

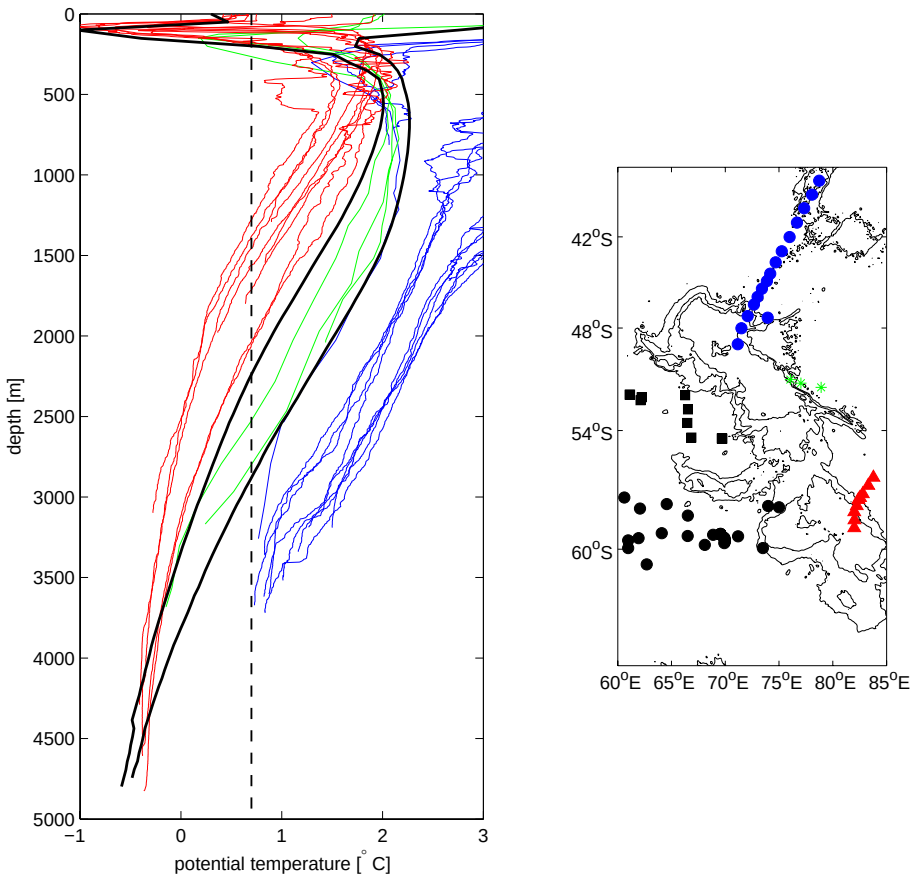

Fig. 18. Potential temperature profiles (left panel) in °C for selected stations near the Kerguelen Plateau with locations plotted in the right panel. Blue lines are stations in the Kerguelen–St Paul Island Passage. The green lines are three Eltanin stations from the area north of Chun Spur on the eastern slope of Kerguelen Plateau northeast of Fawn Trough. The black lines are the two average profiles shown in Fig. 15 from west of Fawn Trough (northern and southern groups). Red stations are from the western boundary current regime off the eastern slope of the southern Kerguelen Plateau (I8S). The vertical dashed line at 0.7°C represents the coldest limit for deep water flowing eastward through the Kerguelen–St Paul Island Passage.

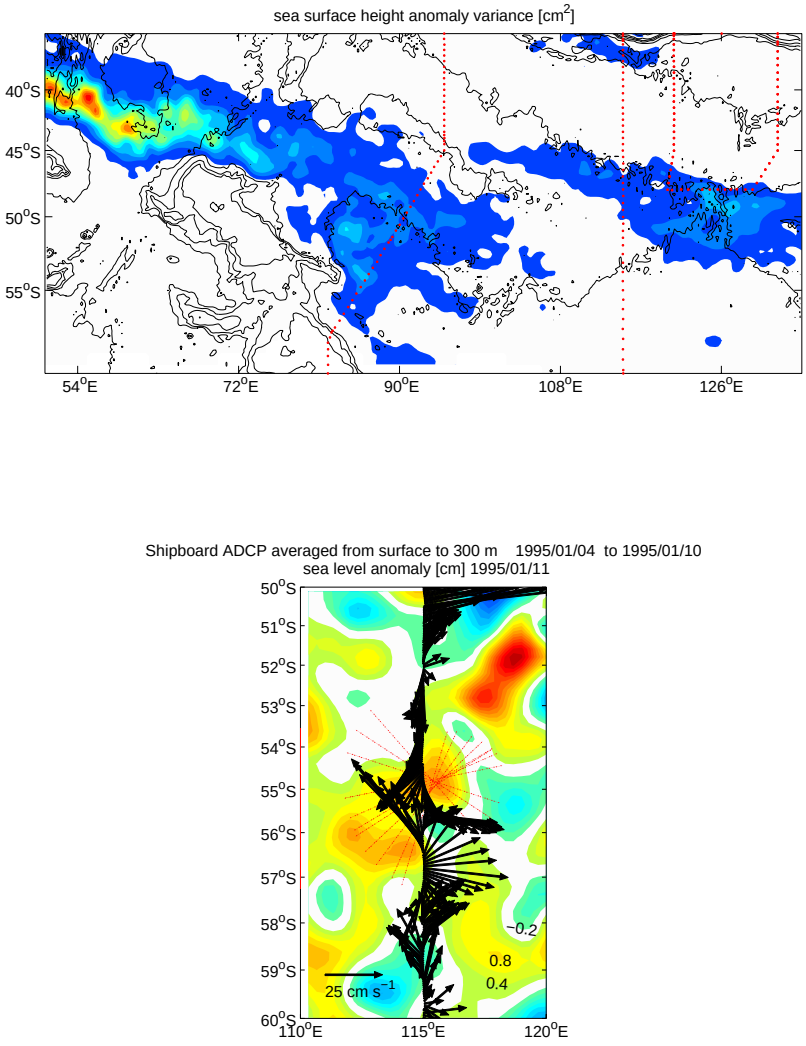

Fig. 19. Top and bottom panels show sea surface height data from merged TOPEX/POSEIDON and ERS-1/2 gridded data products (Le Traon and Dibarboure, 1999; AVISO, 2002). Data maps are produced for 7 day periods with a Mercator 1/3º resolution and available via ftp from ftp://ftp.cls.fr/pub/ oceano/enact/msla/merged/. Sea Level anomalies are relative to a 7-year mean (January 1993 to January 1999). The altimeter products were produced by the CLS Space Oceanography Division as part of the Environment and Climate EU ENACT project (EVK2-CT2001-00117) and with support from CNES. Here we use maps encompassing October 1992 to January 2004.

Top panel: Sea surface height anomaly variance in cm^2, shade interval 1.0 cm^2, white area indicating < 1.0 cm^2.

Bottom panel: I9S SADCP velocity vectors averaged from the surface to 300 m depth superimposed on sea level anomaly map for 11 January 1995 contoured every 2 cm (white denotes range –0.2 to + 0.2). The center of an eddy near 55ºS is indicated by the intersection of lines normal to the velocity vectors (red lines) and a local maximum in the sea level anomaly.

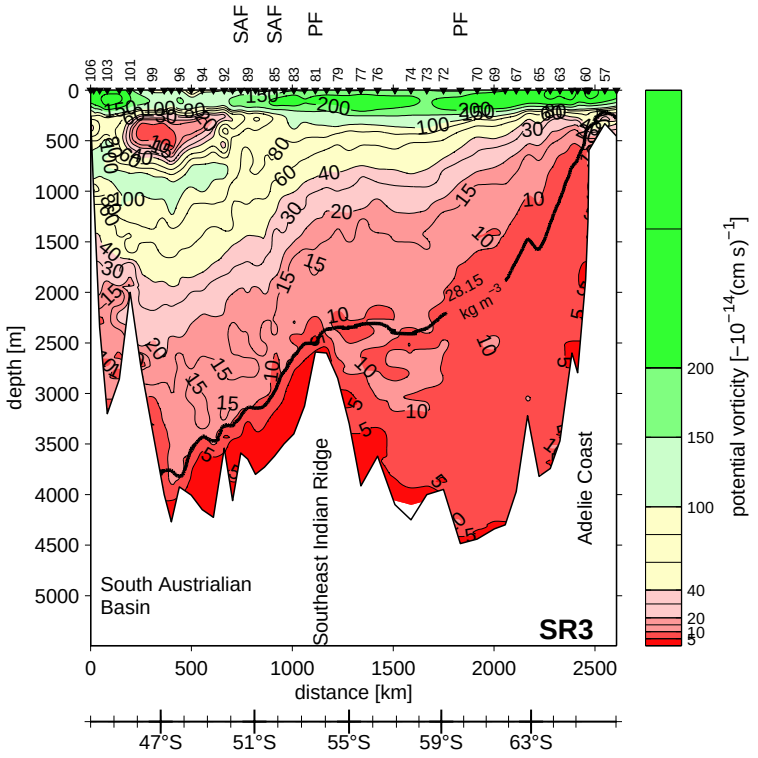

Fig. 20. SR3 distribution of potential vorticity in 10^{-14} (cm s)$^{-1}$. Solid thick line is the neutral density $\gamma^n = 28.15$ kg m^{-3} isopleth. Note the patch of elevated potential vorticity south of the crest of the Southeast Indian Ridge. The December 1994-January 1995 SR3 section is shown here but other SR3 repeat sections have similar structure (not shown).

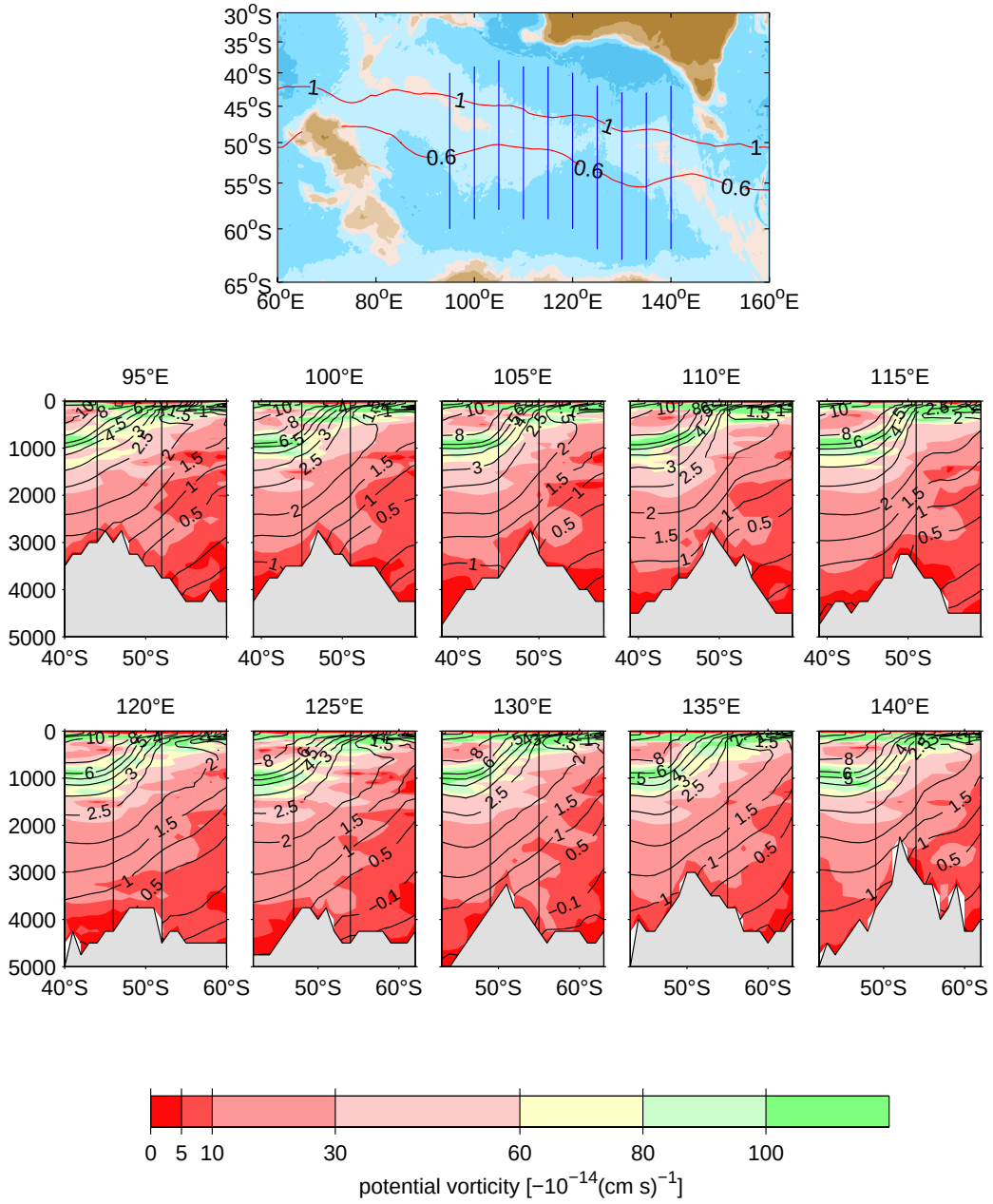

Fig. 21. Upper panel: Dynamic height values at 100 db referenced to 1000 db, calculated from the Gouretski and Jancke (1998) climatology. The 1.0 and 0.6 dynamic meter contours are shown in red. These contours straddle the bulk of the eastward flow through the Kerguelen–St. Paul Island Passage. Bathymetry is color shaded every 1000 m depth. Meridional lines demark sections from the climatology that are contoured in the lower panels. Lower panels: Slices through the Gouretski and Jancke (1998) climatology showing potential temperature (black lines) and potential vorticity (colors). A deep potential vorticity maxima centered near the 0.5ºC isotherm extends across the breadth of the Australian–Antarctic Basin south of the crest of the Southeast Indian Ridge.

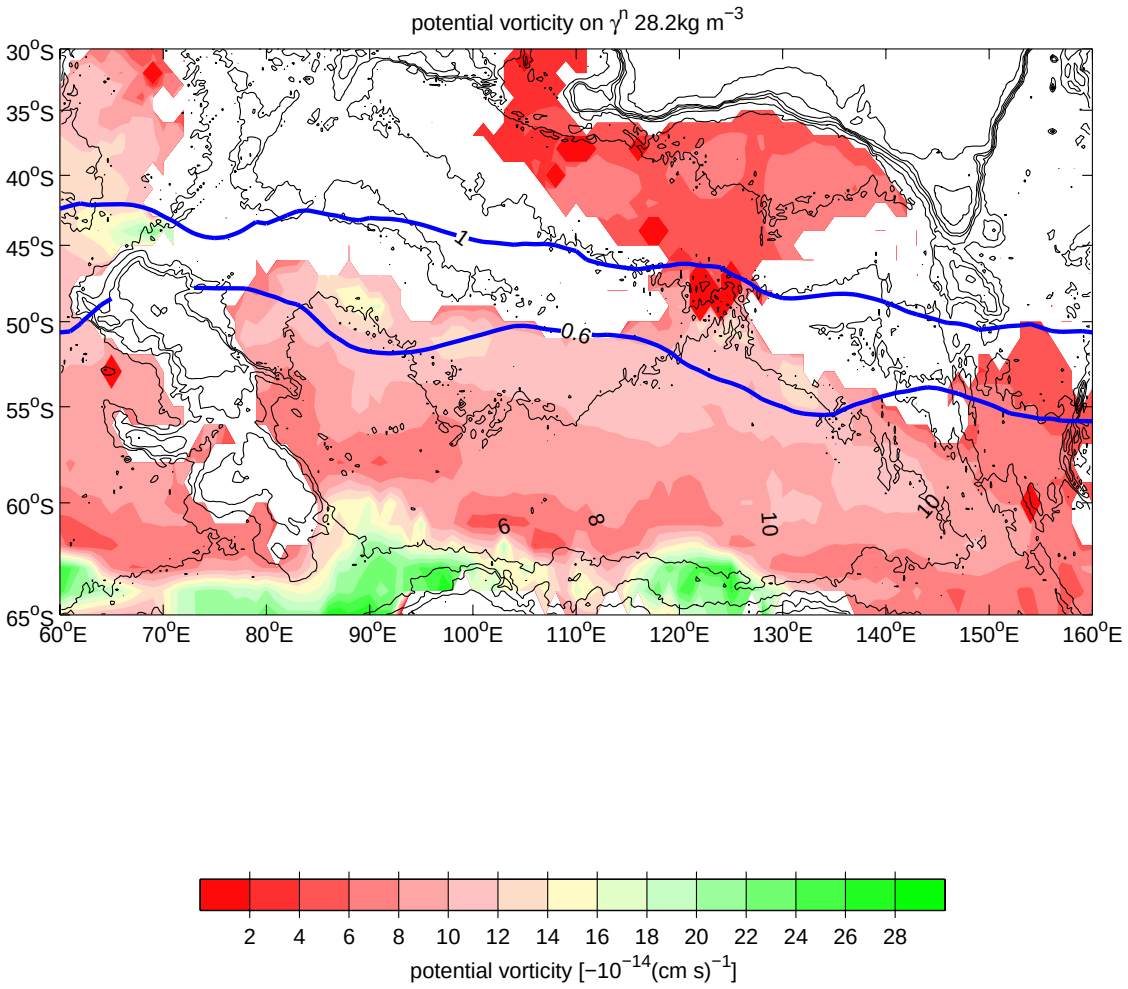

Fig. 22. Potential vorticity in 10^{-14} (cm s)$^{-1}$ on the 28.2 kg m^{-3} γ^n surface from the Gouretski and Jancke (1998) climatology with a 2 x 10^{-14} (cm s)$^{-1}$ contour interval showing that the deep potential vorticity maxima extends across the Australian-Antarctic Basin. White denotes area where that surface is not found in the standard level gridded data. Dynamic height values at 100 db referenced to 1000 db are also calculated from the climatology: the 1.0 and 0.6 dynamic meter contours are shown in blue. Bathymetry is contoured every 1000 m depth.

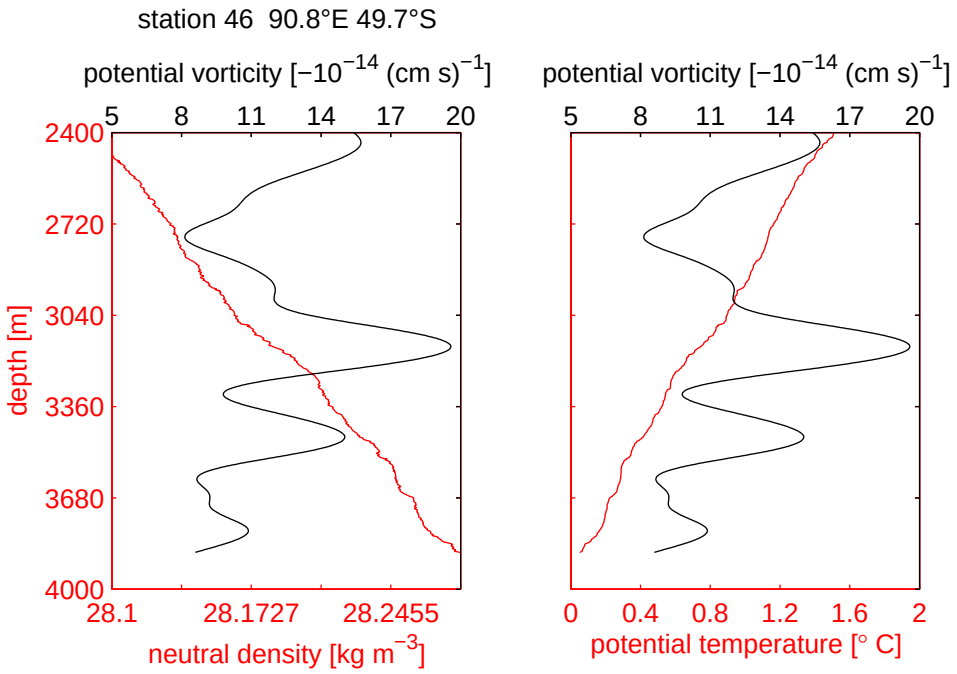

Fig. 23. Potential temperature and neutral density exhibit steppiness within the deep potential vorticity maxima. Left panel: Potential vorticity (black, in 10^{-14} (cm s)$^{-1}$) and neutral density, γ^n (red, in kg m^{-3}), plotted against depth. Right: potential vorticity (black line, in 10^{-14} (cm s)$^{-1}$) and potential temperature (red line, in °C) plotted against depth.

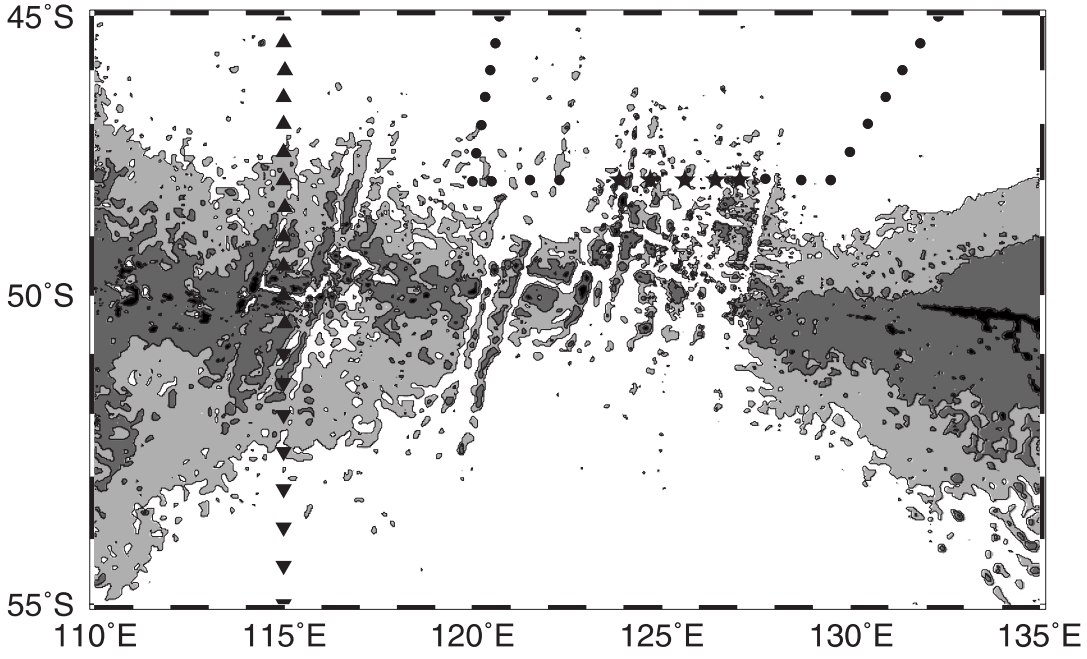

Fig. 24. Topography of the Australian–Antarctic Discordance region (Smith and Sandwell, 1997) with black indicating depths less than 3000 m, shade breaks and contours at 3000, 3500 and 3800 m, with white indicating depths greater than 3800 m. Triangles are I9 stations with bottom temperatures ≥ +0.37°C; inverted triangles are I9 stations with Temperatures ≤ -0.02°C; dots are S5 stations with Bottom Temperatures ≥ +0.47°C; stars are S5 stations with temperatures in the range 0.28 to 0.40°C.

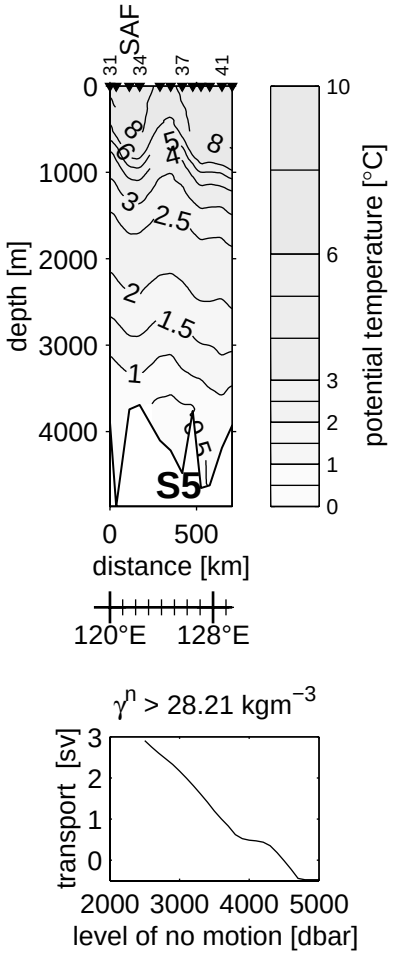

Fig. 25. Top panel: potential temperature (ºC) distribution along the 48ºS part of the S5 section. Bottom panel: Integrated volume transport in Sv across the section as a function of the level of no motion for neutral densities greater than 28.21 kg m^{-3} (potential temperature about 0.5°C.

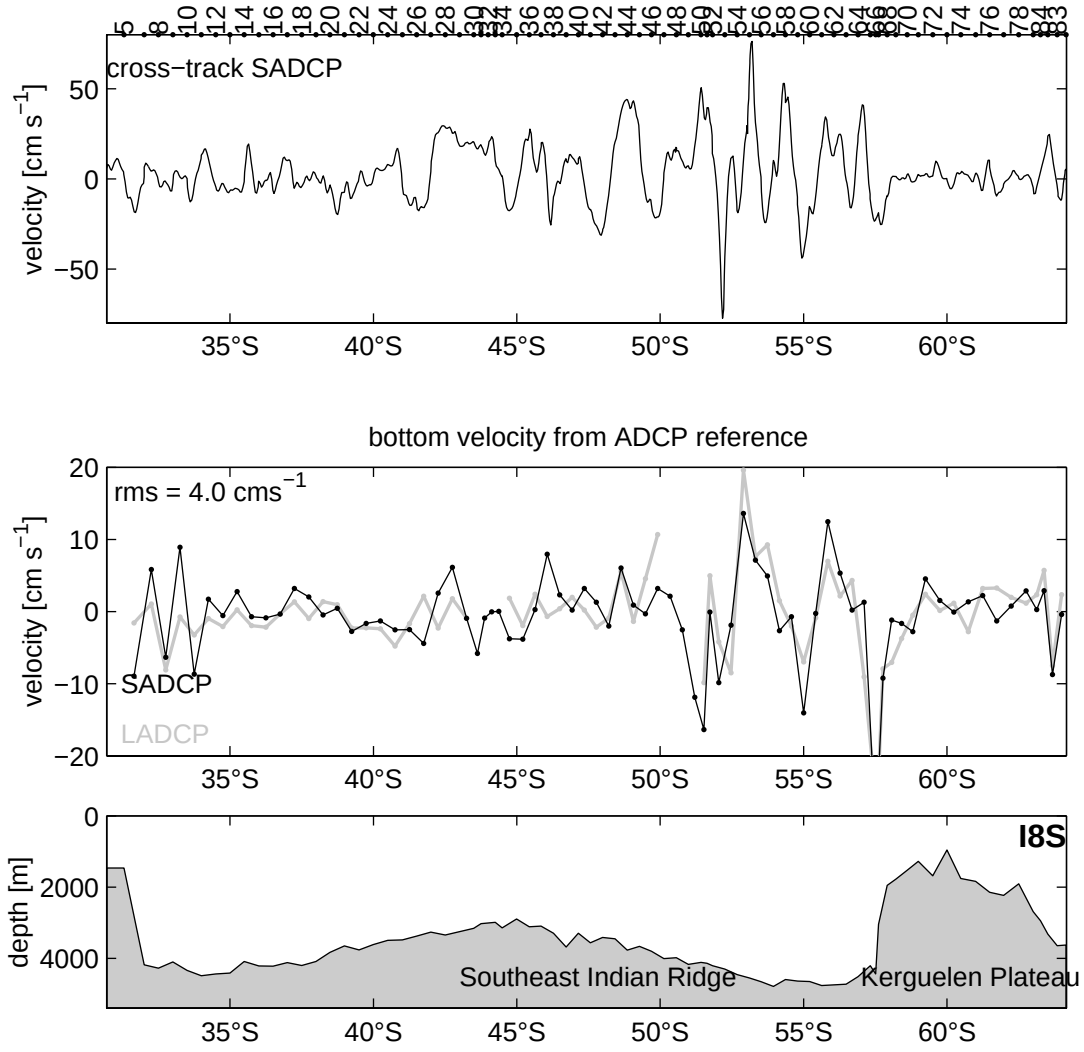

Fig. 26A. Upper panel: Detided cross-track SACP velocities (averaged between 150 and 250 db) along I8S. Middle panel: Bottom velocities (deepest common level) determined from the SADCP (black) and LADCP (grey) referenced geostrophic velocity profiles. reveal similar structure. Bottom velocities tend to be in the same direction as upper-layer cross-track velocity. The root-mean-square difference between the ADCP-derived bottom velocities is 4.1 cm s^{-1}. Lower panel: Bathymetry.

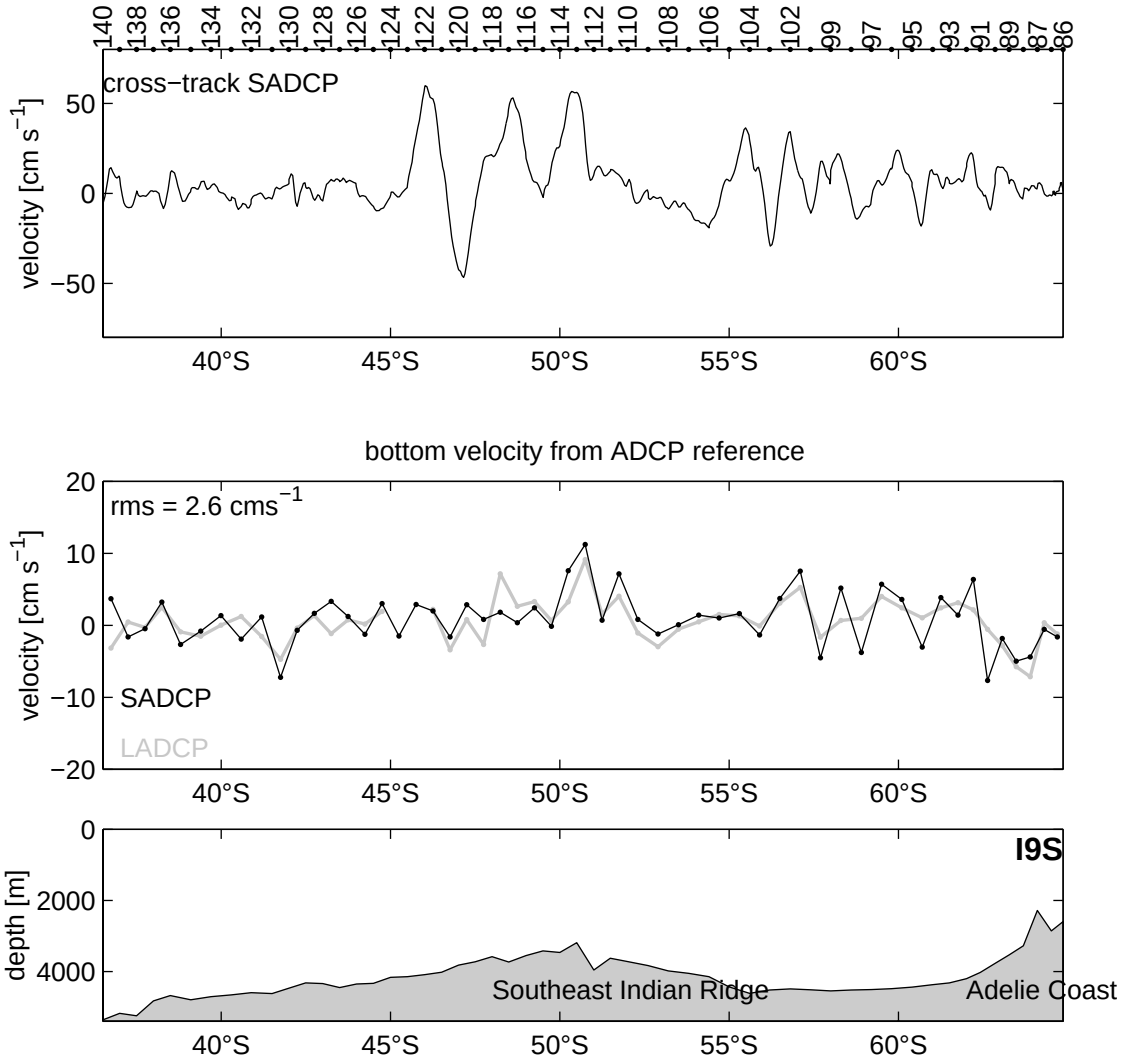

Fig. 26B. Same as Fig. 26A, but for I9S. Similar to the results for I8S, the ADCP-determined bottom velocities tend to be in the same direction as near-surface cross-track velocities. The root-mean-square difference between the LADCP and SADCP bottom velocities is 2.7 cm s^{-1}. Note that the horizontal station spacing does not always resolve the horizontal velocity scales especially along the southern portion of the section. This limits the utility of the LADCP – referenced field.

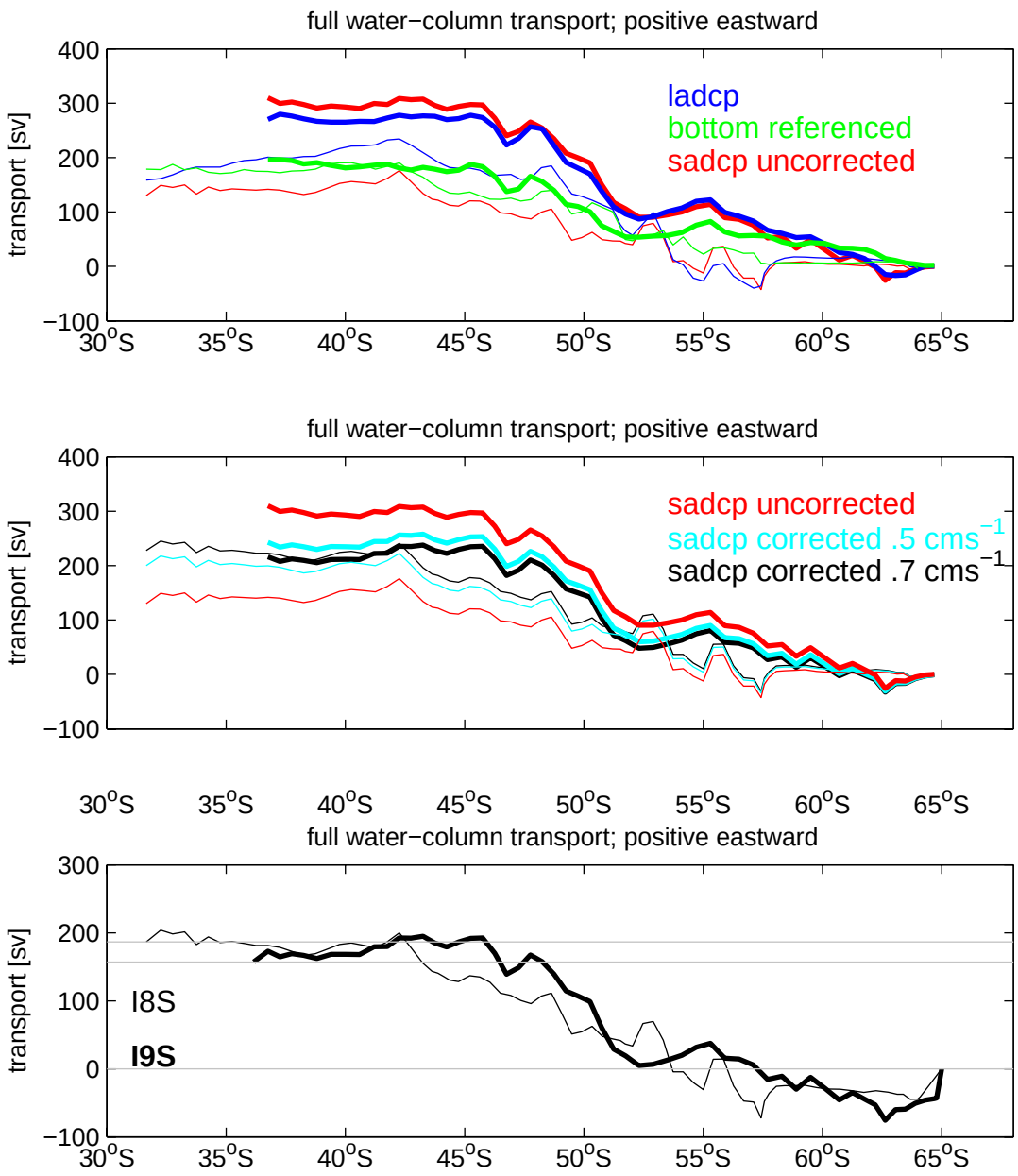

Fig. 27. Full water column transports integrated northward from Antarctica for I8S (thin contours) and I9S (thick contours). See text for details. Upper panel: using bottom-referencing (deepest common level), LADCP-referencing, and SADCP-referencing with no bias applied. Middle panel. The evolution of the estimated northward-integrated transport for SADCP-referencing reflecting the impact of the initial estimate of SADCP bias -0.5 cm/sec and the final estimate of -0.7 cm/sec that results from consideration of large scale transport constraints. Lower panel: The final estimates of total transport using the 0.7 cm/sec bias and with transports for the "missing pieces" along I8S and I9S included. There are three such regions: between the southern end of each section to Antarctica (I8S, 41Sv; I9S, 43Sv) and the northern tip of I9S where the SADCP was not operational (16 Sv).

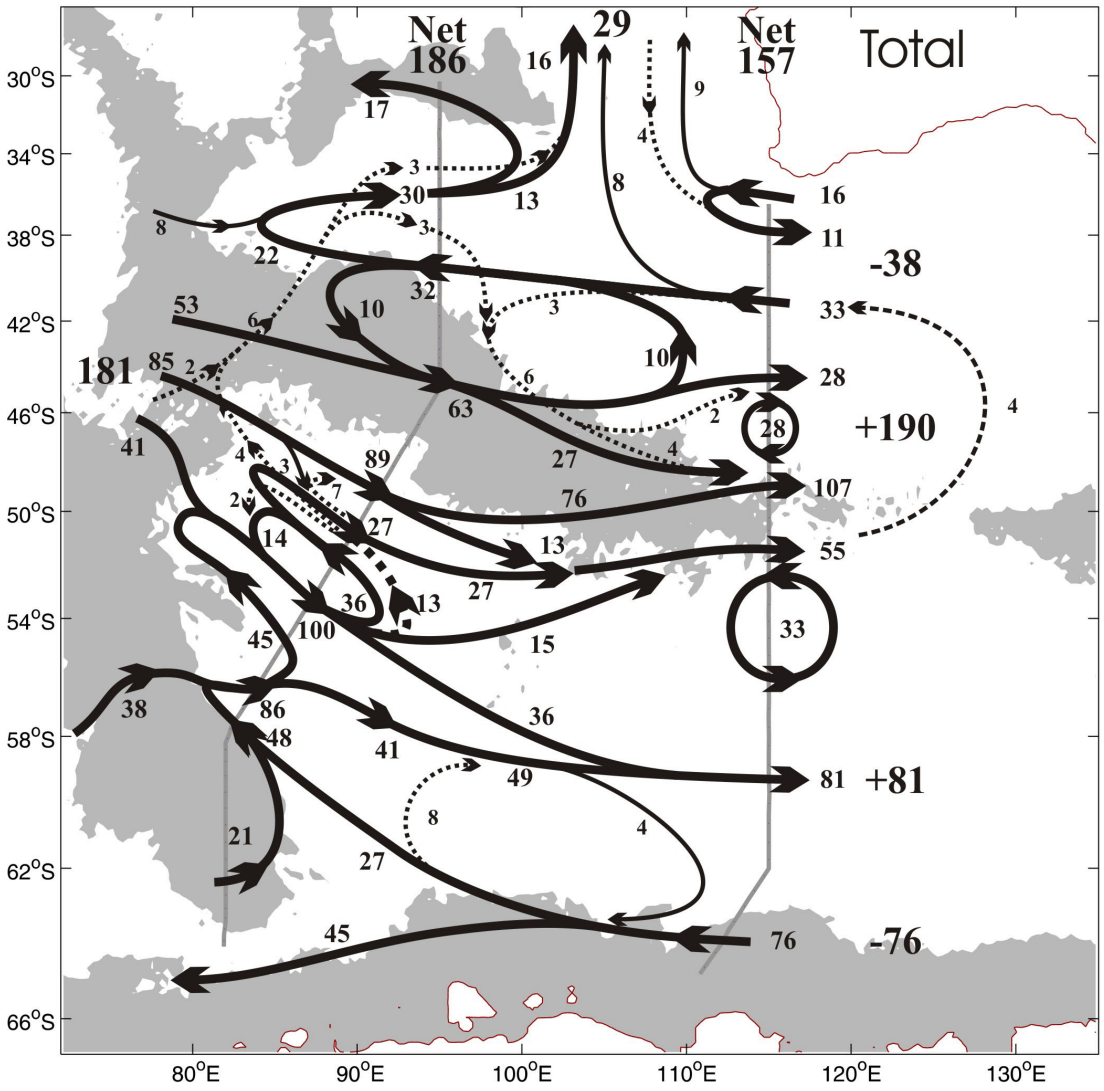

Fig. 28. Plan view of full water column transports for I8S and I9S in Sv. We retain eddy/meander features stronger than 20 S along the sections, but suppress the weaker features. Thin contours represent circulation elements less than 10 Sv, while the thicker contours indicate the principal axes of various stronger flows. Several dashed contours are included in this field and represent pathways along which bottom waters from the cyclonic gyre regime intrude into the Antarctic Circumpolar Current Regime and escape northward into the South Australian Basin. Without that artifice, the total transport field would be somewhat misleading: the relatively small bottom water flows would be masked by the larger transports of the total water column. The schematic is quantitatively accurate to within ±1 Sv relative to the computed transports across the sections. Bathymetry is shaded grey for depths less than 3500 m and land is white.

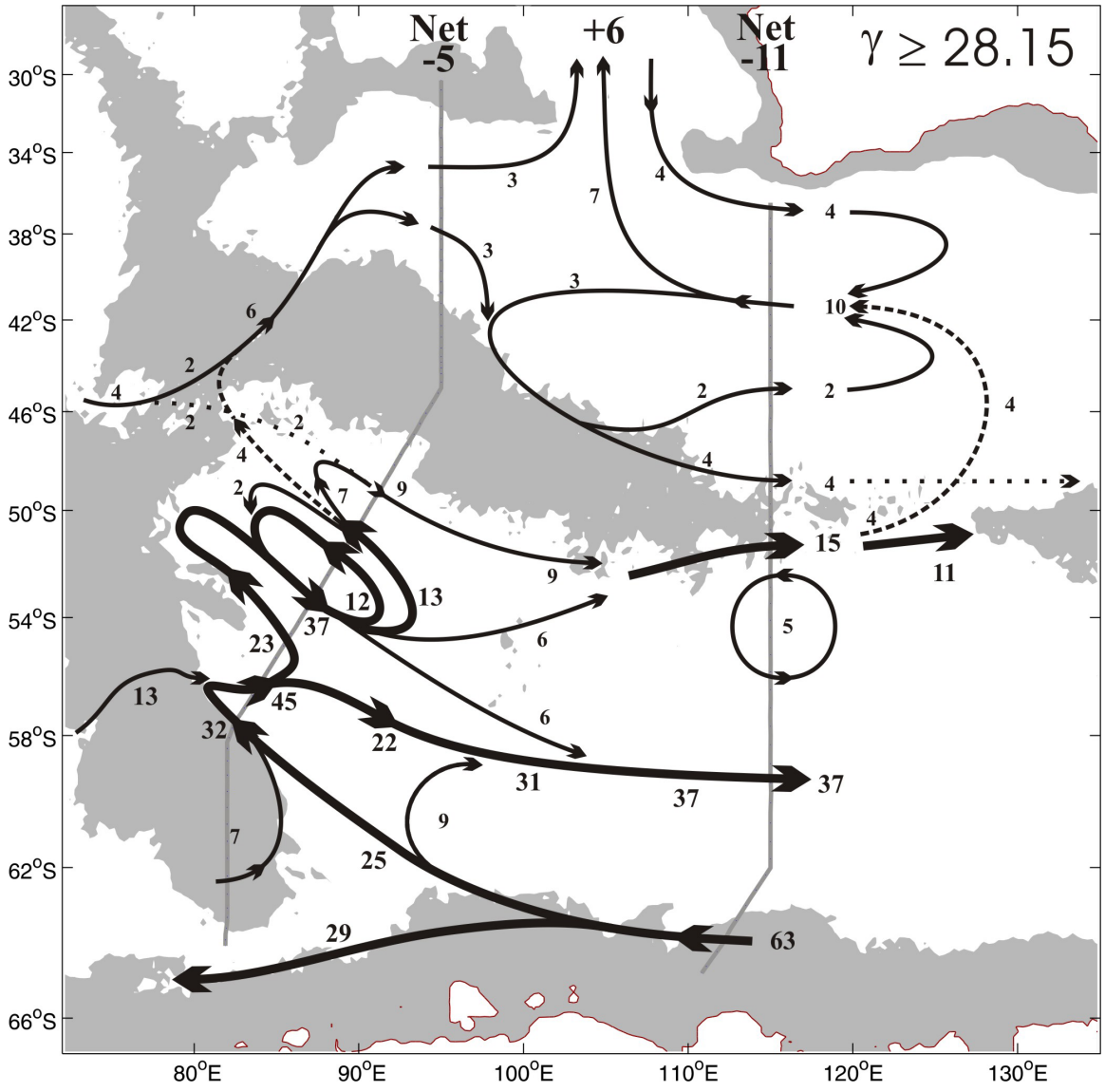

Fig. 29. Same as Fig. 28 but for layers with neutral density, $\gamma^n \geq 28.15$ kg m^{-3} (about 1°C). The dashed contour in the north east indicates 4 Sv of bottom water with $\gamma^n \geq 28.21$ kg m^{-3} (about 0.7ºC) that cross over the Australian–Antarctic Discordance from the 15 Sv concentrated eastward flow just south of the Southeast Indian Ridge crest in I9S. It crosses under a zonal 4 Sv flow along the northern flank of the Ridge of somewhat lighter water, $28.21 \geq \gamma^n \geq 28.15$ kg m^{-3}, that originates from northward flow through the Geelvinck Fracture Zone farther west. A similar artifice of crossing streamlines is used in the west to indicate 4 Sv of denser water undercutting 2 Sv of not so dense water flowing east from the Kerguelen–St. Paul Island Passage to enter the Geelvinck Fracture Zone.

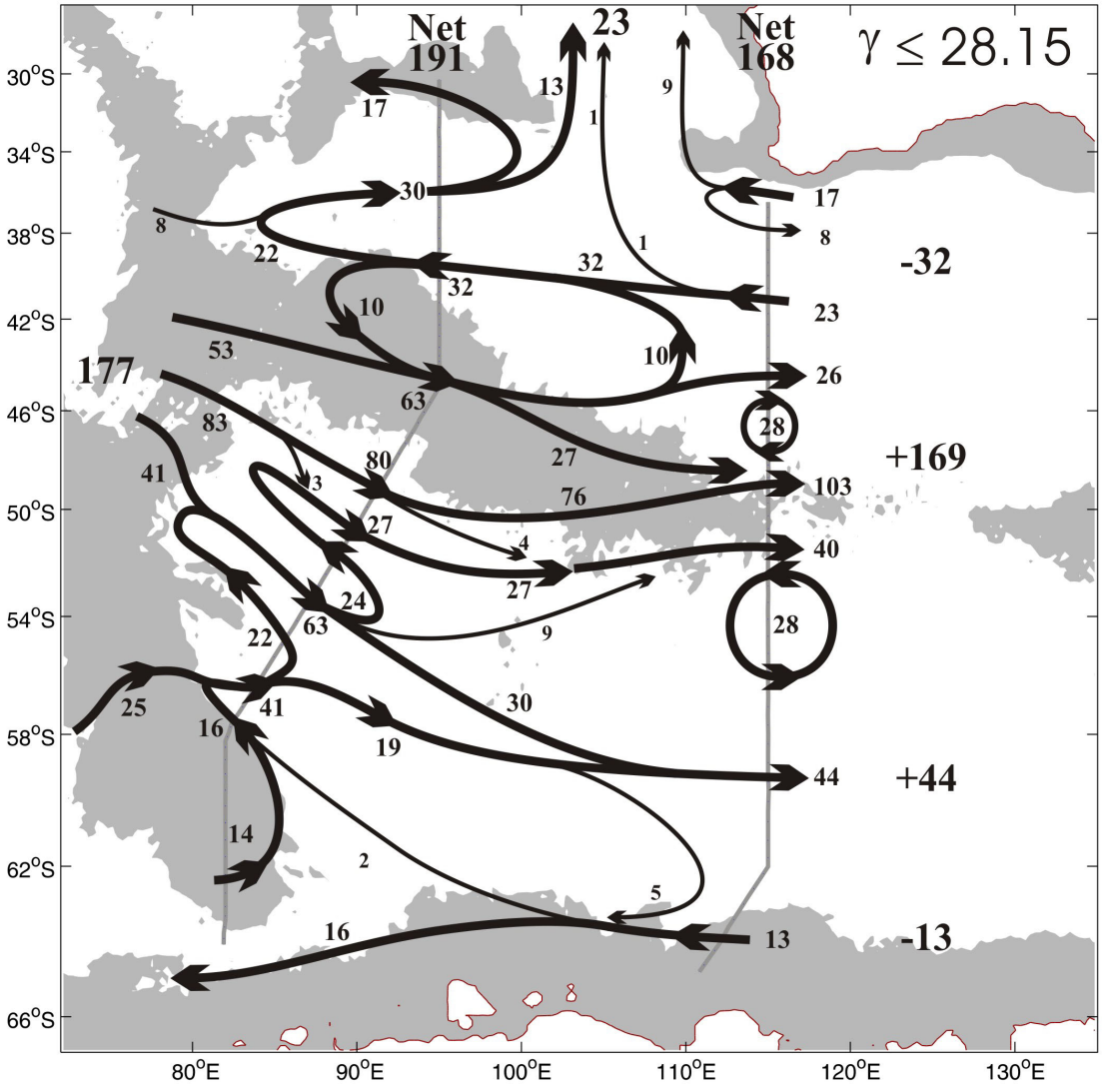

Fig. 30. Same as Fig. 28 but for layers with neutral density, $\gamma^n \leq 28.15$ kg m^{-3} (about 1°C).

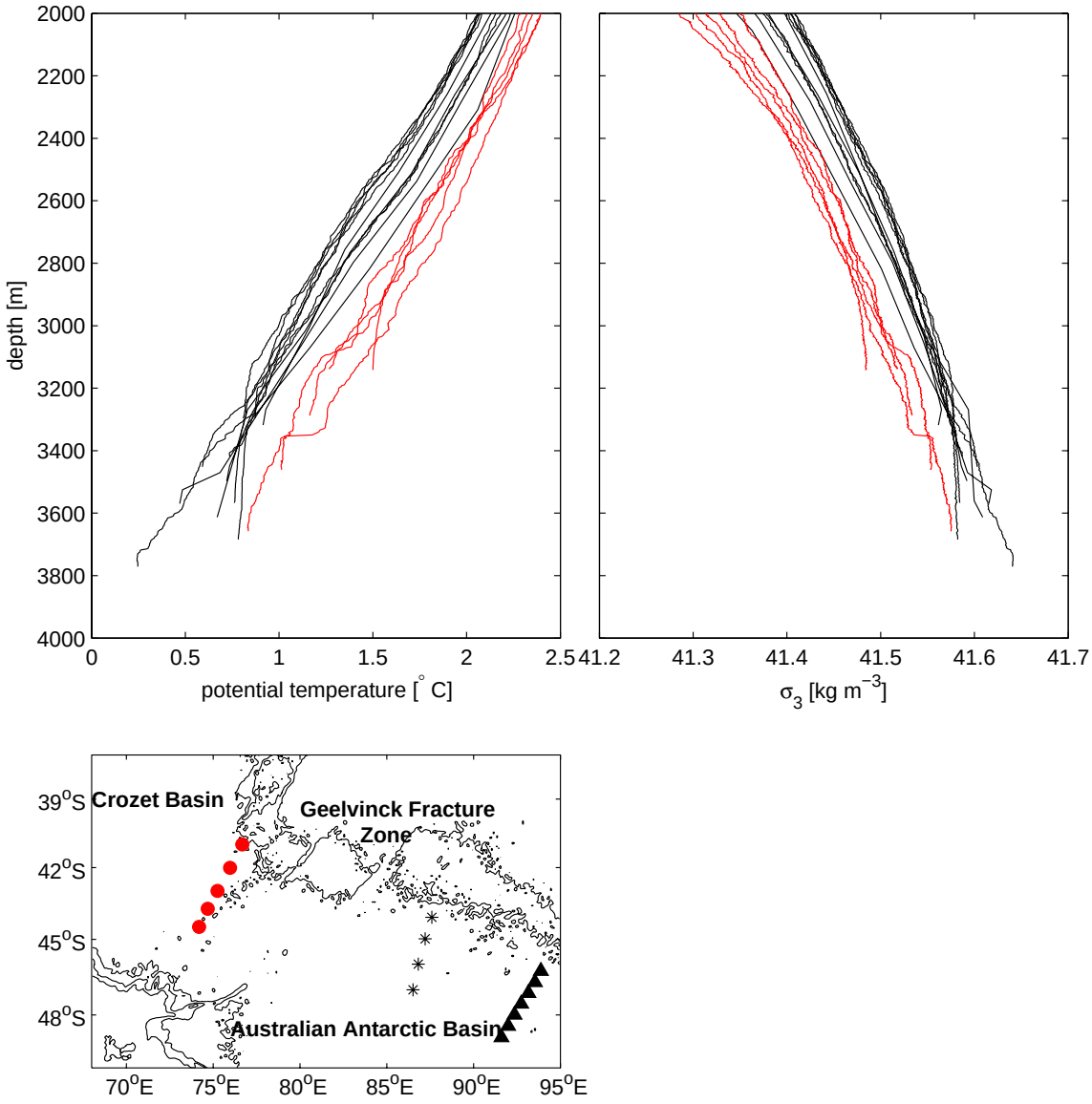

Fig. 31. Upper left (right): Potential temperature versus depth (potential density referenced to 3000 dbar, σ_3) for three groups of stations. Positions are shown in Fig. 16 and in the bottom panel of this figure. Red stations are located 450 km west of the sill (about 3400-3450 m) in the Kerguelen Plateau–St Paul Island Passage (Park et al. 1993). The maximum depths of these stations, 3250–3650 m, bracket the sill depth to their east, the stations plotted (stations 51-55 in section plot, Fig. 17) are north of the compressed front in the central Passage. Black stars and triangles are from the 1972 Eltanin dataset (stars) and the 1994 I8S data set (triangles); the stations shown are in the same depth range along the southern flank of the Southeast Indian Ridge east of the Geelvinck Fracture Zone as the red stations west of the sill.

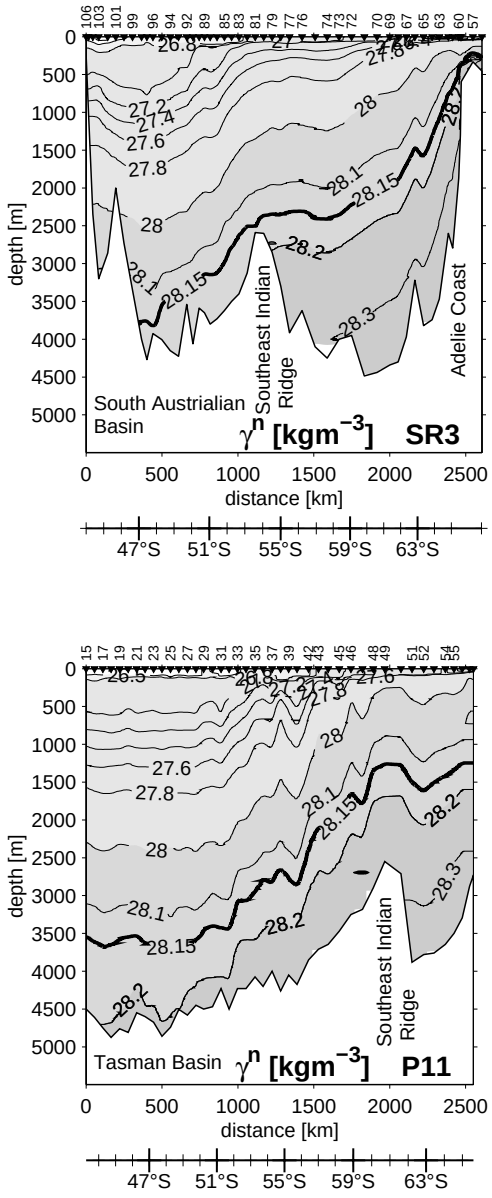

Fig. 32. Distribution of neutral density, γ^n, in kg m^{-3} for SR3 (top) and P11 (bottom). Station locations are shown in Fig. 1.

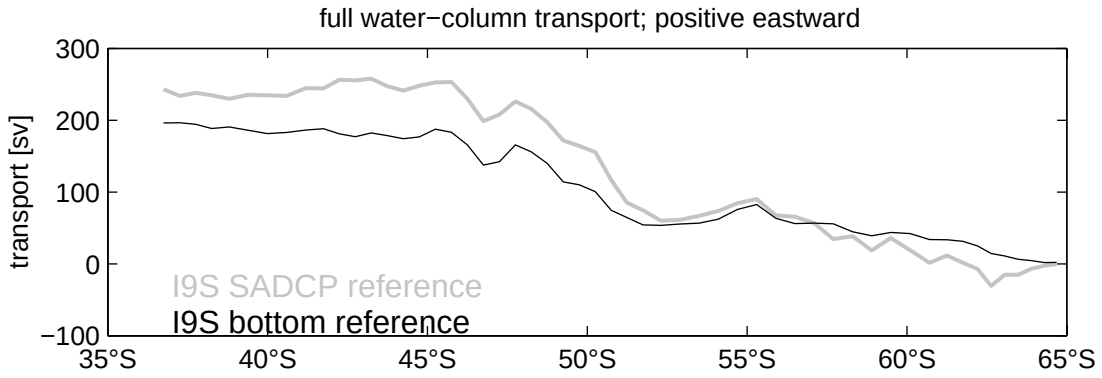

Fig. 33. Full water column transport along I9S integrated northward from the southernmost station over the Antarctica continental slope. The black line derives from a deepest common level reference while the gray line results from the SADCP reference.

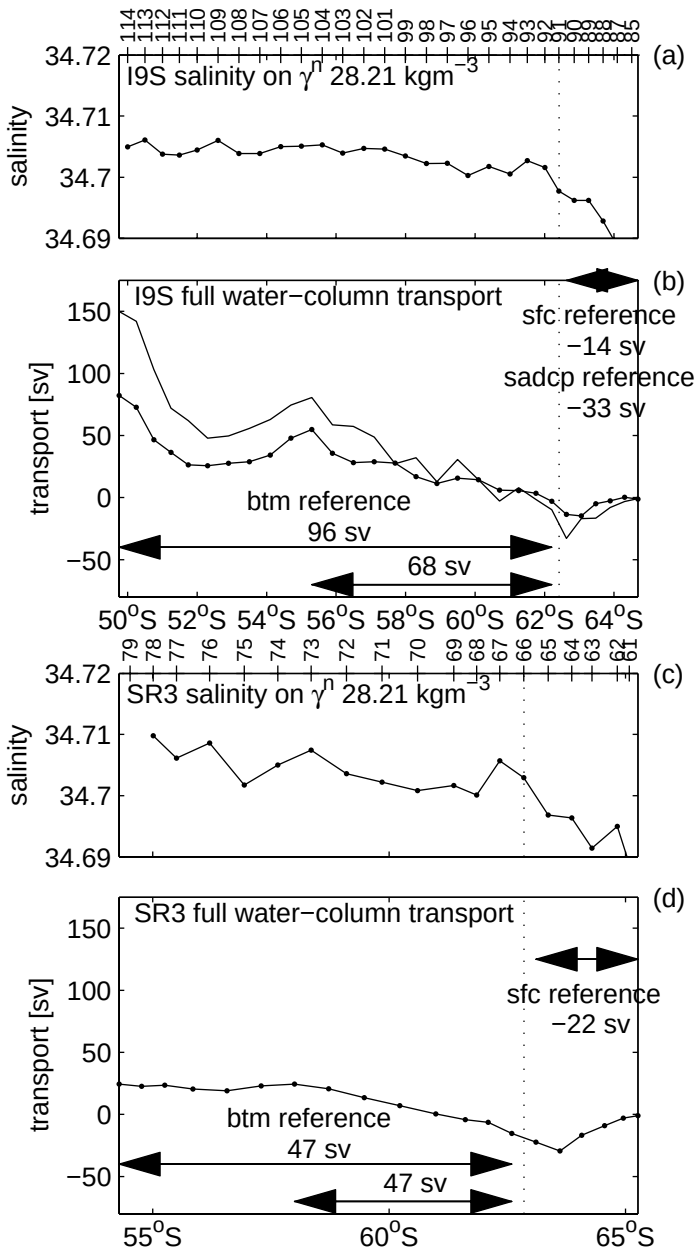

Fig. 34. Salinity on the 28.21 kg m^{-3} neutral density surface for I9S, 115 º E (a) and SR3, 140ºE (c). Volume transport in Sv for neutral densities greater than γ^n 28.21 kg m^{-3} along I9S, 115ºE (b) and SR3, 140ºE (d) integrated from the southern end of each section to the Southeast Indian Ridge crest. Positive is eastward. See text discussion of referencing and domains.

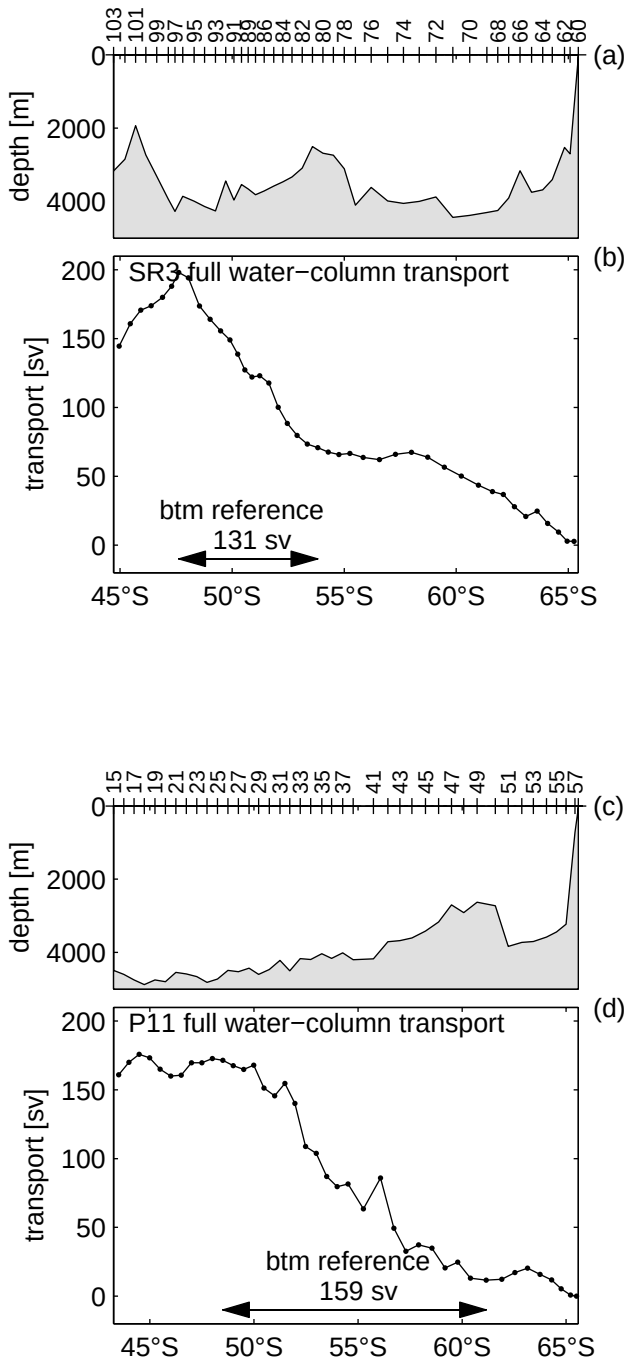

Fig. 35. Bathymetry along SR3 (a) and P11 (c). Full water column volume transport in Sv for a bottom reference level along SR3 (b) and P11 (d) 115ºE (b) and SR3,140ºE (d) integrated northward from the southern end of each section. Positive is eastward.